Tribological response of thermally sprayed high entropy alloys for aerospace applications

Raunak Supekar

A Thesis
in the department of
Mechanical, Industrial and Aerospace Engineering

Presented in Partial Fulfillment of the
Requirements for the Degree of
Master of Applied Science (Mechanical Engineering)
at
Concordia University
Montréal, Québec, Canada

September 2022

CONCORDIA UNIVERSITY

School of Graduate Studies

This is to certify that the thesis prepared

By: **Raunak Supekar**

Entitled: **Tribological response of thermally sprayed high entropy alloys for aerospace applications.**

and submitted in partial fulfillment of the requirements for the degree of

Master of Applied Science (Mechanical Engineering)

complies with the regulations of the University and meets the accepted standards with respect to originality and quality.

Signed by the final examining committee:

_____ Chair
Dr. Carole El Ayoubi

_____ Examiner
Dr. Melanie Hazlett

_____ Examiner
Dr. Carole El Ayoubi

_____ Supervisor
Dr. Pantcho Stoyanov

Approved by _____

Martin D. Pugh, Chair
Department of Mechanical, Industrial and Aerospace Engineering

September 2, 2022 _____

Mourad Debbabi, Dean
Gina Cody School of Engineering and Computer Science

Abstract

Tribological response of thermally sprayed high entropy alloys for aerospace applications

Raunak Supekar

Aerospace components operating in extreme environments commonly face severe degradation due to wear, corrosion, oxidation and fatigue. Conventional materials used for such components face limitations with such degradation issues and thus, there is a need to develop new alloy systems capable of operating effectively in extreme conditions. High entropy alloys (HEAs) have gained a lot of attention recently due to their outstanding mechanical properties and tribological behavior. These advance HEAs need to be deposited in the most effective way suitable for tribological applications. Thermal spraying techniques have proven to be one of the most efficient technologies for mitigating wear and corrosion damage that occurs due to harsh environmental conditions. The modularity of these techniques has made it possible to spray and/or repair intricate components in an effective manner.

The main purpose of this research is to evaluate the tribological performance of a novel AlCoCrFeMo HEA system deposited via cold spraying, flame spraying and HVOF spraying technologies and identify the most suitable thermal deposition technique. This thesis comprises of two research studies in which the first study focuses on tribological behavior of cold sprayed and flame sprayed HEA at room temperature under varying loads (5N and 10N) and the effect of polishing. The second study investigates the temperature response (room temperature and 450^{O}C) on tribological behavior of the HEA deposited via cold spraying, flame spraying and HVOF for the first time in scientific community.

In both the studies, the tribology tests were performed using ball-on-flat tribometer and the wear profiles were extracted using a laser confocal microscope. The ex-situ characterization of the coatings was done using scanning electron microscope (SEM), energy dispersive spectroscopy (EDS), x-ray diffraction (XRD), image analysis, and Vickers micro-hardness testing. The HVOF sprayed HEA showed the least wear rates followed by flame sprayed HEA coating and cold sprayed HEA at both temperatures (room temperature and 450^{O}C). The research suggests that HVOF is the most suitable thermal spray deposition technique for high entropy alloy systems involving tribological applications.

Acknowledgement

I would like to express my immense gratitude towards my supervisor, Dr. Pantcho Stoyanov for providing me an opportunity to work on such an interesting research project. This project turned out to be a huge success due to his unconditional support, expert guidance and enthusiastic mentorship. I would also like to appreciate the contributions of Dr. Andre McDonald, Dr Javad Mostaghimi, Dr. Yu Zou, Dr. Rakesh Nair, Dr. Seyyed Morteza Javid and Ms. Wandong Wang for collaborating in this research work and supporting the study by providing valuable reviews.

I would like to thank all the members of the Thermal Spray Laboratory group for providing expert knowledge and guidance throughout my experiments. I also appreciate the technical assistance of Dr. Dmytro Kevorkov, Mr. Mazen Samara in experimental work. I specially thank Mr. Payank Patel, Mr. Amit Roy and Mr. Parikshit Tonge for helping me throughout my research and for their excellent mentorship.

I am grateful to Concordia University and the Green-SEAM network for providing a platform and resources to carry out my valuable research in an effective way.

Finally, I would like to appreciate the support and motivation I received from my parents and my friends throughout my academic career.

Contribution of Authors

This thesis composes of peer-reviewed and under-review research articles. All the manuscripts have been produced by me as a principal author and my supervisor, Prof. Pantcho Stoyanov as a co-author in collaboration with others. Most of the experimental and technical writing work was performed by the principal author while the supervisor aided in providing analytical vision and technical guidance over the project. I acknowledge the contribution of the co-authors of the produced articles:

- Chapter 3: Supekar, R.; Nair, R.; Javid, S.; Wang, W.; Zou, Y.; McDonald, A.; Mostaghimi, J.; Stoyanov, P. High entropy alloy coatings deposited by thermal spraying technologies: A review of strengthening mechanisms, performance assessments and perspectives on future applications. *Submitted to Journal of Thermal Spray Technology*
    - Supekar R was responsible for conducting an in-depth literature review, writing the original manuscript draft and revising the final manuscript. Nair R was responsible for providing a critical review of the manuscript and addressing the shortcomings of the original draft. McDonald A, Mostaghimi A, Zou Y, Javid A and Wang A were responsible for providing feedback through a secondary review. Stoyanov, P was responsible for supervision and guidance for the literature review.
- Chapter 4: Supekar, R.; Nair, R.; McDonald, A.; Stoyanov, P. Tribological Response of AlCoCrFeMo High Entropy Alloys Deposited via Flame Spraying and Cold Spraying: A Comparative Evaluation. *In Review*
    - Supekar R was responsible for performing all tribological tests, data analysis and writing the entire manuscript. Nair R was responsible for providing the deposited samples for tribological evaluation. McDonald A and Stoyanov P were responsible for critically reviewing the work.
- Chapter 5: Supekar, R.; Patel, P.; Nair, R.; McDonald, A.; Cromik, R.; Moreau, C.; Stoyanov, P. Temperature Response on Tribological Evaluation of AlCoCrFeMo High Entropy Alloys Deposited via Thermal Spraying Techniques: A Novel Study. *In Review*
    - Supekar R was responsible for performing all tribological tests, data analysis and writing the original manuscript. Patel P was responsible for providing deposited samples and coating characterization. Nair R was responsible for providing the deposited samples for tribological evaluation. McDonald A, Cromik R, Moreau C and Stoyanov P were responsible for critically reviewing the work.

Table of Contents

List of Figures

List of Tables

Abbreviations

HEA – High Entropy Alloys

CS – Cold Spray

FS – Flame Spray

HVOF – High Velocity Oxy-Fuel

SEM – Scanning Electron Microscope

EDS – Electron Dispersive Spectroscopy

XRD – X-Ray Diffraction

PVD – Physical Vapor Deposition

CVD – Chemical Vapor Deposition

Organization of thesis

i. Chapter 1 provides the introduction the thesis and its objectives and motivation.

ii. Chapter 2 introduces tribology and thermal spraying as a concept.

iii. Chapter 3 presents the introduction to HEAs, thermally sprayed HEAs, their microstructure, strengthening mechanisms, corrosion, oxidation behavior and their potential applications.

iv. Chapter 4 presents the tribological evaluation of cold sprayed and flame sprayed AlCoCrFeMo high entropy alloy coatings. The tests were performed at room temperature on polished as well as unpolished surfaces at varying loads (5N and 10N) and a comparison was drawn.

v. Chapter 5 presents a novel work of temperature response on tribological behavior of cold sprayed, flame sprayed and HVOF sprayed AlCoCrFeMo high entropy alloy coatings. The tests were conducted at room temperature and 450^{O}C for all the coating systems and a comparative evaluation was deduced. The most suitable thermal spray deposition technique for high entropy alloy coatings involving tribological applications was suggested.

vi. Chapter 6 draws the overall conclusions of the entire thesis and proposes future work on thermally sprayed high entropy alloy coatings.

Chapter

1. INTRODUCTION & OBJECTIVES

In this chapter…

The motivation and brief introduction to the thesis is presented with its objectives.

1.1. Introduction

Almost every industry is affected by the degradation of materials due to wear, oxidation and corrosion damages. Conventional alloy systems prove to be incapable of preventing all these degradation issues at once [1,2]. For, instance, gas turbines blades are constantly wearing at the interface and cause severe losses in efficiency of the engines [3,4]. The wear damages lead to failure of components in extreme environmental conditions which result in economic losses, accidents and environmental consequences [5]. It is crucial to develop new alloy systems that are able to withstand severe wear losses and also resist corrosion and oxidation damages at the same time. The advances in scientific research have led to the discovery of a new species of alloys termed as High Entropy Alloys (HEAs) coined by *et al*. [6] and Cantor *et al*. [7]. Ever since, the curiosity towards HEAs have been increasing exponentially to their remarkable mechanical properties and tribological performance.

HEAs consists of five or more principal elements in equimolar or near equimolar proportions within the range of 5 at% and 35 at% [6,7]. HEAs are mostly found possessing face-centered cubic (FCC) or body-centered cubic (BCC) molecular structures due to their high configurational entropies (more than 1.5 times R, R being the gas constant $8.3144\ \mathrm{J\ mol^{-1}K^{-1}}$) and stability of phases. The four core effects namely (1) high configurational entropy, (2) sluggish diffusion, (3) severe lattice distortion and (4) cocktail effect are responsible for its superior properties and stable microstructure [8,9].

Several researchers have shown that HEAs exhibit exceptional tribological behavior in the form of a coating [8,10-14]. More precisely, thermal spray deposition techniques have the ability to produce excellent HEA coatings for wear resistant applications. Thermal spraying is beneficial as compared to Chemical Vapor Deposition (CVD), Physical Vapor Deposition (PVD) or sputtering since it can produce a coating of larger thickness suitable for tribological applications [15]. Also, thermal spraying is advantageous in situations where repair work or protective layers need to be deposited over complex geometries due to its versatility and flexibility of operation. Cold spray, flame spray and HVOF are some of the most widely used thermal spraying techniques to produce thick wear resistant coatings. Cold spraying is a high velocity low temperature deposition technique where the temperature ranges are kept below the melting point of the feedstock [16]. This process is beneficial for producing thick coatings with minimal amounts of porosity and oxide inclusions [17]. Flame spraying and HVOF are high temperature deposition techniques where particles are melted and deposited over the

substrate in the form of splats [15,18-20]. The rapid solidification of the melted splats tends to increase the porosity of the coating which can be controlled through modification of spraying parameters [18,20,21]. However, the oxide phases formed during high temperature deposition increase the wear resistance significantly due to enhanced hardness of the coating [15,22-24].

While a significant amount of research has been performed on the microstructure and mechanical behavior of HEAs deposited via thermal spraying, their tribological behavior has received less attention. In particular, very few articles can be found on tribological evaluation of cold sprayed and HVOF sprayed HEAs however, the tribological response of flame sprayed HEAs have never been explored. The main purpose of this thesis is to critically evaluate flame spraying for HEAs as well as provide a comparative tribological evaluation between three thermal spray deposition techniques to identify the most suitable method of producing wear resistant HEA coatings. A novel AlCoCrFeMo HEA has been synthesized which was derived from widely used AlCoCrFeNi HEA by replacing Ni with Mo.

1.2. Thesis objectives

The primary objective of this thesis is to evaluate the tribological response of thermally sprayed HEAs for aerospace applications and identify the most suitable deposition process. The following specific objectives (SO) have been identified for this thesis:

SO 1 → To identify existing research gaps for the deposition of high entropy alloys and design an approach to corelate deposition parameters with coating performance.

SO 2 → To identify the effect of polishing and response of varying loads on cold sprayed and flame sprayed AlCoCrFeMo HEA coatings on the tribological performance.

SO 3 → To evaluate the response of temperature on tribological behavior of cold sprayed, flame sprayed and HVOF sprayed AlCoCrFeMo HEA coatings.

1.3. Author's comments

All the manuscripts in this master's thesis have already been submitted to the journal or under internal review. The chapters 3, 4 and 5 contains information that may overlap or repeat within the introduction or experimental procedures sections of the individual manuscripts. Repetitive information in the results has been minimized and referred properly to the overlapping chapters wherever required and retained at some instances for ease of the readers.

References:

1. F.L. LaQue, Marine corrosion: causes and prevention, (1975)
2. I. Finnie, Some reflections on the past and future of erosion, Wear, 186, 1-10 (1995)
3. B. Wang, G. Geng, A.V. Levy, W. Mack, Erosivity of particles in circulating fluidized bed combustors, Wear, 152(2), 201-222 (1992)
4. J.R. Laguna-Camacho, L.Y. Villagrán-Villegas, H. Martínez-García, G. Juárez-Morales, M.I. Cruz-Orduña, M. Vite-Torres, L. Ríos-Velasco, I. Hernández-Romero, A study of the wear damage on gas turbine blades, Engineering Failure Analysis, 61, 88-99 (2016)
5. U.S.Bureau, U.S. Bureau of Labor Statistics. Employer-reported workplace injuries and illnesses, U S Bureau of Labor statistics, (2015)
6. J.W. Yeh, S.K. Chen, S.J. Lin, J.Y. Gan, T.S. Chin, T.T. Shun, C.H. Tsau, S.Y. Chang, Nanostructured High-Entropy Alloys with Multiple Principal Elements: Novel Alloy Design Concepts and Outcomes, Advanced Engineering Materials, 6(5), 299-303 (2004)
7. B. Cantor, I.T.H. Chang, P. Knight, A.J.B. Vincent, Microstructural development in equiatomic multicomponent alloys, Materials science & engineering. A. Structural materials : properties, microstructure and processing., 375(1), 213 (2004)
8. D.F. Rojas, H. Li, O.K. Orhan, C. Shao, J.D. Hogan, M. Ponga, Mechanical and microstructural properties of a CoCrFe0.75NiMo0.3Nb0.125 high-entropy alloy additively manufactured via cold spray, Journal of Alloys and Compounds, 893, (2022)
9. B.S. Murty, J.-W. Yeh, S. Ranganathan, High-entropy alloys, 1 ed., Elsevier, 2014
10. J.M. Torralba, P. Alvaredo, A. García-Junceda, High-entropy alloys fabricated via powder metallurgy. A critical review, Powder Metallurgy, 62(2), 84-114 (2019)
11. E. Ma, X. Wu, Tailoring heterogeneities in high-entropy alloys to promote strength–ductility synergy, Nature Communications, 10(1), (2019)
12. R.B. Nair, H.S. Arora, A. Ayyagari, S. Mukherjee, H.S. Grewal, High Entropy Alloys: Prospective Materials for Tribo-Corrosion Applications, Advanced Engineering Materials, 20(6), (2018)

13. Y. Shi, B. Yang, P. Liaw, K.T.N. Univ. of Tennessee, K.T.N.U.S.A. The University of Tennessee, Corrosion-resistant high-entropy alloys: A review, Metals, 7(2), (2017)

14. M. Vaidya, G.M. Muralikrishna, B.S. Murty, High-entropy alloys by mechanical alloying: A review, J. Mater. Res., 34(5), 664-686 (2019)

15. A. Meghwal, A. Anupam, B.S. Murty, C.C. Berndt, R.S. Kottada, A.S.M. Ang, Thermal Spray High-Entropy Alloy Coatings: A Review, Journal of Thermal Spray Technology, 29(5), 857-893 (2020)

16. F. Gärtner, T. Stoltenhoff, T. Schmidt, H. Kreye, The cold spray process and its potential for industrial applications, J. Therm. Spray Technol., 15(2), 223-232 (2006)

17. G. Munday, J. Hogan, A. McDonald, On the microstructure-dependency of mechanical properties and failure of low-pressure cold sprayed tungsten carbide-nickel metal matrix composite coatings, Surf. Coat. Technol., 396, 125947 (2020)

18. N. Espallargas, Future development of thermal spray coatings : types, designs, manufacture and applications, ed., Woodhead Publishing is an imprint of Elsevier, 2015

19. Y. Shuo, C. Jan, S. Xinkun, L. Wenya, L. Hanlin, Thermal Spray Technology, Advances in Materials Science and Engineeringed.

20. S. Chandra, P. Fauchais, Formation of Solid Splats During Thermal Spray Deposition, Journal of Thermal Spray Technology, 18(2), 148-180 (2009)

21. R.C. Dykhuizen, Review of impact and solidification of molten thermal spray droplets, Journal of Thermal Spray Technology, 3(4), 351-361 (1994)

22. M. Lobel, T. Lindner, T. Lampke, High-temperature wear behaviour of AlCoCrFeNiTi_{0.5} coatings produced by HVOF, Surface and Coatings Technology, 403, (2020)

23. A. Silvello, P. Cavaliere, S. Yin, R. Lupoi, I. Garcia Cano, S. Dosta, Microstructural, Mechanical and Wear Behavior of HVOF and Cold sprayed High-Entropy Alloys (HEAs) Coatings, Journal of Thermal Spray Technology, (2022)

24. P. Patel, A. Roy, N. Sharifi, P. Stoyanov, R.R. Chromik, C. Moreau, Tribological Performance of High-Entropy Coatings (HECs): A Review, Materials (Basel, Switzerland), 15(10), (2022)

25. R.B. Nair, G. Perumal, A. McDonald, Effect of Microstructure on Wear and Corrosion Performance of Thermally Sprayed AlCoCrFeMo High-Entropy Alloy Coatings, Advanced Engineering Materials, 2101713 (2022)

Chapter

2.BASIC CONCEPTS & BACKGROUND

In this chapter…

A brief introduction to tribology involving the concepts of friction, wear and lubrication have been discussed and basic concept of thermal spraying technology has been presented.

2.1. History of tribology

Tribology has been in existence since ancient times of human history including the process of fire generation involved rubbing of two objects. One of the pioneers in the field of tribology was the famous Leonardo Da Vinci, who is believed to have developed several laws governing the friction between objects in the 15th century. Further in the late 16th century, Amonton put forward the theory saying that the surfaces of all objects are covered by small sphere particles which are now known as impurities or asperities. This developed the concept of coefficient of friction. However, it was not researched into the depths. Hence, the field of tribology saw no development until 1886 when Osborne Reynolds published his famous paper on hydrodynamic lubrication [1]. Osborne's research on hydrodynamic lubrication proved that hydrodynamic pressure of a liquid between the two sliding surfaces is enough to keep the surfaces separated even at an exceptionally low sliding speed. This paper paved the way for numerous research and developments in the field of tribology, but even till now, the field of tribology is yet to be explored in depths [2]. It can be said that the domain of tribology is very new as compared with other fields of mechanics, thermodynamics, etc. and there is a massive research gap that needs to be filled to further enhance the efficiency of systems involving tribological systems [2] [3].

2.2. What is tribology?

The word "tribology" is composed of two words, which are "tribos" (Greek origin) meaning rubbing or sliding, while "ology" means study. Thus, tribology can be defined as the study of interaction and movement of two surfaces in contact with each other. These two surfaces can be both in motion at once or one object in motion and other at rest. While the science of tribology is still an evolving subject, unknowingly, humans and animals have been using this concept since ancient times. Numerous examples include generation of fire by rubbing two different objects, walking, and running, sweating on palms or feet, which in turn increases the friction enabling ease in walking or running, etc. [2,4]. Recently, interest in the field of tribology is increasing primarily aiming to manipulate the existing wear and friction between the two contact surfaces by making use of several technologies including newer materials and manufacturing techniques. Overall, it can be said that the field of tribology consists of

three main components: (1) Friction, (2) Wear and (3) Lubrication (depicted in Figure 2.1) [2,4].

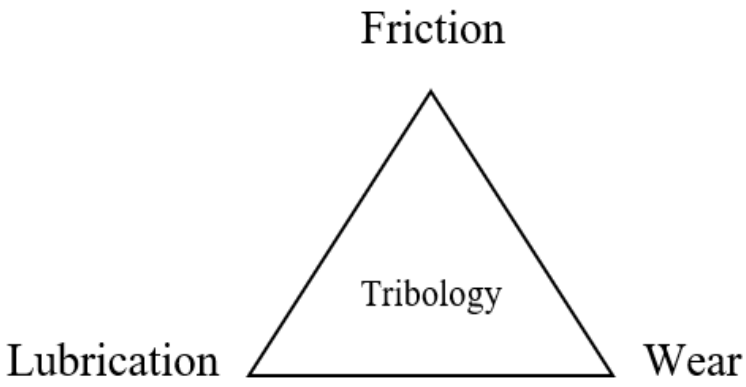

Figure 2.1 Three main components of tribology [3].

2.2.1. Friction

The force of friction can be defined as the resistance to motion when one object moves tangentially over the other body, while in contact [3,4]. Further, this resistance is encountered in direction opposite to the direction of motion when the objects are sliding with respect to each other [3,4]. Figure 2.2 depicts the two surfaces in sliding contact with each other. The load/weight of the block is denoted by 'W' and acting downwards. The friction force is denoted by 'F' and is opposite to the direction of motion. Also, the coefficient of friction can be defined as the ratio of friction force (F) to the normal load, (W) which is 'μ = Frictional force/Normal Load'.

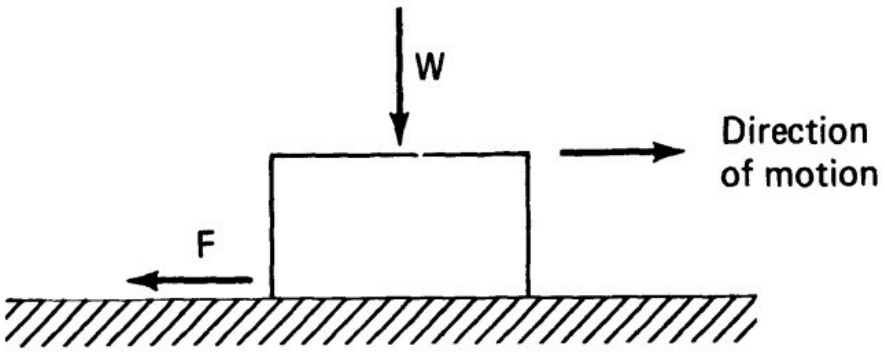

Figure 2.2 Illustration of a horizontally sliding body [5].

In addition, frictional force between the two objects can be categorized in two separate ways: (1) based on the presence or absence of lubricating fluid between the contacting surfaces (Dry and Wet friction) and (2) based on the current condition of the system,

i.e., whether the objects are already in motion or at rest at that particular instance (Static and Dynamic Friction) [3,4]. Dry friction exists when there is no lubricating fluid present in between the contacting surfaces, while wet friction exists when the two surfaces in contact/motion have a film of lubrication present in between them. On the other hand, static friction exists between the surfaces in contact when the whole system is at rest, i.e., when motion is about to be initiated, while dynamic friction exists when the surfaces are already in motion (sliding). The presence of frictional force between the two surfaces can be desirable or non-desirable based on the application [3,4]. For example, we need frictional force to be able to walk or run, for smooth application of car/bike brakes, handwriting on paper, etc. Whereas there are various cases where we desire to have lower/no force of friction, examples are, gears, cams sliding surfaces, pistons in engine blocks, etc. In conclusion, frictional force is a system property (depends on environment, lubrication, temperature, humidity, etc.) and is not dependent on a specific material [3,4].

2.2.2. Wear

Wear can be defined as the phenomenon of loss of material from either of the two surfaces in contact during relative motion. The material loss from the surfaces of objects in contact can be transferred to the other surface (case of no net loss of material of the system) or it can be accounted for as the loss into the atmosphere (case of loss of material to the atmosphere lowering the net weight of system) [3]. Similar to friction, wear is a system phenomenon and can also be desirable in some cases. For instance, wear is desired in the case of writing with a pencil on a sheet of paper. However, the aim is to always avoid wear in case of tires of an automobile, gears etc [3]. Wear in a system can be caused by six different wear mechanisms: (1) adhesion, (2) abrasion, (3) fatigue, (4) impact by erosion and percussion, (5) tribo-chemical and (6) oxidative type [3,6]. The wear mechanisms followed by the bodies in contact largely depend on the operating conditions and the environment of the system [3].

2.2.3. Lubrication

In cases where wear and friction are not desired in between the two surfaces in contact, a lubricant is used in between the surfaces to lower the amount of wear/friction. Depending on the system requirements, this lubricant can be a liquid or solid [7]. Fluid film lubrication is used in case of low-speed application and greases are used for high-

speed systems. On the other hand, solid lubricants, for example graphite or MoS2, are used for elevated temperature applications or space applications where liquid lubricant fail due to their volatility. While the lubrication of two surfaces in contact is broadly categorized into two categories which are hydrostatic and hydrodynamic lubrication [7]. In the case of hydrostatic lubrication, the two sliding or rolling surfaces are separated by a film of lubricant fluid which is pumped by making use of a pump. Thus, overall, the efficiency of lubrication system is dependent on the performance of pump. This fluid tends to keep the two surfaces separated from each other and reduces friction as a result [7]. While in the case of hydrodynamic lubrication, the motion of one surface is at a high speed as compared with the other surface. This leads to the gathering of the lubricating fluid under the sliding surface and the bodies in contact can be separated which results in reduction in friction. One such example of hydrodynamic friction is water ski sport, in which the ski is at a higher speed than the water below [7].

2.3. Concept of thermal spraying technology

Manufacturing techniques largely influence the mechanical properties and the microstructure of the materials and as a result determine their friction and wear behavior [8-10]. Bulk manufactured modern alloy systems (Ni-based, Ti-based, Al-based, Co-based and High Entropy Alloys) have shown promising wear behavior under extreme conditions. However, producing entire components with these alloys increase the usage of expensive alloys and place a burden on alloying technologies for developing new materials. For example, Ni-based alloys are well known for their wear resistance however, if the aerospace components are manufactured using these alloys, the overall weight and economy will greatly increase. To mitigate these issues, wear resistant coatings can be sprayed over cheaper and lighter metals instead of using expensive bulk alloys. In addition to reduction in costs and weight, coatings have proved to be advantageous in repairing damaged components instead of replacing them completely [11].

Thermal spraying is a widely used modern technology for developing thick wear resistant coatings. Thermal spraying is termed as a technique in which the feedstock is in the form of powder particles. These powder particles are sprayed over a metallic substrate in either molten or unmelted state depending on the process parameters. These particles are impinged over the substrate at high velocities (50 to

>1000 m/s) and form solid splats that agglomerate and form a thick coating (>100 μm) [12,13]. Thermal spray operates at a wide range of deposition temperatures lying between 200 K to 2500 K [10]. Plasma spray, flame spray, high velocity oxygen fuel and detonation gun are some of the commonly used high temperature deposition processes. These techniques are useful for developing hard wear resistant coatings due to the oxide inclusions at elevated temperatures [10]. However, in some applications, oxide contamination is undesirable. In addition, the rapid solidification of molten splats leads to increased porosity due to which low temperature deposition techniques such as cold spraying are preferred [14].

This thesis compares the tribological behavior of cold sprayed, flame sprayed and HVOF sprayed coatings. Thus, these technologies have been discussed briefly in the following sub-sections.

2.3.1. Cold Spray

Cold spray or cold gas-dynamic spray is a relatively newer technology used to produce thick metallic or ceramic coatings over a metallic or mixed metal composite substrates [15]. Being a low temperature deposition process, the operating temperatures lie between 0^{O}C to 1000^{O}C. In order to increase the adhesion of powder particles over the substrate, the particles are accelerated and sprayed at very high velocities ranging between 300 m/s to 1200 m/s and the particle size ranges between 1 to 50 μm in diameter [12]. Many researchers studied the microstructures of high entropy alloys (AlCoCrFeNi, CoCrFeMnNi, CrFeMnNi, and AlCoCrFeNiTi) developed by cold spray and found that the phases were fine and homogenous with negligible presence of oxide phases and very less porosity (< 1%) [16-19]. Figure 2.3 shows a schematic of a typical cold spray technology [12]. Pressurized gas (typically Nitrogen) is first brough to the gas control module with the help of high- or low-pressure compressor and then heated with the help of an electric or a combustion type heater. The heating of the gas helps in improving the particle impact velocities and benefits the quality of coatings. This heated high-pressure gas is passed through a De Laval (convergent-divergent) nozzle and the flow changes to supersonic velocities at the exit. The feedstock powder is fed through a powder feeder and brought in the gaspath with the help of precision robotic

equipment. The accelerated gas bombards the feedstock powder over the substrate and eventually forms layers of thick coating.

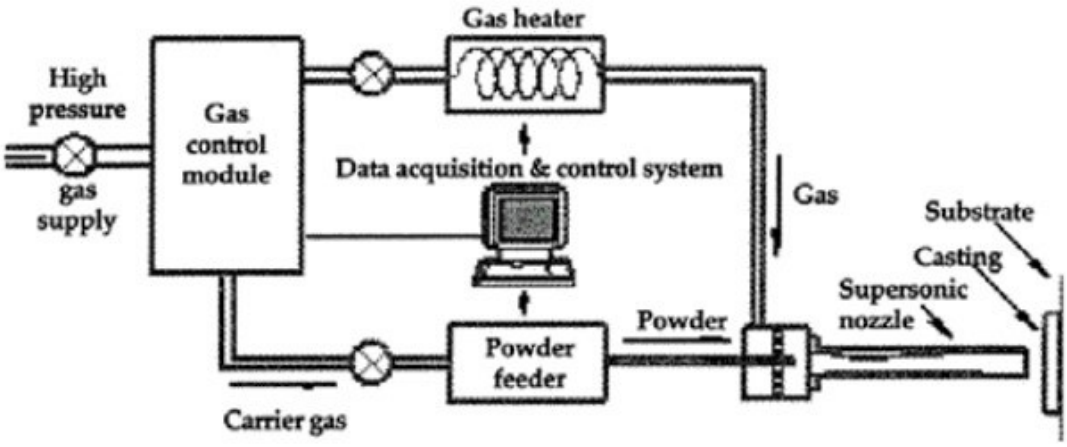

Figure 2.3 Schematic of cold spray technology [12].

2.3.2. Flame Spray

Flame spraying is one of the highest temperature deposition processes with the values as high as 2600^{O}C [12]. The elevated temperatures lead to formation of oxide phases which raises the hardness of the coating resulting in improved wear performance as compared to cold sprayed coatings [20]. Traditional flame spraying technology was one of the initial methods of coating deposition. The particle velocities are relatively low in the range of 80 m/s to 100 m/s and the powder particles are impinged over the substrate in molten state which then solidify rapidly leading to increased porosity [12,14]. Figure 2.4 illustrates the schematic of a flame spraying equipment [12]. In this figure, it can be seen that feedstock powder is carried through the feeder to the nozzle with the help of a carrier gas (usually Air or Nitrogen). Acetylene in presence of Oxygen is used as fuel for combustion and generate high temperatures that are able to melt the powder particles. Feed power is introduced axially into the path of these combustion gases and is melted for increased adhesion over the substrate. The molten particles are accelerated towards the substrate due to high velocities generated as a result of combustion of fuel exiting the nozzle in the form of a flame torch. The concentrations of oxygen can be reduced (fuel-rich) to minimize the oxide contaminations formed in the coatings. Flame spraying is a very primitive technology with a very basic set of required equipment and hence is highly cost effective.

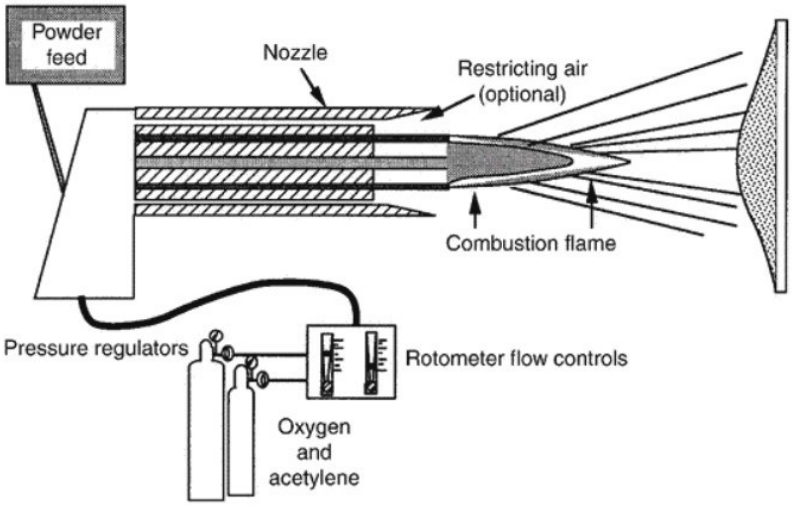

Figure 2.4 Schematic of flame spray technology [12].

2.3.3. High Velocity Oxy-Fuel (HVOF)

Like flame spraying, HVOF is also a high temperature deposition technique with temperatures ranging between 2200^{O}C to 3000^{O}C with particle velocity between 500 m/s to 2000 m/s [21]. High particle velocities favor the formation of coatings with less porosity similar to cold sprayed coatings, but higher deposition temperatures give rise to oxide phases which are similar to flame sprayed coatings. Few researchers studied flame sprayed of AlCoCrFeNi, AlCoCrMoNi and AlTiCrFeCoNi coatings deposited using HVOF [22-25]. It was observed that the porosity levels were as low as 3% and the overall hardness of the coatings were much more than that obtained using cold spray. Figure 2.5 shows the schematic diagram of HVOF technology [26]. It can be seen that HVOF is a specialized type of flame spray where the exit velocities of the nozzle are supersonic. The fuel used is usually gas or kerosene which is fed to the combustion chamber and ignited. The combustion gases are passed through a water-cooled nozzle where they expand and reach high velocities. The carrier gas is usually oxygen and air by which the powder feed particles are fed into the flame and bombarded over the substrate at high particle velocities. The high kinetic energy associated with supersonic flow of gases tends to produce thick and dense coatings even though some of the particles might be unmelted due to high impact forces. In some application the oxyacetylene fuel is used or simply air is used for combustion. This special variant of

HVOF, where air is the main combustion fuel, is widely known as High Velocity Air Fuel (HVAF) spraying.

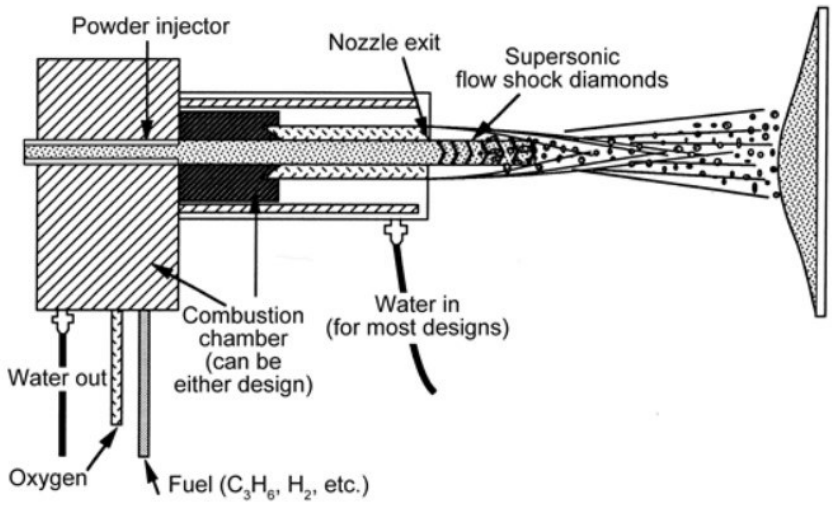

Figure 2.5 Schematic of HVOF spray technology [26].

References:

1. O. Reynolds, IV. On the theory of lubrication and its application to Mr. Beauchamp tower's experiments, including an experimental determination of the viscosity of olive oil, Philosophical transactions of the Royal Society of London, (177), 157-234 (1886)
2. A.W.B. Gwidon W. Stachowiak, Engineering Tribology, Elsevier, (2013)
3. B. Bhushan, Introduction to tribology, Wiley, 2013
4. W.E. Jamison, Introduction to tribology, Journal of Vacuum Science & Technology, 76-81 (1976)
5. B. Bhushan, Friction, Tribology and Mechanics of Magnetic Storage Devicesed., Springer, 1996, p 231-365
6. K. Razavizadeh, T.S. Eyre, Oxidative wear of aluminium alloys, Wear, 79(3), 325-333 (1982)
7. K.C. Ludema, Friction ,Wear, Lubrication: A textbook in tribology, CRC Press, 1996
8. P. Hariharasakthisudhan, B.S. Rajan, K. Sathickbasha, Inspiration of reinforcements, manufacturing methods, and microstructural changes on wear behavior of metal matrix composites—a recent review, Materials Research Express, 7(1), 012006 (2020)
9. W. Kuang, Q. Miao, W. Ding, H. Li, A short review on the influence of mechanical machining on tribological and wear behavior of components, The International Journal of Advanced Manufacturing Technology, 1-13 (2022)
10. A. Meghwal, A. Anupam, B.S. Murty, C.C. Berndt, R.S. Kottada, A.S.M. Ang, Thermal Spray High-Entropy Alloy Coatings: A Review, Journal of Thermal Spray Technology, 29(5), 857-893 (2020)
11. S. Pathak, G.C. Saha, Development of sustainable cold spray coatings and 3D additive manufacturing components for repair/manufacturing applications: A critical review, Coatings, 7(8), 122 (2017)
12. J.R. Davis, Associates, A.S.M.I.T.S.S.T. Committee, Handbook of thermal spray technology, ed., ASM International, 2004
13. S. Chandra, P. Fauchais, Formation of Solid Splats During Thermal Spray Deposition,

Journal of Thermal Spray Technology, 18(2), 148-180 (2009)

14. R.B. Nair, G. Perumal, A. McDonald, Effect of Microstructure on Wear and Corrosion Performance of Thermally Sprayed AlCoCrFeMo High-Entropy Alloy Coatings, Advanced Engineering Materials, 2101713 (2022)

15. S. Grigoriev, A. Okunkova, A. Sova, P. Bertrand, I. Smurov, Cold spraying: From process fundamentals towards advanced applications, Surface & Coatings Technology, 268, 77-84 (2015)

16. S. Yin, W. Li, B. Song, X. Yan, M. Kuang, Y. Xu, K. Wen, R. Lupoi, Deposition of FeCoNiCrMn high entropy alloy (HEA) coating via cold spraying, Journal of Materials Science & Technology, 35(6), 1003-1007 (2019)

17. A. Yurkova, D. Hushchyk, A. Minitsky, Synthesis of High-Entropy AlNiCoFeCrTi Coating by Cold Spraying, Powder Metall. Met. Ceram., 59(11), 681-694 (2021)

18. J. Lehtonen, H. Koivuluoto, Y. Ge, A. Juselius, S.-P. Hannula, Cold gas spraying of a high-entropy CrFeNiMn equiatomic alloy, Coatings, 10(1), 53 (2020)

19. A. Anupam, S. Kumar, N.M. Chavan, B.S. Murty, R.S. Kottada, First report on cold sprayed AlCoCrFeNi high-entropy alloy and its isothermal oxidation, J. Mater. Res., 34(5), 796-806 (2019)

20. P. Patel, A. Roy, N. Sharifi, P. Stoyanov, R.R. Chromik, C. Moreau, Tribological Performance of High-Entropy Coatings (HECs): A Review, Materials (Basel, Switzerland), 15(10), (2022)

21. N. Espallargas, Future development of thermal spray coatings : types, designs, manufacture and applications, ed., Woodhead Publishing is an imprint of Elsevier, 2015

22. T. Li, Y. Liu, B. Liu, W. Guo, L. Xu, Microstructure and Wear Behavior of FeCoCrNiMo0.2 High Entropy Coatings Prepared by Air Plasma Spray and the High Velocity Oxy-Fuel Spray Processes, Coatings, 7(9), (2017)

23. M. Löbel, T. Lindner, T. Mehner, T. Lampke, Microstructure and wear resistance of AlCoCrFeNiTi high-entropy alloy coatings produced by HVOF, Coatings, 7(9), 144 (2017)

24. M. Löbel, T. Lindner, T. Mehner, L.-M. Rymer, T. Lampke, S. Björklund, S. Joshi,

Microstructure and Corrosion Properties of AlCoCrFeNi High-Entropy Alloy Coatings Prepared by HVAF and HVOF, Thermal Spray 2021: Proceedings from the International Thermal Spray Conference (ITSC), H.J. O. Ozdemir, F. Toma, Ed., May 24-28, 2021 (Quebec City, Canada), ASM International, pp 416-421

25. W.-B. Liao, Z.-X. Wu, W. Lu, M. He, T. Wang, Z. Guo, J. Huang, Microstructures and mechanical properties of CoCrFeNiMn high-entropy alloy coatings by detonation spraying, Intermetallics., 132, 107138 (2021)

26. R.C. Tucker, A.S.M.I.T.S. Society, ASM handbook. Volume 5A, Thermal spray technology, ed., ASM International, 2013

Chapter

3. HIGH ENTROPY ALLOY COATINGS DEPOSITED BY THERMAL SPRAYING TECHNOLOGIES: A REVIEW OF STRENGTHENING MECHANISMS, PERFORMANCE ASSESMENTS AND PERSPECTIVES ON FUTURE APPLICATIONS

In this chapter…

A detailed literature review on thermally sprayed high entropy alloys has been presented.

3.1. Abstract

Thermal spray deposition techniques have been well established owing to their flexibility in addressing degradation due to wear and corrosion issues faced due to extreme environmental conditions. With the adoption of these techniques, a broad spectrum of industries is experiencing continuous improvement in resolving these issues. To increase industrial level implementation, state-of-the-art advanced materials are required. High entropy alloys (HEAs) have recently gained considerable attention within the scientific community as advanced materials, mainly due to their exceptional properties and desirable microstructural features. Unlike traditional material systems, high entropy alloys are composed of multi-component elements (at least five elements) with equimolar or nearly equimolar concentrations. This allows for a stable microstructure that is associated with high configurational entropy. While most of the research on HEAs has primarily been focused on high-temperature deposition methods, there is continuous interest in identifying research gaps in the development and study of high entropy alloys fabricated using semi- and solid-state deposition techniques.

This review article provides a critical assessment observed in various high entropy alloys developed by means of thermal deposition techniques and their strengthening mechanisms. The wear, corrosion, and oxidation responses of these alloys are reviewed in detail and correlated to microstructural and mechanical properties and behavior. In addition, the review undertakes a comparative evaluation of HEAs and conventionally utilized materials, with a strong focus on material design principles for developing next-generation HEAs that can significantly benefit the aerospace, marine, energy, oil and gas, and mining sectors. Despite having shown exceptional mechanical properties, the article describes the need to further evaluate the tribological behavior of these HEAs in order to show proof-of-concept perspectives for several industrial applications in extreme environments.

Keywords: Aerospace materials, High entropy alloys, microstructure, phase formations, strengthening mechanisms, Tribology

3.2. Introduction

3.2.1. Introduction to high entropy alloys

Traditional alloy design strategies generally consist of combining one or two principal elements with few minor elements in order to achieve the desired microstructural features and mechanical properties. However, these strategies restrict the plausible number of combinations for developing advanced alloys since most of the dominant elements would be either iron, aluminum, or nickel. A paradigm shift in the alloy design concept occurred in 2004, when Cantor et al. [1] and Yeh et al. [2] developed advanced metallic alloys by mixing multiple elements, without differentiating solvent and solute atoms. Cantor et al. [1] reported this design concept as "multi-component alloy systems", whereas the term "high entropy alloys (HEAs)" was derived from the pioneering work of Yeh et al. [2]. Since then, the term HEAs has become popular among the scientific communities, and researchers had put significant efforts in investigating the microstructural features and phase formations that formed for different HEAs, as well as their impact on different industrial applications, including wear and corrosion. Studies have shown that the HEAs possess unique microstructural characteristics that result in the stabilization of solid solution structure with adjustable properties depending upon the chemical compositions used.

High entropy alloys are defined based on chemical compositions – containing five or more principal elements with equimolar concentrations or close to equimolar concentrations unlike the traditional alloy design strategies [1,2]. The concentrations of major elements ranges between 5 at% and 35 at%, with the possibility of adding minor elements less than 5 at% [3]. It has been reported that the HEAs possess inherently high configurational entropy (>1.5*R*, where *R* is the ideal gas constant) compared to traditional alloys (<1.0*R*) (Figure 3.1). In their book of "High Entropy Alloys", Murty *et al* [156] have mentioned that the configurational entropy ($\Delta S_{conf} = -R\ (X_A \ln X_A + X_B \ln X_B)$) of a binary alloy is maximum when the elements are in equiatomic proportion and this configurational entropy increases with increasing number (N) of elements ($\Delta S_{conf,\ max} = R \ln N$). More information on calculating the configurational entropy of high entropy alloys can be found in this book [156]. Thus, a new definition for HEAs arose based on high configurational entropy per mole, where the alloy should exhibit a configurational entropy greater than 1.5*R*. If the configurational entropy values are less than 1.5*R*, the alloys are classified as medium entropy systems (see Figure 3.1). However, it has been argued that the high configurational entropy effect bestows the

single-phase solid solution structure (disordered or partially ordered) for HEAs, either in the form of face-centered cubic (FCC), body-centered cubic (BCC), or the combination. The contribution of enthalpy of mixing and the high configurational entropy is key in reducing the Gibbs free energy of the system for obtaining the single-phase structure. Debates on the formation of intermetallic compounds (i.e., B2, σ phases) in HEAs are still going on. However, the combination of disordered and ordered structure may significantly play a crucial role in desirable properties based on the selection of compositions. HEAs also go by the names such as complex concentrated alloys [4], compositionally complex alloys [4], multi-component alloys [1], and baseless alloys [5].

Low Entropy Alloy	Medium Entropy Alloy	High Entropy Alloy
$\Delta S_{Conf} \leq 1.0R$	$1.0R \leq \Delta S_{Conf} \leq 1.5R$	$\Delta S_{Conf} \geq 1.5R$
One or two dominant elements. Formation of solid solution and/or compounds	Two to four dominant elements	Five or more dominant elements. Single phase solid solution phase formations (FCC/BCC or both)

Figure 3.1 Differences between low, medium and high entropy alloys [1].

Owing to the compositionally complex structures, HEAs possess superior strength, excellent fracture toughness, fatigue strength, high-temperature oxidation and corrosion resistance, as well as improved wear resistance [3,6-8]. While earlier studies focused mainly on understanding the mechanical behavior of arc-melted HEAs, the advancement of HEA coatings by means of thermal spray techniques has recently gained more attention. Indeed, with the advent of these advanced materials, there is a demand for the development of time-efficient, reliable and environmentally friendly deposition techniques that benefits the HEAs in controlling degradation-related problems. As shown in Figure 3.2, the demand for HEAs by means of thermal spraying technologies has been increasing in accordance with the number of research publications per year since 2016. Thermal spraying technologies are well-established in many industrial sectors for developing thick coatings due to their ability to deposit wide range of feedstocks to protect industrial components against extreme environments caused by wear, corrosion, and oxidation [9-11].

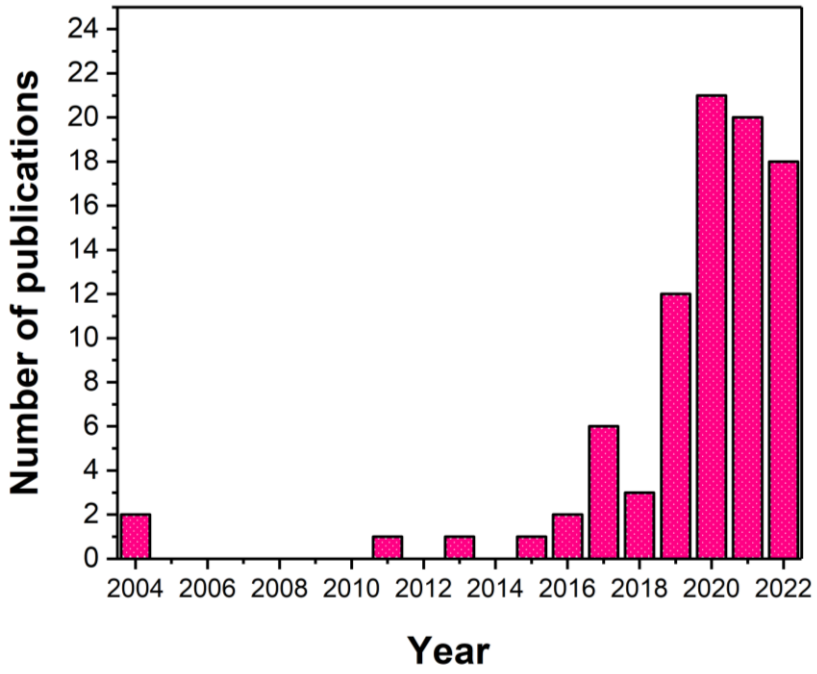

Figure 3.2 The number of publications of thermal spray high entropy alloy coatings per year until March 2022.

With the increasing demand for HEA materials and coatings, the synthesis of feedstock needs to be optimized since it plays a vital role in producing coatings with negligible microstructural inhomogeneities. This will pave the way for desirable mechanical properties, such as strength, hardness, and toughness, which in turn, provide better industrial sustainability. Nevertheless, the quality and characteristics of the feedstock powders are determined by the fabrication routes, which includes particle size and morphology, homogeneity, powder yield, and flowability [12,13]. The capability of HEAs to be developed as a coating has increased the scope for various industrial applications due to the reduced amount of feedstock consumptions and the ability to deposit on intricate components compared to bulk alloy counterparts. Despite the versatility of using these techniques, studies related to thermal-sprayed HEA coatings are limited and not fully understood. Therefore, this review article provides a critical assessment on the microstructural and strengthening mechanisms. The wear, corrosion and oxidation responses of various HEAs are reviewed and discussed in detail. In addition, the feasibility of next generation high entropy alloys is reported, emphasizing on the development of high-performance coating materials and their potential benefits for sustainable industrial futures.

3.2.2. Preparation of HEA Feedstock

Many researchers have been devoted to fabricating HEA feedstocks for the thermal spraying by means of mechanical blending, mechanical alloying, gas atomization, mechanical milling of as-casted HEAs, and more recently radio frequency inductively coupled plasma (RF-ICP) [14-19]. Mechanical blending involves mixing of each elemental powder without any bonding formation, and the features of powder particles remain unchanged [14,15]. Lobel *et al.* [14] investigated the impact of three feedstocks prepared by mechanical blending, mechanical alloying and gas atomization of AlCoCrFeNiTi HEAs and deposited on S235 steel substrates via the atmospheric plasma spray system. Figure 3.3 shows the microstructure for all three HEA coatings prepared by different feedstock routes. Among these HEA coatings, the gas-atomized showed homogeneous microstructure with lower defects compared to that of mechanically blended and mechanically-alloyed powder based coatings. The authors also reported that the hardness showed a significant difference in the values for the coatings prepared by three different feedstocks. The highest average hardness (Vickers micro-hardness test) was found for the gas atomized powder deposited coatings with around 5.8 GPa, followed by mechanical alloyed and mechanical blended deposited coatings of approximately 4.6 GPa and 3.4 GPa, respectively. This was most probably related to the formation of a homogeneous microstructure for the gas atomized powder deposited coatings (see Figure 3.3). The mechanical blended powders showcase the presence of titanium and nickel contents along with BCC and FCC phases, highlighting inappropriate formation of alloy microstructure compared to the coatings deposited with gas atomized powders. This implies that mechanical blending may not the most appealing approach for preparation of HEA feedstocks for thermal spray technologies.

Mechanical alloying and gas atomization are the most widely used synthesis routes due to their homogenous nature in forming an alloy [12,20]. Due to the exceptional flowability and homogeneity in microstructural formations, the gas atomization method is a feasible method for synthesizing the HEA feedstocks. Mechanical alloying, on the other hand, provide superior elemental distribution and may form solid solution structure due to melting and solidification; however, the flowability might be challenging due to their irregular morphologies and varying particle distributions compared to that of gas atomized counterpart.

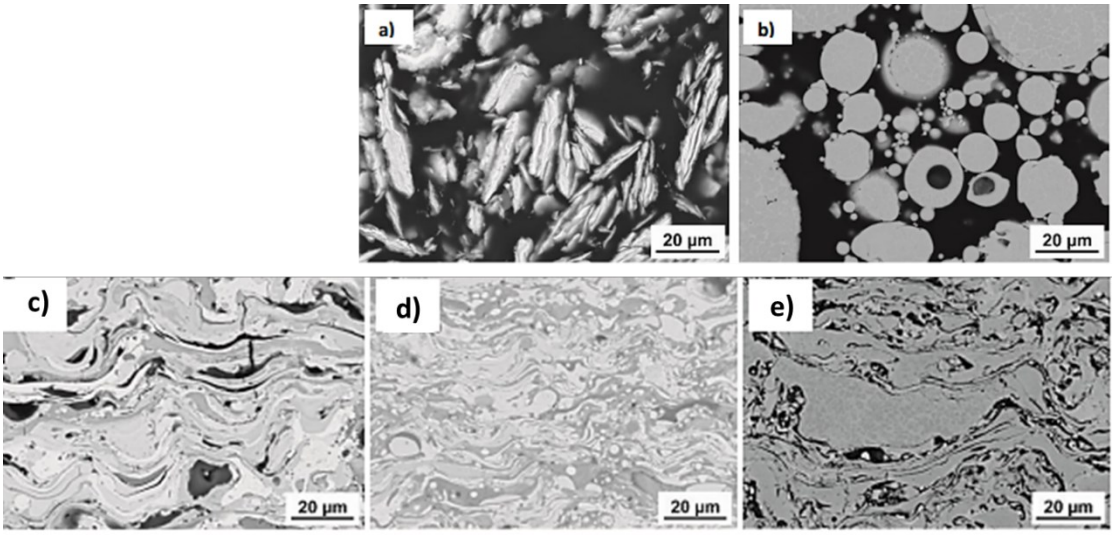

Figure 3.3 Scanning electron microscope images of (a) mechanically-alloyed and (b) gas-atomized feedstocks of AlCoCrFeNiTi powders. Coating microstructure of the AlCoCrFeNiTi HEA coatings for (c) mechanically blended, (d) mechanically-alloyed and (e) gas atomized feedstock powders. The different microstructural features with respect to different feedstock powders are clearly visible in the figure, with the gas atomized powder coatings showing homogeneity compared to the other two coatings [14].

A new powder metallurgical technique has been introduced by Zhu *et al*. [21] to synthesize HEA powders rapidly by means of a plasma source provided by radio frequency inductively coupled plasma (RF-ICP). As shown in Figure 3.4, RF current, which is passed through a load coil wound around a dielectric tube (i.e., ICP torch) provides an intense electromagnetic (E.M.) field inside the torch leading to ionization of the working gas [21]. The mixed powders are placed on a water-cooled copper crucible which is able to tolerate the high temperatures of RF-ICP during the process (Figure 3.4). The ignited RF-ICP will rapidly heat the powder bed and build up a high-temperature environment for HEA synthesis. Generally, the speed of material preparation in an alloy synthesis method is a critical factor. The process temperature provided by ICP can reach up to 5000 – 8000 K [21], which is significantly higher than 3000 K for arc-melting [22] and 4500 K for laser-melting [23]. Therefore, the efficiency of alloy synthesis by RF-ICP is higher. At the end of the process, the plasma is turned off while the argon gas will keeps running to rapidly cool the sample while protecting it from the air [21]. As shown in Figure 3.5, the total time is within 40 s for the fabrication of HEA, which is followed by fast cooling the sample by argon for ~15 s. This method features a high fabrication temperature ensuring homogenous mixing, high heating and cooling rate (~10^5 K/s), high fabrication speed preventing the material from

volatile evaporation, reduction of the non-uniform distribution of microstructures caused by uneven diffusion due to high heating rate, eco-friendly heat source without the emission of harmful gases or secondary products to the environment, elimination of the unstable impurities improved controllability of the process in comparison with the free burning arc due to the absence of arc instability, minimization of the contamination of the synthesized samples from electrode erosion due to electrodeless design of the RF-ICP, formation of a natural shroud gas around the sample by the plasma jet minimizing the entrainment of the surrounding air, and use of any kind of precursor in different physical forms or chemical compositions [21].

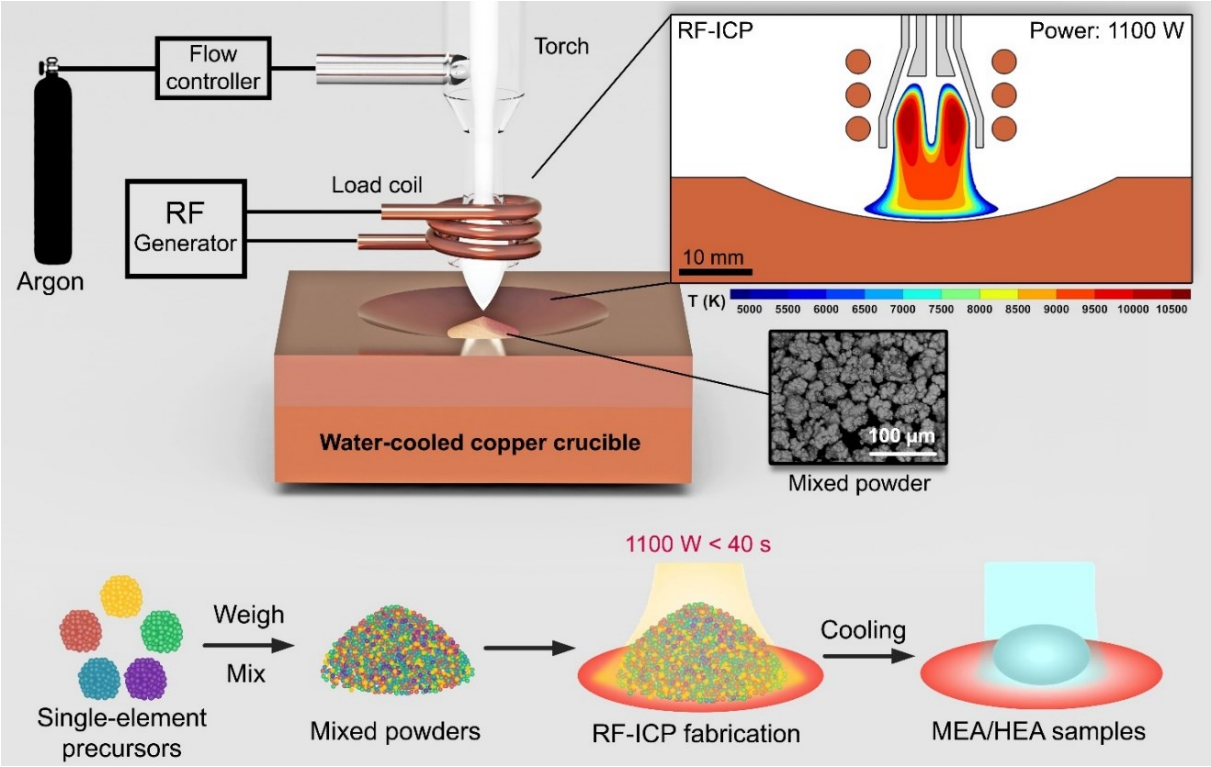

Figure 3.4 Setup of HEA synthesis with RF-ICP. Well-mixed powder bed is directly synthesized by RF-ICP under 1100 W with 5000 – 8000 K and becomes HEAs within 40s [21].

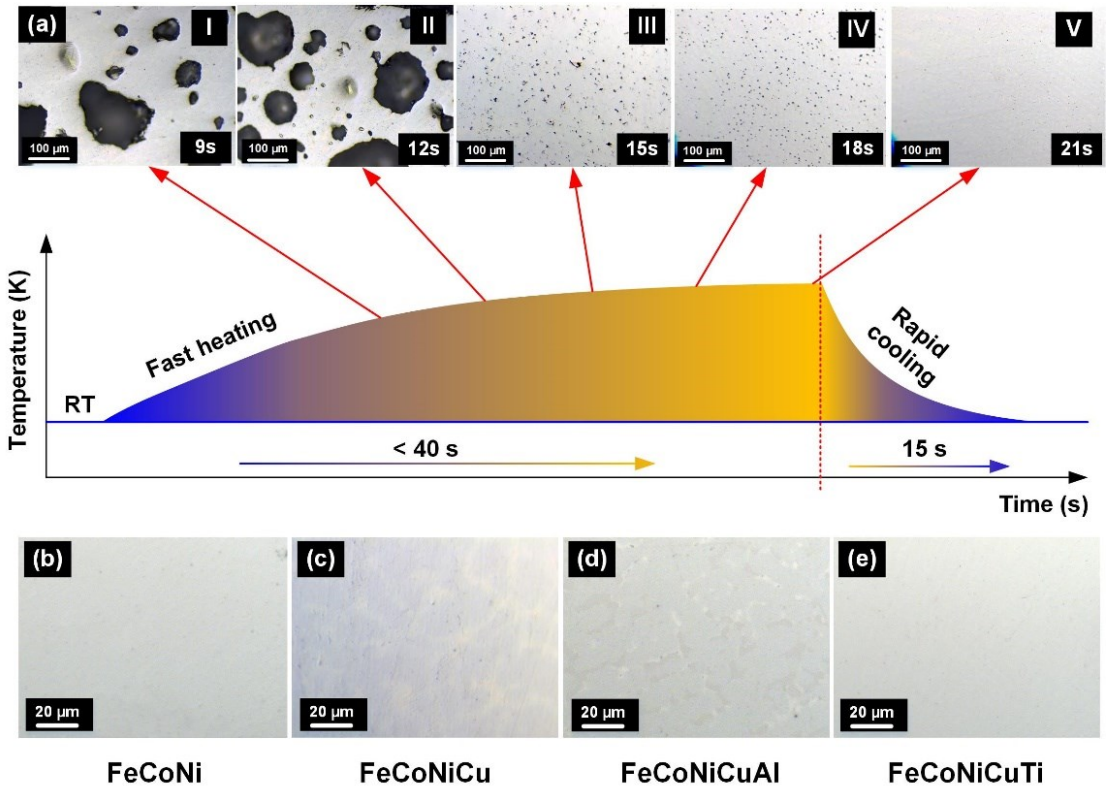

Figure 3.5 Rapid synthesis of alloys. (a) The temperature profile of CuNi alloy using the RF-ICP synthesis. The OM images demonstrate the evolution of porosity of CuNi alloy during HEA synthesis process. (b)-(e) OM images of synthesized FeCoNi MEA, FeCoNiCu MEA, FeCoNiCuAl HEA and FeCoNiCuTi HEA [21].

3.3. Microstructure and strengthening mechanisms of HEA coatings

3.3.1. Microstructure

Thermal-sprayed deposits usually contain defects, such as porosities, un-melted or partially melted particles, some level of oxidates forming in the whole stages of the spray process [24-27]. A schematic diagram and scanning electron microscope (SEM) images in Figure 3.6 show different types of defects. The density of these defects highly depends on the specific spray process used, the operating parameters chosen, and the feedstock sprayed. Several studies have indicated that investigating the relationships between defect formation and processing are vital for the improvement of as-sprayed coating properties [25,28-30]. All the HEA coatings developed through thermal spraying and their phase formations have been illustrate in Table 3.1.

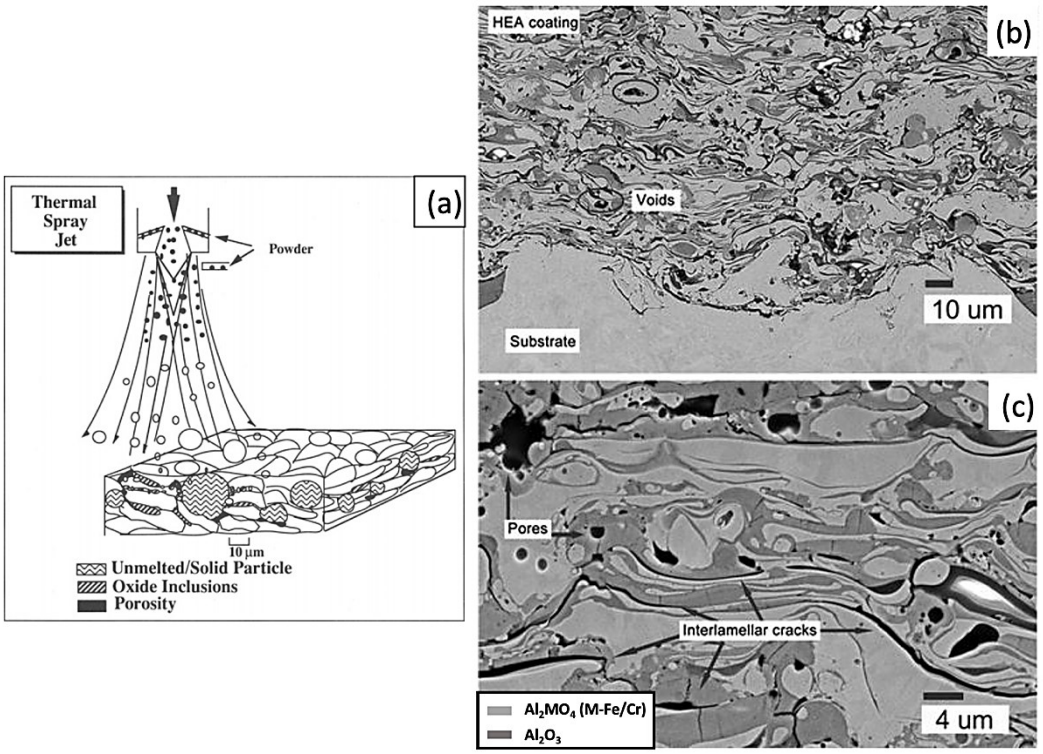

Figure 3.6 (a) A schematic diagram of defects generated in a thermal spray process [27]. SEM images of plasma-sprayed (b) AlCoCrFeNi and (c) MnCoCrFeNi showing the formation of oxides, pores and interlamellar cracks [24].

Table 3.1 Different high entropy alloy compositions and their phase formations and porosity levels according to deposition techniques.

High entropy alloy coatings	Feedstock routes	Substrates	Deposition routes	Phases	Porosity (%)	Ref.
AlCoCrFeNi	MA	Mild steel	APS	BCC + FCC + oxides	9.5±2.3	[24]
	Gas atomized	AISI 1045 steel	APS	BCC and B2	-	[58]
	Gas atomized		APS	BCC and FCC	-	[17]
	MA	Mild steel	HVOF	B2	-	[63]
	MA	Mild steel	HVAF	B2	-	[63]
	Water atomized	06Cr13Ni5Mo martensitic stainless steel	HVOF	FCC and BCC	-	[64]

	MA	SS 316L	APS	Al-rich oxides + AlCrFe oxides + Al-depleted regions	-	[70]
	MA	Low carbon steel	APS	BCC + FCC + oxides	-	[59]
$Al_{0.5}CoCrFeNi_2$	Gas atomized	SS 304	APS	FCC	-	[71]
AlCoCrFeNiTi	MA	SS 316	APS	BCC and oxides	-	[20]
	MA	S235 steel	APS	BCC and FCC	-	[14]
	Gas atomized	S235 steel	APS	BCC and FCC	-	[14]
	Gas atomized	S235 steel	HVOF	BCC + B2 + A12	-	[80]
$Al_{0.6}CoCrFeNiTi$		A572 steel	HVOF	BCC	-	[81]
MnCoCrFeNi	MA	Mild steel	APS	BCC + FCC + oxides	7.4±1.3	[24]
MnCoCrFeNi	Gas atomized	SS 304	APS	FCC	-	[152]
	Gas atomized	SS 316L	Detonation	FCC and oxides3	-	[65]
$FeCoCrNiMo_{0.2}$	Gas atomized	Low carbon steel	APS	FCC and oxides	-	[72]
	Gas atomized	Low carbon steel	HVOF	FCC and oxides	-	[72]
WC-10Co /AlCoCFeNi	Water atomized	06Cr13Ni5Mo martensitic stainless steel	HVOF	FCC + BCC	-	[65]
Ni60/AlCoCrFeNiTi	MA _+ gas atomized	SS 316	APS	BCC and oxides	-	[15]
Ag/ $Al_{0.2}CrCo_{1.5}FeNi_{1.5}Ti$	Mechanically blended	Carbon steel	APS	BCC + B2 + FCC + Cr Carbides	-	[71]
Al_20_3-13 wt.% TiO_2 /MnCoCrFeNi	Gas atomized	Mild steel	APS	FCC and oxides	-	[76]

Nano oxides/MoCrCoFeNi	Gas atomized	-	APS	BCC + FCC + oxides	-	[16]
AlCoCrFeNiSi	MA	SS 316	APS	B2 and BCC	-	[60]
AlCoCrFeNi	MA	Ni-base super alloy	CS	BCC	7	[16]
MnCoCrFeNi	Gas atomized	Al 6082 alloy	CS	FCC	-	[41]
AlCoCrFeNiTi	MA	Steel	CS	B2 + TiC+σ	0.5±0.18	[50]
MnCrFeNi	Gas atomized	Fe52 steel	CS	BCC	-	[40]
MnCrFeNi	Gas atomized	Fe52 steel	CS	BCC	-	[40]
$Ni_{0.2}C_{0.6}Fe_{0.2}CrSi_{0.2}AlTi_{0.2}$	Gas atomized	SS 304	APS	BCC and Cr_3Si	-	[153]
$NiC_{0.6}Fe_{0.2}CrSiAlTi_{0.2}$	Gas atomized	SS 304	APS	BCC and Cr_3Si	-	[153]
$Ni_{0.2}C_{0.6}Fe_{0.2}Cr_{1.5}SiAlTi_{0.2}$	Gas atomized	SS 304	APS	BCC and Cr_3Si	-	[153]
CrMnFeCo	-	-	APS	FCC	2.9	[45]
MnCoCrFeNi	-	-	CS	FCC	0.47±0.17	[41]
$NiCo_{0.6}Fe_{0.2}Cr_{1.5}SiAlTi_{0.2}$	Arc melting + mechanical milling	-	APS	BCC	1-5	[47]
$Al_{0.6}TiCrFeCoNi$	Gas atomized	-	HVOF	BCC	1.68	[48]
AlCoCrMoNi	Mechanical alloying	-	HVOF	BCC	1.03	[154]
$FeCoCrNiMo_{0.2}$	Gas atomized	-	HVOF	FCC + AB_2O_4	0.6	[155]
	Gas atomized	-	APS	FCC + AB_2O_4	3.1	[155]
$Ni_{0.2}Co_{0.6}Fe_{0.2}CrSi_{0.2}AlTi_{0.2}$	Arc melting + mechanical milling		HVOF	BCC	2.8±0.5	[33]
			APS	BCC	4.3±0.5	[33]

The main defect of thermal sprayed HEA coatings is oxidation. The existence of oxides breaks the chemical uniformity of coatings. Compared to the relatively soft HEA matrix, randomly distributed oxides are rigid. It has been reported that oxides play an important role in tribological applications [25,31-33]. In addition to increasing the hardness of HEA specimens, in certain conditions, oxides can act as self-lubricating materials. However, in some cases, oxides with high porosity deteriorates the corrosion resistance, which can result in premature failure of the component [32,34,35].

Oxide formation takes place at different stages during spray process [31]. The content of oxides highly relies on thermal sprayed processing. For atmospheric plasma spray (APS), where particle temperatures may reach up to 2500 K [36,37], the oxygen will react with fully molten or semi-molten powders before and after impact on a substrate. Oxide precipitates can be a major issue, when HEAs have oxygen-sensitive constituents, such as aluminum (Al), titanium (Ti), chromium (Cr), and molybdenum (Mo) [20,38,39]. On the contrary, minimal oxidation was observed for the coatings deposited using cold spraying. The temperature used for this process is far below their melting points, which in turn results in lower oxidation [16,40,41]. More recently, a significant amount of effort has been put forward to reduce the content of oxidates for APS [42-44]. By introducing a vacuum chamber in APS, the oxide inclusions will be efficiently reduced. However, apart from the limited workpieces, the cost of such installation is high. Instead, adding a coaxial shrouding gas is an efficient method to minimize oxidation.

HEA coatings developed via thermal spraying feature varying levels of porosity. The fraction of the porosity ranges from less than one percent to over ten percent. It is reported that the amount, size, and even the location of pores can strongly affect the mechanical properties (e.g., hardness, elastic modulus, wear behavior) and physical properties (e.g., thermal conductivity) of HEA coatings [25,27,45-51]. Table 3.1 lists porosity data as a function of thermal spray processes. It can be seen that the HEA coatings prepared via APS possess higher porosity compared to that of the HEA coatings developed via high-velocity oxygen fuel (HVOF) and cold spraying, respectively. In addition to that, varied particle distribution sizes of mechanically-alloyed powder particles may induce microstructural defects with high amount of porosity and cracks, which also depend on the exposed zones of powder particles in the

plasma stream as reported by Anupam *et al.* [38]. The particles travelling around the periphery of the plasma stream are not exposed to high temperatures completely, leading to partially melted regions or scattered fragments of oxides, which in turn, affects the homogeneity of the coatings and leads to undesirable properties.

A unique characteristic of thermal spray processes is the extremely high heating and cooling rates (>10^6 K/s) [27]. Such rapid cooling rates result in fine-grain structures. Meanwhile, large numbers of solute atoms are also beneficial to limit grain growth in HEAs. Coatings with fine-grain structures often possess a good combination of strength and ductility. Another advantage of a high cooling rate is preventing elemental segregation. Therefore, as-sprayed HEA coatings may possess different phases constitution compared with their as-cast counterparts [17,24,52,53]. For example, both $AlSiTiCrFeCoNiMo_{0.5}$ and $AlSiTiCrFeNiMo_{0.5}$ fabricated via thermal spray manifest a supersaturated BCC phase due to rapid solidification. For as-cast counterparts, they are dual-phase alloys (BCC+FCC) [52]. The phase components of HEAs are affected by the feedstock synthesis techniques and thermal spray methods. Mechanical alloying allows powders mix in nanoscale with enhanced solid solubility, which favors the formation of solid solution phases before thermal processing [54]. Those post-alloyed powders melted or partially melted in APS and HVOF will further undergo phase transformation. On the contrary, for cold spraying, due to relatively lower processing temperatures, materials will maintain their feedstock compositions. Taking Al-Co-Cr-Fe-Ni alloying system as an example, it was observed that the BCC phase dominates after mechanical alloying because aluminum acts as a BCC stabilizer [16]. This phase composition was retained in cold spray HEAs [16]. For plasma sprayed AlCoCrFeNi coatings, the FCC phase was observed as being the major phase [24]. However, this can be affected by the particle size, argon flow rate, and the spraying current. Coarse powders with an increment of argon flow rate favor the formation of the FCC phase [17].

The microstructure and phase constitutions can generally be adjusted by post-processing treatments. As-sprayed coatings, especially for those forming under high processing temperatures, have a high density of pores. Post-processing treatments have a strong influence on eliminating the pores. Yue *et al*. [55] proved that a dense surface with only very few isolated small pores can be found in the laser-remelted layer (shown in Figure 3.7a). Besides, the growth of columnar dendrites was observed as the result

of laser remelting (shown in Figure 3.7b). As mentioned above, rapid cooling rates allow HEA coatings to possess a precipitate-free microstructure. Annealing and/or laser remelting often promote the formation of precipitates [33,47,48,56]. The size and distribution of precipitates can be changed by tuning process parameters. Those precipitates as hard phases may increase the strength and hardness of HEAs and can be a good candidate in tribological applications. Wang *et al*. [56] applied a transmission electron microscope (TEM) on thermal sprayed $NiCo_{0.6}Fe_{0.2}CrSiAlTi_{0.2}$ HEA coatings. After heat treatment, nano-precipitates are randomly distributed on the matrix (shown in Figure 8a), which results in a higher hardness (935 HV) compared to its as-sprayed counterpart (450 HV). A high density of dislocations was observed after heating, and semi-coherent interfaces were formed, which is energetically favorable (shown in Figure 8b).

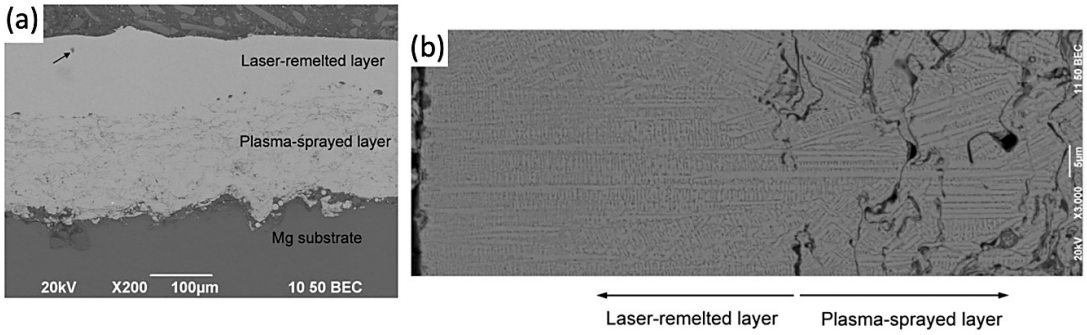

Figure 3.7 (a) A cross-sectional SEM image of AlCoCrCuFeNi coated on a Mg substrate showing the as-sprayed layer and a laser-remelted layer. (b) A high-resolution SEM image showing the epitaxial growth of columnar dendrites at the laser-remelted layer [84].

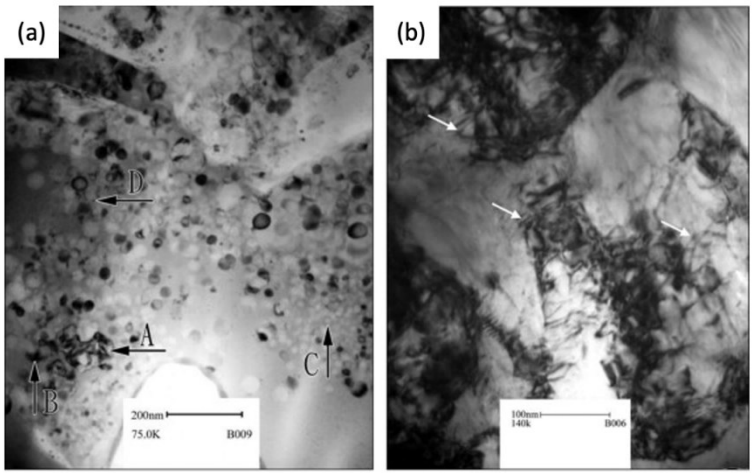

Figure 3.8 TEM images of thermal sprayed NiCo0.6Fe0.2CrSiAlTi0.2 after annealed under 1100 °C for 10 h showing (a) large amount of nano-sized precipitates (labeled with A, B and C); (b) high density of dislocations (marked with white arrows) [56].

3.3.2. Strengthening mechanisms of HEA coatings

3.3.2.1. Solid solution strengthening

Based on the results from recent studies, solid solution strengthening mechanism plays a major role in improving the hardness for most of the thermal-sprayed HEA coatings. It has been reported that the solid solution strengthening for HEAs is mainly attributed to the pronounced lattice distortion associated with mismatch parameter of atomic size differences of different elements [57]. The atomic radius of each constituent element studied for thermal sprayed HEA coatings are illustrated in Table 3.2. As shown in Table 3.2, the elements with large atomic radius (i.e., Al, Ti and Mo) induce strain energy in the lattice structure causing severe lattice distortion, which is one of the core effects of high entropy materials [6]. The pronounced lattice distortion effect act as a large barrier against the dislocations and their movements by effectively pinning the dislocations, yielding solid solution strengthening/hardening. A study by Wang *et al.* [58] explored the deposition of gas atomized AlCoCrFeNi feedstock on AISI 1045 steel by means of APS. The hardness was around 4.5 GPa (468 HV), which is likely due to the solid solution strengthening caused by the disordered BCC (A2) and ordered (B2) phase formations. It has been argued that the occurrence of ordered B2 phases is more prominent when the lattice distortion effect is too large [57]. The movement of dislocations is inhibited by the hard B2 phases causing resistance to plastic deformation, which further yields to improved strength for the HEA coatings. The effect of annealing temperature on hardness has also been investigated for the AlCoCrFeNi coating, and the results showed an increase in hardness with lower annealing temperature and a gradual decrease as the function of annealing temperature (600 to 900 ^{0}C). The higher hardness obtained after annealing at 600 ^{0}C (5.64 GPa) was approximately 1.2 times than that of the as-sprayed HEA coatings at room temperature. The authors claimed that the area fraction of B2 phases (i.e., possible increase in the solid solution strengthening effect) increased at 600 ^{0}C and thus, significantly contributing to enhanced hardness. However, it is anticipated that the presence of B2 phases decline the toughness/ductility of the coatings that have not been reported to date.

Table 3.2 shows the atomic size radius of the constituent elements used for high entropy alloy coatings.

Elements	Al	Co	Cr	Fe	Ni	Ti	Si	Mn	Nb	Mo
Atomic size radius (nm)	0.143	0.125	0.128	0.127	0.125	0.146	0.111	0.126	0.246	0.139

Mu *et al.*[59] explored AlCoCrFeNi equimolar compositions deposited by means of atmospheric plasma spraying. The authors showed that the average hardness increased as the function of spraying power, with the highest observed around 5.97 GPa when using a voltage and current of 55.4V and 550A, respectively. Cheng *et al.* [17] investigated similar AlCoCrFeNi HEA composition deposited using APS with varying gas atomized feedstocks (10-60 μm and 60-90 μm). The hardness was higher (4.18 GPa) for the coatings deposited with coarser feedstock (60-90 μm) and a high spraying current of 650A. This was mainly attributed to the solid solution strengthening associated with BCC phases compared to finer feedstock (which has major FCC peaks). It should be noted that the absence of oxides was reported and compared to other literature on APS-based HEA coatings. However, it can be inferred that the solid solution strengthening due to the presence of high aluminum content (20 at%) is the major responsible factor for high hardness.

The microhardness and wear properties of mechanical-alloyed AlCoCrFeNiTi HEA coatings were first investigated by Tian *et al.* [20]. The authors used the APS technology to fabricate the coatings on stainless steel 316 substrates. The result showed that the average hardness value was around 6.3 GPa (642 $HV_{0.2}$), which was higher compared to the AlCoCrFeNi HEAs fabricated by means of atmospheric plasma spraying. The higher average hardness of 3.8 GPa was also obtained at the coating/substrate interfaces, signifying adequate adhesion. The low porosity, severely distorted lattice structure (solid solution strengthening) due to large atomic radii of aluminum and titanium, as well as the hard oxides are the determinative factors that contribute to the improved hardness of AlCoCrFeNiTi coatings. Generally, silicon can also increase the strength of the materials through solid solution strengthening due to

its small atomic size. In terms of HEAs, the addition of silicon favors to phase transitions and mechanical properties due to its high negative enthalpy of mixing with other constituent elements and lattice distortion effect. To date however, the influence of silicon content on the mechanical properties has been limitedly examined. Tian *et al.* [60] fabricated the equimolar AlCoCrFeNiSi HEA coatings using the APS technique on stainless steel 316L. The average hardness was found to be approximately 6 GPa (612 $HV_{0.2}$), which is due to the solid solution strengthening associated with the presence of B2 and disordered BCC phases.

3.3.2.2. Grain boundary strengthening

Grain boundary strengthening or fine grain strengthening are often observed in thermal-sprayed HEA coatings, particularly in cold spraying, which can significantly contribute to the enhancement in the hardness/strength. For grain boundary strengthening, the strength/hardness primarily depends on the pinning of dislocations around the fine grains contributing to Hall-Petch effect. This phenomenon has been observed in cold sprayed HEA coatings, reported by Nair *et al*. [61] and Rojas *et al.* [62]. The high velocity impact offered in thermal spraying techniques (cold spraying, HVOF and HVAF) improves the strengthening by inhibiting the grain growth due to dynamic recrystallization and high dislocation density [62]. A comparative study of AlCoCrFeNi HEA coatings developed using HVOF and HVAF thermal spray technologies was reported by Lobel *et al.*[63]. The microhardness exhibited higher (6.6 GPa) for HVAF fabricated HEA coatings compared to that of HVOF based HEA coatings (5.8 GPa). The authors concluded that the low porosity levels and influence of grain boundary strengthening (fine grain size) due to high velocity impact could be the possible reasons for improved hardness. Furthermore, the absence of oxides and low porosities also resulted in a low standard deviation of hardness for the HEA coatings developed using HVAF.

In a different study reported by Wei *et al.* [64], for similar composition HEA fabricated by means of HVOF, the average hardness obtained was around 5.4 GPa (552 $HV_{0.3}$), which was attributed to the presence of FCC and BCC phases. Nano indentation studies were performed on each phase of the HEA coatings to determine the nano hardness and elastic modulus. Higher nano hardness (i.e., 9.5GPa) and lower elastic modulus (i.e., 208 GPa) were obtained for the BCC phases (9.5 GPa) when compared

to that of the FCC (i.e. H=5.9 GPa and E=250 GPa), highlighting solid solution strengthening. The work of elastic deformation was high in BCC phases indicating the capability of large elastic recovery after deformation compared to FCC phases. The study concluded that the combined interaction of solid solution strengthening and grain boundary strengthening are the contributing factors for the improvement in hardness of the HEA coatings. Similarly, Liao *et al.* [65] investigated the hardness of the Cantor (CoCrFeMnNi) HEA deposited by means of detonation spraying on stainless steel 316L substrates. The average hardness obtained in this study was around 4.6 GPa, which outperforms the alloys fabricated using casting (1.6 GPa) [66] and spark plasma sintering (4 GPa), respectively [67]. Despite the presence of FCC phases in the MnCoCrFeNi coatings, the grain boundary strengthening associated with fine grains and oxide formations augmented the high hardness.

While thermally sprayed HEAs exhibited outstanding microstructural features and mechanical properties, as shown by several studies in literature, there is limited work specifically focusing on HEAs fabricated via cold spray techniques. The trend in cold spray HEA coatings is increasing among researchers due to its feasibility in producing high strength coatings [68,69]. The high velocity (typically between 500 m/s and 1200 m/s) during the deposition process results in severe plastic deformation, which further contributes to improved strength due to fine grain size and work hardening. Anupam *et al.* [16] reported the first AlCoCrFeNi HEA fabricated by means of cold spraying. The mechanically-alloyed powder feedstocks were used to deposit the coating on nickel base superalloy substrates. The major BCC phase obtained for the HEA resulted in an average coating hardness of 3.8 GPa. The high hardness could possibly be explained by the fine grain structure, which occurred due to severe plastic deformation. However, the obtained hardness value for the cold sprayed AlCoCrFeNi HEA coatings was lower compared to HVOF, and APS deposited HEA coatings [17,63], which is due to the absence of oxides lamellae in the cold spray HEA coatings. The influence of Mn on CoCrFeNi HEAs was investigated by Yin *et al.* [41]. The high-pressure cold spray system was utilized to deposit atomized MnCoCrFeNi feedstock on aluminum 6082 alloy substrates. The overall hardness showed to be around 3.2 GPa, which was three times the hardness of powder particles. The improvement in the hardness was attributed to the significant grain refinement (fine grain strengthening) and increased dislocation density after cold spraying.

3.3.2.3. Oxide-based strengthening

The evolution of oxides and their impact on mechanical properties for thermal spray coatings has been previously reported on several occasions. The occurrence of oxides during oxidation in-flight for high temperature deposition techniques is a common artifact. Nevertheless, the occurrence of these oxides plays a dominant role in changing the behavior of the coatings in terms of hardness and wear performance. Meghwal *et al.* [70] conducted nano-indentation studies on similar compositions fabricated using APS. The oxide phases were dominant in the case of APS HEA coatings compared to the HVOF HEA coatings. The Al-rich and oxide-rich phases were found to have the highest nano hardness of 15 GPa, followed by AlCrFe oxides and Al depleted HEA regions with 13 GPa and 5 GPa, respectively. The H/E_r (hardness to reduced elastic modulus) ratio was reported to be lower for the Al-depleted HEA phase, indicating the ability to resist plastic deformation. Although the Al-rich oxide phases exhibited high hardness, the Weibull plot assessment signifies the Al-rich oxides phases with the largest variations, which explained the inhomogeneity of property distribution. These oxides improved the overall microhardness of the AlCoCrFeNi HEA coatings, which was around 4.13 GPa. Liang *et al.* [71] investigated APS-based non-equimolar $Al_{0.5}CoCrFeNi_2$ high entropy alloy coatings using gas atomized powders. The average hardness reported was around 2.7 GPa, which was lower than that of the same coatings developed using magnetic sputtering (5.5 GPa). The reason might be the homogenous microstructure with low defects and voids, resulting in two times high hardness for the sputtered HEA coatings.

More recently Nair *et al*. [61] investigated novel AlCoCrFeMo HEA using cold spraying and flame spraying technologies to understand their effects on microstructural formation and hardness property. The average hardness showed approximately 40% improvement for the flame sprayed HEA coatings owing to the formation of high fraction of spinel oxides (25 wt%) compared to cold sprayed HEA coatings. A comparative study using APS and HVOF was investigated by Li *et al*. [72] using non-equimolar $FeCoCrNiMo_{0.2}$ HEA as feedstock. An average hardness reported for APS and HVOF coatings was around 3.4 GPa and 3.8 GPa, respectively. The reported values also outperform the $FeCoCrNiMo_{0.3}$ HEA fabricated via arc melting (2 GPa) investigated by Shun *et al.* [73]. Although the coatings and arc-melted HEAs exhibited FCC phases, the improvement in the hardness for the HEA coatings was mainly

attributed to the occurrence of oxide contaminations compared to that of arc-melted HEAs.

3.3.2.4. Dispersion strengthening

The addition of particulate reinforced high entropy alloy coatings developed by means of thermal spraying techniques has been reported in literature [74-76]. The hard particle reinforcement enhances the mechanical properties such as hardness and toughness due to the different possible mechanisms, namely, i) dispersion strengthening – associated with micro size particles, ii) misfit in coefficient of thermal expansion – resulted in occurrence of geometrically necessary dislocations, iii) load transfer effect – transferring loads from the matrix to the particles and iv) Orowan strengthening mechanism associated with nano size particles [77]. It has been reported that the addition of micron sized particles induces high dislocation densities and twinning around the reinforced particle regions, which contributes to improvement in the hardness/strength [78]. Many studies have been reported on the effect of dispersion strengthening through particle reinforced HEA coatings. Wei *et al.* [65] investigated the effect of hard WC-10Co reinforcement of AlCoCrFeNi HEA by mixing using a mechanical mixer prior to deposition. The HVOF system was used to spray in different proportions (0 to 50 wt.% of WC-10Co) on 06Cr13Ni5Mo martensitic stainless steel. The average hardness showed a linear function with the reinforced particles with highest value obtained for equi-proportional HEA composite coatings (7.3 GPa), which was around 1.5 times than non-reinforced counterparts. The solid solution strengthening associated with high atomic radii elements (aluminum) as well as the dispersion strengthening mechanisms (due to hard WC-Co) further result in improved hardness for the HEA coatings. In addition, the addition of reinforcement enhanced the plastic deformation resistance of the coatings obtained from nano indentation results. The nano-hardness and elastic modulus of BCC phases were around 11.52 GPa and 232 GPa, respectively, for the equi-proportional HEA composite coatings, which was higher than that of values reported previously [64]. This can be explained based on the bonding force enhancement of the lamellae after reinforcement addition, which further resulted in enhancement in the average hardness.

In the work reported by Tian *et al.* [15], the atomized Ni60 alloy was added as reinforcement to AlCoCrFeNiTi and developed using APS technique. An increase in

the average hardness from 6.3 GPa to 6.6 GPa was found after reinforcement addition, which is attributed to the dispersion strengthening and solution hardening. The coating/substrate interface hardness was also enhanced noticeably after the reinforcement additions compared to non-reinforced counterparts. Zhu *et al*. [76] investigated MnCoCrFeNi composite HEA by adding Al_2O_3-13 wt.% TiO_2 as a reinforcement and fabricated via APS. The powders were blended with a 3D motion mixer with a frequency of 50 Hz for 4 hours before spraying. The average hardness was 1.29 times higher for the HEA coatings after reinforcement, signifying the dispersion strengthening. The *H/E* ratio was also enhanced, indicating the resistance to plastic deformation and elastic recovery for the Al_2O_3-13 wt.% TiO_2 reinforced HEA composite coatings.

Nano oxides reinforced FeCoCrNiMo HEA using APS was investigated by Mu *et al.* [16]. The authors concluded that the dispersion strengthening (possibly Orowan strengthening) due to addition of nano oxides as well as solid solution strengthening due to high atomic size of molybdenum contributed towards high microhardness of 3.1 GPa despite the FCC structure. The obtained average hardness was almost similar to the result obtained using APS $FeCoCrNiMo_{0.2}$ HEA coatings [72] and higher than arc-melted HEAs [73].

3.3.2.5. Precipitation strengthening

The effect of precipitation strengthening on mechanical properties of thermal-sprayed HEA coatings has been reported in literature. Fine particles that precipitate creates large strain fields, which act as barriers to the movement of dislocations and improves the hardness through Orowan strengthening [77]. Very recent study by Rojas *et al.* [62], reported the formation of nano sized fine precipitate (226 nm) for cold sprayed $CoCrFe_{0.75}NiMo_{0.3}Nb_{0.125}$ HEA coatings. The authors concluded that the fine precipitates, coupled with lattice distortion induced by molybdenum and niobium (solid solution strengthening), and fine grains (grain boundary strengthening associated with cold spraying) pinned the dislocations resulting in high compressive yield strength of 1745 MPa. Jin *et al.* [79] investigated the effect of silicon in different molar fractions (x = 0.5 to 2) on $Al_{0.5}CoCrFeNiSi_x$ HEA fabricated by means of APS on Q235 steel substrates. The developed coatings were post-processed using laser re-melting. The hardness showed linearity with the molar fractions, wherein the maximum hardness was observed for $Al_{0.5}CoCrFeNiSi_2$ coatings (10.7 GPa) and the lowest hardness was

found for the coatings with low silicon content (4.9 GPa). The area fractions of BCC phases increased (increase in solid solution strengthening effect) by suppressing the FCC phases after laser-remelting, which attributed to the highest hardness for the coatings. However, due to high silicon content, chromium and silicon (which has a high negative enthalpy of mixing) tend to decompose from the matrix and form Cr_3Si precipitates, which also act as precipitation strengthening mechanism and along with solid solution strengthening due to lattice distortion, it further resulted in high hardness.

Li *et al.* [71] reported non-equimolar $Al_{0.2}CrCo_{1.5}FeNi_{1.5}Ti$ HEA by adding silver as a reinforcement to fabricate coatings using APS. The HEA and reinforced particles were mechanically blended and deposited on carbon steel substrates. The coated specimens were then heat-treated to 750 ^{0}C. The average hardness showed to be around 6 GPa for as-sprayed HEA coatings, which further increased up to 1.2 times after heat treatment. The oxidation and precipitation hardening (Ni-Ti and Co-Ti phases) are the contributing factors for improved hardness after heat treatment. A recent study by Yurkova *et al*. [50] explored the MA AlCoCrFeNiTi HEAs deposited using high-pressure cold spraying on steel substrates. The study reported that the average hardness value is around 10 GPa, which outperforms the AlCoCrFeNiTi coatings fabricated by means of APS and HVOF techniques [14,80]. The presence of intermetallic phases, such as B2 (AlNi rich) and CrFe rich precipitate phases along with TiC formations, contributed to high hardness. In addition, the high-velocity impact of feedstock powder particles on the substrate resulted in significant plastic deformation through strain hardening and undergoing dynamic recrystallization, which influences further hardness enhancement.

Another study was performed by Chen *et al.* [81] where the authors reduced the Al content to $Al_{0.6}CoCrFeNiTi$ HEA. The average hardness value obtained for the HVOF sprayed HAE coating was around 7.7 GPa (789 $HV_{0.1}$). The hardness increased up to 9.2 GPa when treated at a temperature of 800 ^{0}C for 1 hour. The improved hardness was probably related to the precipitation hardening after heat treatment. The CrFe rich σ phases were precipitated from the BCC phases at high temperatures (>300 ^{0}C) resulted in high hardness. Furthermore, the fracture toughness was investigated using the Vickers indentation method for the first time in thermal spray coatings. Higher fracture toughness was obtained at room temperature (8.4 MPa.√m). However, the fracture toughness showed to be decreasing after heat treatment (5 MPa.√m). These

trends can possibly be explained by the brittle nature of CrFe rich σ phase precipitations. At high temperatures, the CrFe with high negative enthalpy of mixing tends to decompose from the BCC phases forming σ phase precipitates. The presence of σ phases also increases the work hardening ability due to the formation of deformation twinning and hence, improves the hardness, and lowers fracture toughness. The detailed mechanism needs to be further investigated to provide a correlation between phase formations and mechanical properties. The various high entropy alloy coatings developed through thermal spraying techniques that have been evaluated in terms of their strength/hardness are summarized in Figure 3.9. As shown in Figure 3.9, the precipitation strengthening mechanism together with solid-solution strengthening contributes to higher microhardness when compared to the other strengthening mechanisms of the HEA coatings, irrespective of the chemical compositions and deposition technologies.

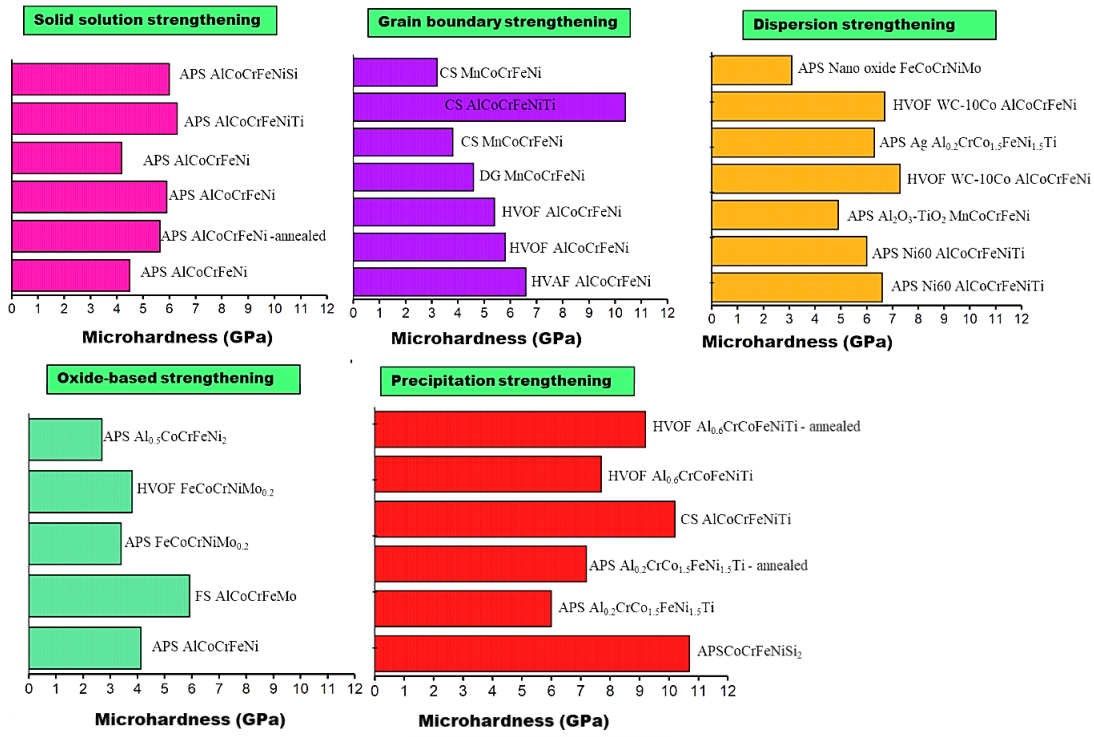

Figure 3.7 Comparative assessment of different strengthening mechanisms for thermal sprayed HEA coatings. The precipitation strengthening seems to have a higher influence on the microhardness compared to all other strengthening mechanism.

3.3.3. Quantitative mechanical performance and property assessment for extreme industrial applications

The influence of microstructure and mechanical properties incline to form in thermal spray HEA coatings are important to understand the failure mechanisms due to loading conditions. The results from the previous studies of HEA coatings are investigated mainly on micro-hardness. Although hardness being a dominant property, the reliability of the coatings under different loading conditions also influenced by various mechanical properties such as yield strength, ultimate strength, ductility, toughness, strain hardening and elastic modulus. Recently, Munday *et al.* [82] studied the correlation between different mechanical properties and microstructural features (porosity, particle-particle mean free path and average particle size) on cold sprayed WC-Ni composite coatings. The features of microstructural defects that influence mechanical properties has been investigated systematically. It was reported that a high variation in tensile strength was found due to variations in WC content and related porosity. Such study may open the door to explore the fundamental understanding of HEA coatings. The high spatial variability is challenging and difficult through experimentations and can be validate and predict through mechanism-based numerical models.

The strength and toughness are the key properties that determines resistance to damage due to loading. For instance, the aircraft and marine components during operations suffer from erosion damages due to impact of high velocity solid particles, which resulted in decline in efficiency of the components and premature failure. Furthermore, the decline in the wear performance may drastically leads to fatigue failure due to cracking [83]. The fatigue crack initiation phenomenon is related to the residual stress, and the coatings with excellent balance of strength and toughness can be able to provide high resilience to fatigue, wear and erosion damages [84,85]. However, the systematic investigations that relate to the HEA coatings and their fatigue failure mechanisms is lacking. It has been reported that the material's capability to absorb strain energy can provide high damage tolerance to fatigue failure. Furthermore, it is well known that the coatings with excellent toughness and ductility can provide resistance to erosion damage when the angle of impact greater than 60^0, whereas the hardness and strength are the dominant parameters at low angles [85,86]. HEAs are reported to have the synergistic response of strength and toughness, which can provide

resistant to micro-cutting, micro ploughing, micro indent and micro-cracks [87-89]. Since the state-of-art-of the field of HEAs is establishing among the thermal spray researchers, such studies have not been explicitly explored till date. Figure 3.10 represents classifications of parameters that should quantify for extreme engineering environments. Correlating the materials-related features of HEA coatings including different mechanical properties (yield strength, ductility, toughness, ultimate strength, fracture strength, elastic modulus, work hardenability, fracture resistance), microstructures (porosities, cracks, inter-splat bonding, adhesion and cohesion) and phase formations (oxides, FCC, BCC and other phases) with extrinsic factors of wear damage, such as shape and size of abrasion particles, particle distribution, hardness of the abrasive particles, density, impact velocity, impact angles, and temperature, which may help in understanding the effect of microstructure, mechanical properties and loading conditions (see Figure 3.10). However, such process parameter evaluations are challenging through experimental investigations and not fully understood. Mechanism through physical-based modelling is a viable approach to predict the damage resistance of thermal sprayed HEA coatings.

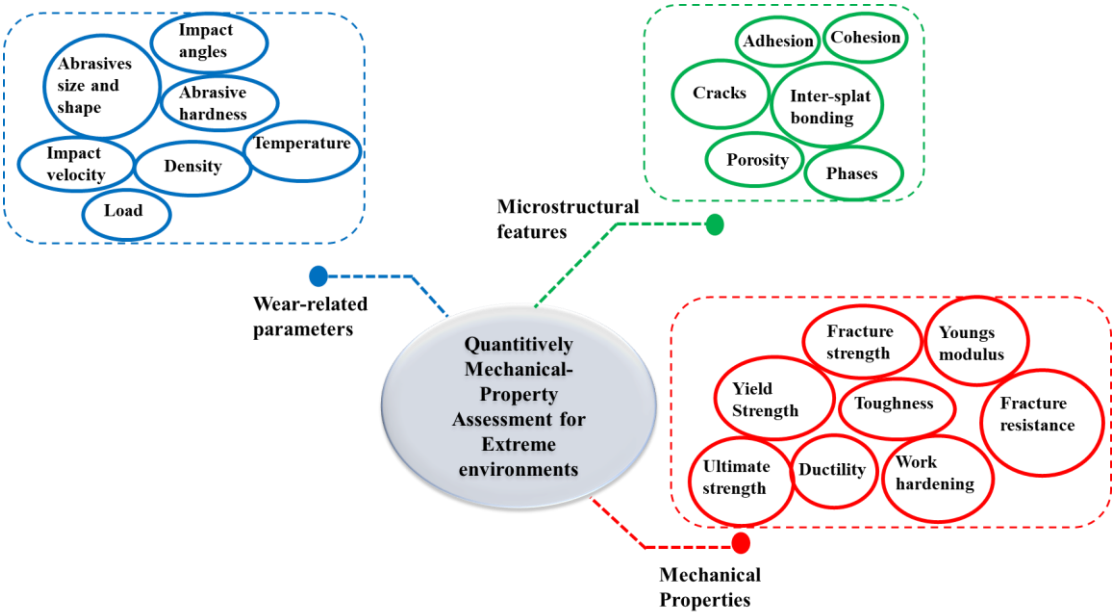

Figure 3.8 Schematic illustrating the classifications of material properties for quantifying the mechanical performance for extreme environmental applications.

Other salient properties that influence the functionality of a coating are the substrate-coating adhesion and cohesion or bonding between splats. The adhesion and cohesion strengths can appreciably affect the coating's performance in various loading

conditions. These studies are not emphasized to date for thermal spray HEA coatings. Thus, the fundamental understanding on the adhesion and strengths and their mechanisms on wear loading need to be explored for HEAs as structural applications. The bond strength can be investigated by various testing, which includes peel adhesion [90,91] laser shock adhesion test [92,93] and three-point bend test [94]. However, the application of these methods on thermal sprayed HEA coatings has not been explored and further research is required.

3.4. Performance assessment of HEA coatings

3.4.1. Wear behavior

Prior studies have mainly focused on the HEA composition of AlCoCrFeNi, where additions of promising elements have been investigated in terms of the wear performance. Since the HEA coatings have the ability to provide high temperature wear performance due to their peculiar microstructural features, many studies were devoted to performing the wear studies at elevated temperatures. Some of the important HEA coatings and their key findings are summarized in this section.

The wear behavior of $AlCoCrFeNiTi_{0.5}$ developed by means of HVOF was studied as a function of temperature (room temperature to 900 ^{0}C) using an Al_2O_3 counterface and a 26 N normal load [95]. A strong dependence of temperature on the wear behaviour was observed, which indicates that the wear resistance decreased as the function of temperature (from room temperature to 500 ^{0}C) due to thermal softening. However, an increase in the wear resistance was found as the temperature increased up to 900 ^{0}C. Figure 3.11 revealed presence of deep grooves with oxide formations (white regions) at the lowest temperature however, oxide film or glazed layers appeared to be compact on the wear tracks at elevated temperatures acting as a protective shield against plastic deformation [95]. The glazed layers formed are comprised of spinel oxides, causing a reduction in coefficient of friction and wear rates. Chen *et al.* [81] investigated the wear performances of HVOF based $Al_{0.6}TiCrCoFeNi$ HEA coatings using pin on-disc testing against a Al_2O_3 counter body. The authors noticed a change in the wear behavior as the function of temperature, where abrasive wear was the dominant wear mechanism together with fatigue failure at increased temperature [81]. A compact glazed layer was also identified on the wear tracks at highest temperature (500 ^{0}C), yielding to reduction in coefficient of friction. The evolution of these compact

glazed layers protect the surface from further damaging due to sliding, and thereby lower wear rates were achieved [81].

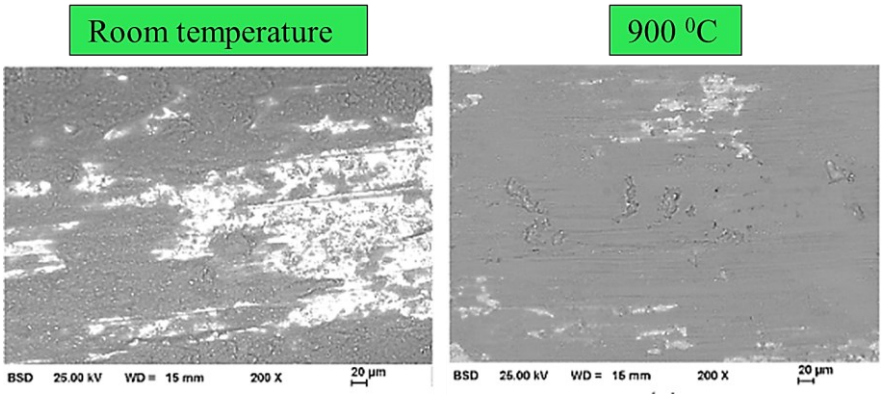

Figure 3.9 Wear morphologies of AlCoCrFeNiTi HEA coatings tested at room temperature and elevated temperature. The presence of contrast oxide regions was more profound when tested at room temperature compared to that at elevated temperature [14].

Tian *et al.* [20] investigated wear performance at varying temperatures using Si_3N_4 counterface for atmospheric plasma sprayed AlCoCrFeNiTi HEA coatings on stainless steel 316L substrates. The study was performed at varying temperatures, i.e., 25 ^{0}C to 900 ^{0}C with a constant normal load. The as-sprayed HEA coatings showed the presence of ordered BCC, disordered BCC and an FCC phase. The authors reported that there were no changes in phases when tested at 500 ^{0}C; however, at elevated temperature (at 700 ^{0}C), CrFe rich precipitates were found on the wear tracks, indicating a phase transformation from the disordered BCC structure. The CrFe precipitates might contributed to reduction in coefficient of friction and lower wear rates compared to that of tested at different temperatures. In general, fine structured precipitates with small fractions may induce pinning of dislocations by Orowan strengthening, which further contributed towards high hardness and reduction in wear rates. Wear morphologies of the AlCoCrFeNiTi HEA coatings at different temperatures are shown in Figure 3.12. As shown in Figure 3.12, the wear tracks obtained at room temperature and 500 ^{0}C showed significant delamination, abrasive grooves and formation of lips after testing. The pronounced delamination could possibly be explained by the large plastic flow and adhesive wear. Ex situ analysis of the counterface and their transfer film formations have not been reported by the authors. Nevertheless, the formation of tribofilms were found for the HEA coatings tested at higher temperatures, i.e., 700 ^{0}C and 900 ^{0}C. The tribofilms consists of compact oxides and mechanically mixed layers – layers that

generated due to chemical and processing conditions during wear, which further helped in reduction in wear rates and coefficient of friction.

A comparative study on $FeCoCrNiMo_{0.2}$ HEA coatings using HVOF and APS over a steel substrate was performed by Li *et al*. [51]. The study concluded that the high fraction of oxides, typically spinel oxides formed for the APS HEA coatings reduced the wear rates compared to that of HVOF based HEA coatings. The spinel oxide contents for APS HEA coatings were almost 4 times higher compared to HVOF HEA coatings. Despite of having high fractions of oxides, the hardness values were similar for both HEA coatings. The high fractions of spinel oxides act as a lubricating behavior for the APS HEA coatings, which in turn reduced the wear rates compared to HVOF HEA coatings in an order of magnitude. The dominant wear mechanisms involved was abrasion for both the HEA coatings [51].

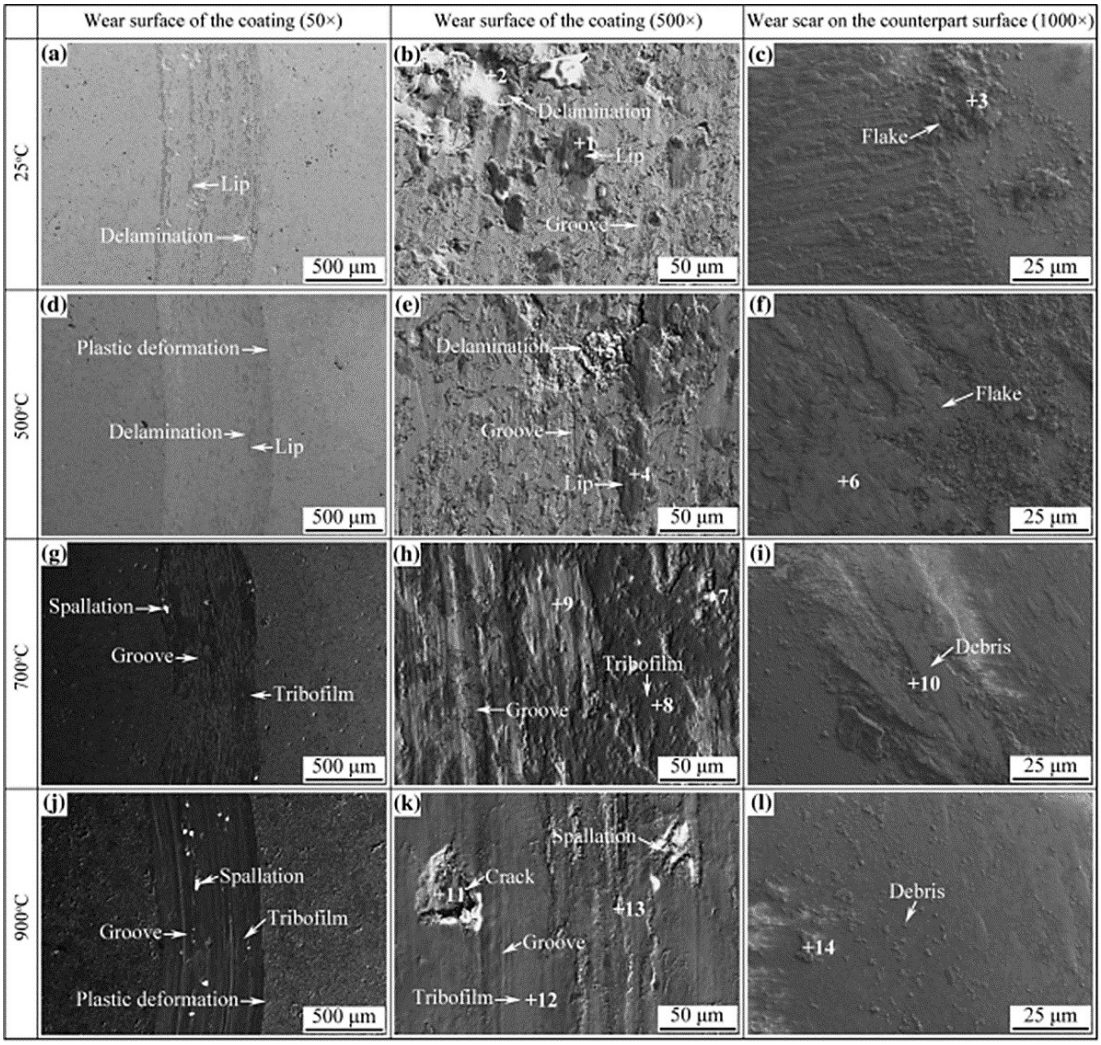

Figure 3.10 Wear morphologies of mechanically-alloyed AlCoCrFeNiTi HEA coatings tested from room temperature to 900 ^{0}C. Delamination, and formations of grooves and lips were more obvious at low temperatures (Figure (a to c)). The tribofilm formations at elevated temperatures (700 ^{0}C and 900 ^{0}C) act as protective layers against wear damage (Figure (g to i)) [20].

More recent by Patel *et al.* [96] investigated the wear behavior of as-sprayed and heat treated CoCrFeMnNi HEA coatings using Al_2O_3 as counter surface tested at 5 N normal load. The study was carried out on rough and polished surfaces, aiming to understand the influence of surface roughness on tribological interfaces. The as-sprayed polished surfaces showed approximately 5 times lower wear rates compared to that of rough surfaces of the HEA coatings, indicating the rough surfaces are not an appealing method for wear applications. However, no variations in wear rates were achieved after heat treating the HEA coatings. The difference in wear rates could possibly be explained by the formation of oxide or glazed layers, which were similar in case of as-sprayed and heat-treated HEA coatings. The authors concluded that the occurrence of

tribolayers (typically mixed oxide layers) act as third-body, which reduced the adhesion between two bodies and thereby increased the wear resistance for both the coatings. Figure 3.13 shows the counterface images after sliding against the as-sprayed and heat-treated HEA coatings at both the surface conditions. As shown in Figure 3.13, material transfer had taken place for all the coatings, wherein, severity of grooves was lesser in case of the polished surface coating compared to that of rough surface counterpart. The authors suggested that the transfer film to counterface was higher for the rough surfaces, which eventually leads to further breakage of the films. Consequently, the fractured particles (wear debris particles) act as third body, resulting in ploughing of asperities and wear rates for the rough surface HEA coatings [96].

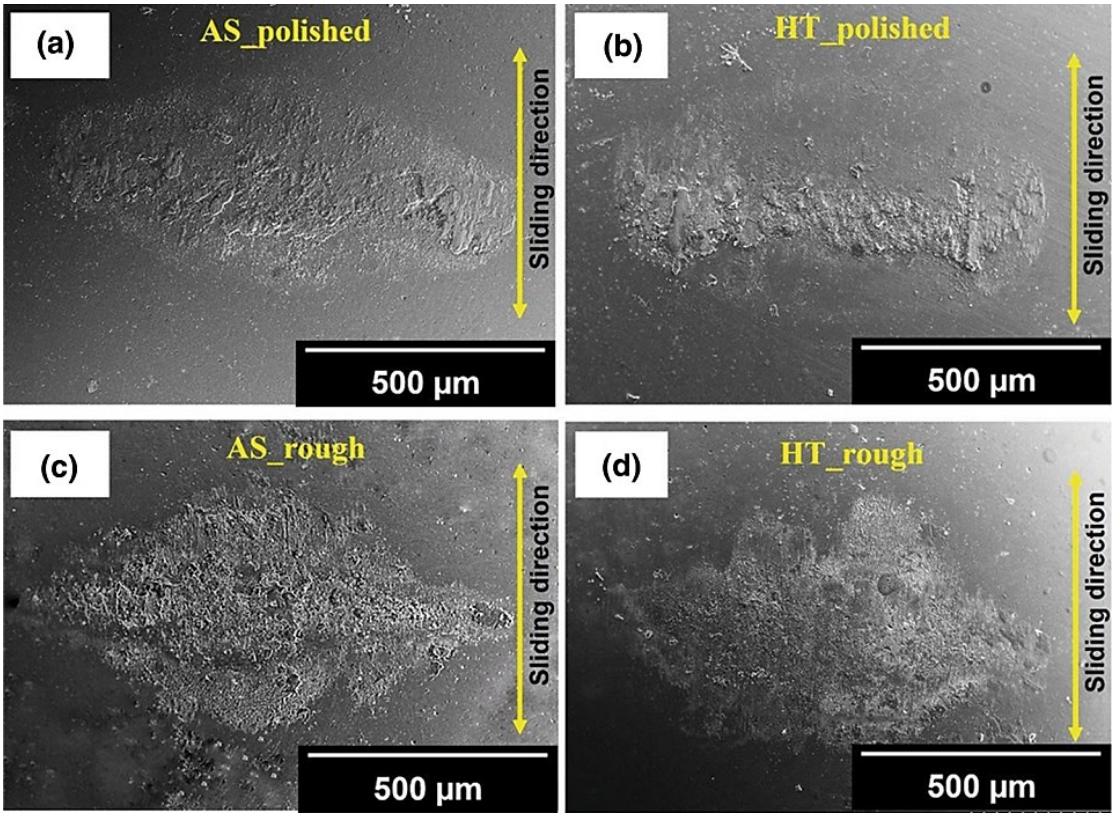

Figure 3.11 Wear morphologies of Al2O3 counter body performed against rough and polished CoCrFeMnNi HEA coating surfaces. The transfer film was more pronounced for the rough (unpolished) HEA coatings, which contributed to increased wear rates [96].

A few articles also investigated the wear behavior of cold sprayed HEA coatings. Yin *et al*. [41] investigated the wear behavior of high-pressure cold sprayed FeCoNiCrMn HEA coatings tested at 5 N load using WC-Co ball as counter body. The authors concluded that the significant work hardening ability and grain refinement due to high velocity impact influenced the wear rates, which was comparatively lower than

that of laser cladded HEA coatings. Similarly, a recent study by Silvello *et al.* [97] investigated the wear behavior of cold sprayed and HVOF sprayed FeCoNiCrMn HEA coatings. The study showed that the cold sprayed HEA coatings exhibited least cohesive strength, which were prone to wear performance. On the other hand, the HVOF coatings showed low wear rates, which was mainly attributed to their formation of spinel oxides. It was observed that the wear track was characterized by microgrooves and fragmented debris, indicating abrasive wear as major wear mechanism for the cold sprayed HEA coatings.

3.4.2. Corrosion behavior

Chromium is considered to be the most influential metal to provide material protections against corrosion species due to its stabilized chromium oxide films. It has been reported that the presence of chromium with more than 20 wt.% in the composition provides corrosion protections for HEAs fabricated via arc-melting [98]. However, some studies on HEAs claimed that the aluminum addition in high fractions declines the protection capability by depleting chromium from the phases [99]. Still, the debate is ongoing on how the alloy chemical compositions, microstructural, and phase formations influence the corrosion characteristics of HEAs. Reported literature in the article was mainly focused on seawater (may consist of NaCl, $CaCl_2$ $MgSO_4$, and $MgCl_2$) and 3.5 wt.% NaCl as electrolytes. Generally, chloride ions cause severe corrosion damages when compared to electrolyte containing acidic or alkaline. However, there is a significant research gaps on the response of different electrolyte conditions on corrosion performances of thermal sprayed HEA coatings. More importantly, different chemical compositions of HEAs utilized for thermal spraying has not studied so far and required further research to understand how the influence of different HEA compositions and their microstructural artifacts could impact the performance under electrochemical damage.

The effect of phase formations and oxidation in HEA coatings can strongly influence the corrosion current density (I_{corr}), pitting potential (E_{pit}), and corrosion rates. Wang *et al*. [100] investigated the corrosion behavior of $(CoCrFeNi)_{95}Nb_5$ HEA coatings using plasma spraying. I_{corr} values showed to be around 7.23 $\mu A/cm^2$, which is lower than that of HEA coatings fabricated using other techniques, highlighting the better corrosion resistance. The presence of stable oxides (Cr_2O_3 and Nb_2O_5) enhances

corrosion resistance for the HEA coatings. Niobium and chromium rich interdentrite phases act as micro-galvanic cells, which leads to inferior corrosion resistance. In another study reported the corrosion rates decreased up to 1.6 times by an increase in the molybdenum additions in $AlCoCrNiMo_x$ ($x = 0.5$ and 1) HEAs fabricated by HVOF [101]. These HEA coatings showed approximately 2.4 times better corrosion performance than that of traditional NiCrSiB coatings under 3.5 wt.% NaCl solution.

Mu *et al*. [59] investigated the corrosion performance on AlCoCrFeNi HEA fabricated by means of APS. They utilized different power sources to study their effects on corrosion behavior. The coatings with high voltage exhibited low I_{corr} values, highlighting the better corrosion resistance. The electrochemical impedance spectroscopy (EIS) study revealed the high charge transfer resistance (R_{ct}) for the HEA coatings fabricated at high voltage, which indicated the better passivation resistance. X-ray photoelectron spectroscopy (XPS) showed the presence of species including Al_2O_3, Co_3O_4, $Cr(OH)_3$, Fe_2O_3, Fe_2O_4, FeO, NiO, and bound water (H_2O) on the corroded surfaces, where the presence of bound water improved the corrosion performance of HEA coatings. Meghwal *et al*. [102] investigated the AlCoCrFeNi HEA coatings using APS in comparison with stainless steel 316L under seawater conditions. The HEA coatings showed slightly higher I_{corr} values (0.83 $\mu A/cm^2$) compared to that of stainless steel 316L (0.26 $\mu A/cm^2$), as shown in Figure 3.14(a). Micrographs of the corroded surface revealed the formation of the pores and pits for the HEA coatings, which indicates the general and localized corrosion attacks (Figure 3.14(b) and 3.14(c)). Stainless steel 316L is known for corrosion resistance material due to its Cr_2O_3 stabilization, which acts as the barrier to selective and localized corrosion. On the other hand, the microstructural inhomogeneities and porosities act as preferential sites that lead to poor corrosion resistance for the HEA coatings. The multiphase formed with oxides may act as micro-galvanic cells, which also increased the I_{corr} values compared to stainless steel 316L.

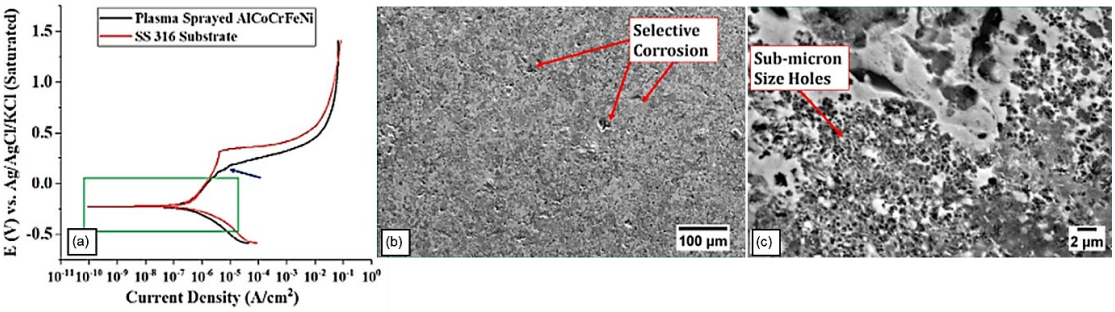

Figure 3.12 (a) Potentiodynamic polarization curves of APS AlCoCrFeNi HEA coatings and SS 316L and (b) and (c) depicts the corroded HEA surfaces [102].

More recently, Nair *et al*. [61] investigated electrochemical corrosion of newly developed AlCoCrFeMo coatings deposited by means of flame spraying and low-pressure cold spraying techniques using a 3.5 wt% NaCl solution. The authors reported that the lack of oxide contaminations and reduced porosity level contributed to an improvement in the corrosion resistance (approximately two times); low corrosion current density and high passivation capability for the cold sprayed coatings compared to that of flame sprayed counterparts, as shown in Figure 3.15. The presence of oxides inclusions during oxidation in-flight, which has different chemical composition gradients, increased the corrosion rates for the flame sprayed HEA coatings due to formation of micro-galvanic cells. Furthermore, the porosity level was higher in the case of flame sprayed HEA coatings, which act as a preferential site for the electrolyte to pass through, resulting in high corrosion rates. The comparative studies of the corrosion current density indicated that the thermal sprayed HEA coatings showed better performance compared to that of the HEA coatings fabricated using different manufacturing routes when tested under 3.5 wt% NaCl solution [61,97,98,100,103-106], as shown in Figure 3.16.

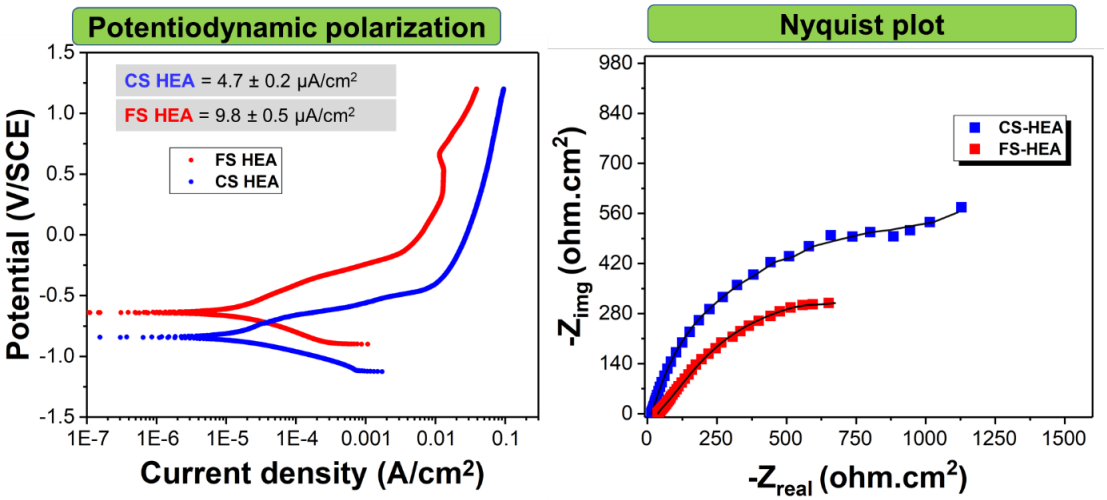

Figure 3.13 Electrochemical corrosion studies representing potentiodynamic polarization curves and Nyquist plot of flame sprayed and cold sprayed AlCoCrFeMo HEA coatings. The figure indicates that the cold sprayed HEA coatings showed better corrosion performance compared to flame sprayed HEA coatings [61].

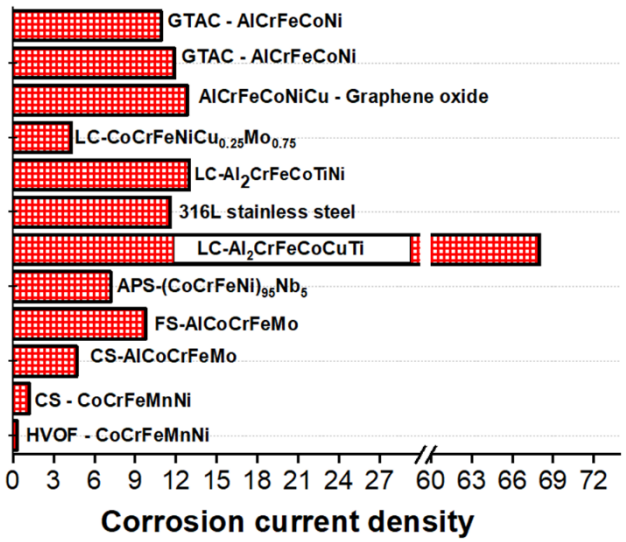

Figure 3.14 A comparative assessment of corrosion current density for thermally sprayed HEA coatings with other HEA coatings fabricated using different methods under 3.5 wt% NaCl solution [61,97,98,100,103-106]. The thermal sprayed HEA coatings showed lower corrosion rates compared to stainless steel 316L and other HEA coatings. GTAC is gas tungsten arc cladding, CS is cold spraying, FS is flame spraying, HVOF is high-velocity oxy fuel, APS is air plasma spraying and LC is laser cladding.

3.4.3. Oxidation behavior

Although the performance of HEA coatings against corrosion was better than traditional materials, studies on the oxidation behavior of thermal sprayed HEA coatings were also shown promising. The literature investigated for oxidation response on thermal sprayed HEA coatings were similar to that of electrochemical corrosion. The studies on oxidation response are crucial for thermal-sprayed HEA coatings that can be served for elevated temperature applications. Hsu *et al.* [33,107,108] fabricated HEAs based on the family of non-equimolar $NiCo_{0.6}Fe_{0.2}Cr_xSi_zAlTi_y$ coatings using APS, HVOF, and warm-spraying. The alloy coatings development strategy aiming at achieving a clearly beneficial property combination, which is required for insertion of new high-temperature coatings, can be summarized as follows. Chromium and titanium, in addition to aluminum, should ensure the formation of protective oxide scales. Addition of silicon also favors in providing oxidation protection with chromium and titanium constituent elements. All the HEA coatings were compared to traditionally utilized NiCrAlY and MCrAlY coatings, respectively. These studies were performed at a temperature of 1100 ^{0}C.

The first study conducted by Hsu *et al.* [33] fabricated used APS-based HEA coatings with an increase in chromium content, and the result showed a similar oxidation response compared to that of NiCrAlY coatings after the completion of 150 hours. The steady-state regime was found for the HEA coatings after 100 hours, indicating stable oxide scales. The mixed Ti-Cr-Al oxides and Al_2O_3 are the major contributing thermally grown oxides (TGO) to provide oxidation resistance. The next study conducted by Hsu *et al.* [107] used two HEA overlay coatings with varying chromium and titanium in $NiCo_{0.6}Fe_{0.2}Cr_{1.3}SiAlTi_{0.2}$ and $NiCo_{0.6}Fe_{0.2}Cr_{1.5}SiAlTi$ fabricated using HVOF, APS, and warm spraying, respectively. The oxidation time increased to 336 hours. A steep rise in the weight gain was observed for all the HEA coatings compared to MCrAlY coatings (Co-30Ni-21Cr-15Al-0.5Y), indicating inferior oxidation performance. The weight gain showed a sudden rise after 250 hours for the HEA coatings. Among the HEA coatings, warm-sprayed coatings showed the highest oxidation resistance, which is mainly due to the non-porous oxide scales. The subsurface layer confirmed the Ti-Cr-Al and Al_2O_3 are the oxide scales formed for all the HEA coatings. Another study was reported by adding Si in $NiCo_{0.6}Fe_{0.2}CrSi_{0.2}AlTi_{0.2}$ was fabricated HEA overlay coatings using APS and HVOF,

respectively [108]. The oxidation studies were performed in comparison with MCrAlY (Co-30Ni-21Cr-15Al-0.5Y) coatings. The weight gain showed a sharp rise until 50 hours, followed by steady-state conditions for the HEA coatings, whereas the MCrAlY coatings showed a steep rise until 168 h. The results conclude that the oxidation resistance was similar to that of MCrAlY coatings at 1100 ^{0}C.

The Al_2O_3 and Cr_2O_3 serve as protective oxide scales, which yield better oxidation resistance for the HEA coatings. For instance, two HEA AlSiTiCrFeCoNi$Mo_{0.5}$ and AlSiTiCrFeNi$Mo_{0.5}$ coatings showed the first increase in oxidation resistance from 900 to 1000 ^{0}C and declines at 1100 ^{0}C, which is due to the formation of unstable TiO_2 scales at the outer layer. Among all the temperatures, both the HEA coatings showed better oxidation performance at 1000 ^{0}C, which is attributed to their strong chromium oxide scales [52]. Another study by Anupam *et al*. [16] reported Al_2O_3 protective oxides are the main contributing factors for oxidation resistance for the cold sprayed AlCoCrFeNi coatings while performed at 1100 ^{0}C for 100 hours. Recently, Xu *et al*. [109] investigated the oxidation performance of FeCoCrNiMn fabricated using cold spraying at 700 to 900 ^{0}C and compared with their bulk forms. The oxidation behavior of cold sprayed CoCrFeMnNi and reported similar oxidation rate ($k_p = 0.0208$ mg^2 cm^{-4} h^{-1}) compared to as-cast HEA ($k_p = 0.0197$ mg^2 cm^{-4} h^{-1}) at 700 ^{0}C, but higher at high temperatures. The multi oxide scales were observed on the sublayer, which includes Mn_2O_3 outer layers, Mn-Cr spinel layers along with Cr_2O_3 inner layers, respectively at 700 to 800 ^{0}C. The significant grain boundaries promote the manganese outer diffusion, which results in the formation of manganese oxide scales, which was not found for the as-cast HEAs. These studies give a new opportunity to explore detailed studies regarding the oxidation response in thermal-sprayed HEA coatings and can be potentially transformative.

3.5. Types of HEA coatings and their potential applications

3.5.1. Refractory-based High Entropy Alloys (RHEAs) for high temperature applications

Refractory-based HEAs (RHEAs) have gained significant attention in the materials science community due to their prospective properties at elevated temperatures. Despite having high-temperature strength and oxidation resistance, the limited capability of nickel superalloys to perform at temperatures above 1000 ^{0}C has

always been a challenge. The features of RHEAs in terms of resistance to high temperature softening, and high melting point that can sustain more than 2000 ^{0}C outperform the superalloys, reported by literature [110-113]. Furthermore, the high-temperature strength and ductility along with superior oxidation and corrosion resistance of RHEAs at elevated temperatures increased the demand to focus on thermal barrier coatings. However, no reports have been provided for RHEAs fabricated using thermal spray technologies so far. Grouping the elements with refractory and transition-based metals offers excellent properties to high-temperature strength and oxidation, which in turn results in poor oxidation performance, high density, and brittleness [113-115]. By employing thermal spraying technologies for HEAs may enable a breakthrough for applications that demand elevated temperatures. However, till now, more than 120 refractory based high entropy materials has been developed using various technologies due to their exceptional high temperature properties. Primarily, RHEAs forms as BCC phases, mostly with single phase BCC structure with high strength at room and elevated temperature (even at high temperature of 1600 ^{0}C) and are high resilience to thermal softening because of the slower diffusion kinetics [61], and thus, capable as coatings for high temperature gas turbine regions in aerospace sectors. More importantly, the combination of refractory (Ta, Nb, etc) and transition metals (Al, Cr, Mo) provide an excellent combination of high melting point and oxidation and corrosion resistance, enable them to use for high-temperature applications replacing super alloys. Recently, Gorr *et al.* [113,114,116-118] proposed novel RHEAs based on the x-Mo-Cr-Ti-Al (x=W, Nb, Ta) alloy system developed by arc-melting and annealing. The alloy development strategy aiming at the achieving a clearly beneficial property combination, which is required for insertion of new high temperature materials, can be summarized as follows. The addition of tungsten, niobium, tantalum, and molybdenum should provide a high melting point, high temperature strength and creep resistance. Additions of titanium and aluminum should guarantee reasonable density, while chromium, in addition to aluminum, should ensure the formation of protective oxide scales. While the equiatomic alloy W-Mo-Cr-Ti-Al possesses a single-phase BCC microstructure, the substitution of tungsten by niobium causes formation of the ordered Laves and A15 phases [113,118]. In addition to the BCC and the Laves phases, the ordered B2 phase becomes dominating in the Ta-Mo-Cr-Ti-Al alloy [117]. Furthermore, the Ta-Mo-Cr-Ti-Al alloy shows very high

oxidation resistance. Oxidation experiments yielded values of the mass gain less than 1 mg/cm^2 and ~ 3 mg/cm^2 at 1000 and 1100°C, respectively, after 48 hours [116,117]. The formation of the protective Al_2O_3 oxide scale along with $CrTaO_4$ explains the high oxidation resistance of the Ta-Mo-Cr-Al-Ti alloy [116]. The remarkable properties of RHEAs such as high melting point, high hardness and oxidation resistance are beneficial for harsh environments and thus, suitable for the components used in gas turbines. However, the exploration of RHEAs in conjunction with thermal spraying technologies for high-temperature applications has not been explored till date and further research is required.

3.5.2. Transition-based High Entropy Alloys for aerospace applications

For aircraft engines, static and dynamic seals are vital components, which prevent the leakage of gases and fluids. One typical example is the usage of face seals to control the oil leakages from the gear boxes. In addition to that, the seals should have capability to withstand high temperature operations. Figure 3.17 shows typical seals used in aircraft engines and their locations. However, due to the severe operating conditions, engine seals undergo pronounced vibrations relative to the interfaces, which results in high friction and wear by reducing their efficiency to control the leakages [119]. Studies are on-going to incorporate advanced materials to mitigate the high friction and wear operating at different working environments, especially in the high-temperature regions. Thermal-sprayed HEA coatings have shown promising wear behavior at elevated temperatures, which can be a potential candidate for such extreme applications. The lightweight nature and superior specific strength at high temperatures offered by AlCoCrFeNi HEAs may be an alternative material than that of the traditional materials utilized for aerospace seal applications [120]. However, further research is required to understand how the different temperatures influence the wear performance of thermal-sprayed HEA coatings.

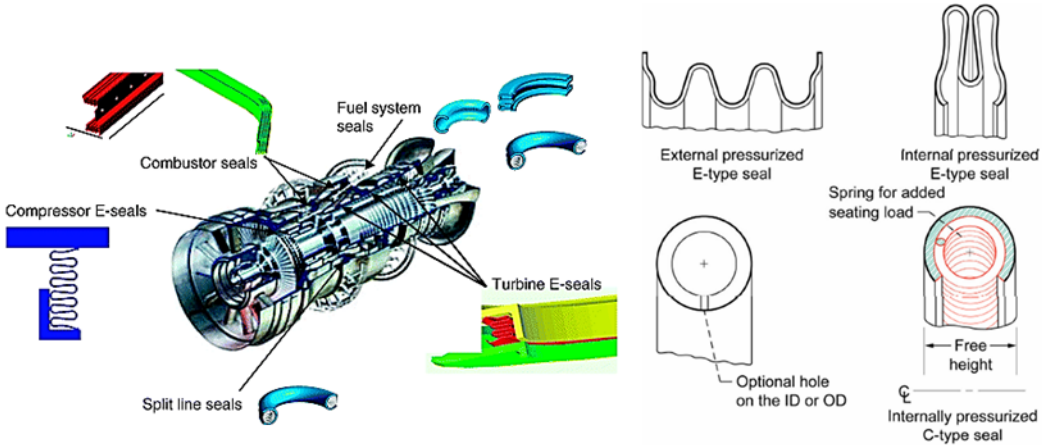

Figure 3.15 Typical seals and their locations in gas turbine engines [119]

Thermal barrier coatings are utilized to protect gas turbines components from extreme temperatures. The thermal barrier coatings consist of metallic bond coat as first layer and ceramic coating as top layer coating. Typically, MCrAlY (M = Co and/or Ni) is used as metallic bond coating as these coatings provide reasonable oxidation performance due to the formation of Al_2O_3 oxide scales, acting as a protective shield for base materials. Most of transition-based HEAs have shown exceptional properties due to their sluggish diffusion kinetics and high configurational entropy effect [121]. Aluminum and its oxide counterparts formed are the protective scales preventing from oxidation; however, utilizing the high-temperature deposition techniques reduce the aluminum content in the HEA coatings, reported by Ang *et al*. [24]. More specifically, the deposition techniques that can work under low temperature is a feasible approach to develop HEA coatings that can provide protective oxide films from further oxidation. Cold sprayed HEA coatings as bond coating for thermal barrier systems has not been explored till date and opens a new research direction to explore transition-based HEA coatings.

3.5.3. High Entropy Carbides

High-entropy-driven materials provide a challenging aspect to design materials based on certain applications. Although transition and refractory metals endow a scope in terms of structural materials for harsh environments, the researchers extend their focus in designing and developing carbides from the group of IVB, VB, and VIB transition metals known as high entropy carbides (HECs) [122-125]. The most attractive features of HECs are their ability to persist in single-phase structures at extreme temperatures and local chemical environments. By the advantages of slow

diffusion kinetics and distorted lattices favor the HECs to provide thermal protection, improved strength and hardness, and better oxidation resistance. Furthermore, the HECs are defined as materials with ultra-high melting points (>3000 ^{0}C), which increase their demand in extreme operational conditions in structural applications such as rocket nozzles, and nuclear reactors. The plausible elements based on the vulnerability of the applications should have to be explored to develop high-entropy-driven carbides.

3.5.4. High Entropy Oxides

The rapid development of high entropy materials and their strong correlations between compositions and properties opens up a new window to study the prospects of these materials in the form of oxides. High entropy oxides (HEOs) are emerging branch of high entropy materials, which can fulfil the requirements in applications such as catalyst, dielectrics, and magnetic properties [126-131]. The distinct nature of anion and cation sublattices in HEOs bestow better solubilities and stabilizations. Although the field of research based on HEOs is in its inception, the understanding of developing the HEOs by means of thermal spraying and cold spraying is critical and challenging. The structural formation and properties of thermal spraying and cold spraying HEO coatings should have to be explored to expand their research for applications such as, catalysis, water splitting, thermal protection, supercapacitors, and thermoelectric and thermal barrier coatings. HEOs developed through arc-melting process had been proved for their magnetic [127,128] and energy storage [129,132] applications, and hence, the thermal-sprayed HEO coatings may provide a fascinating research topic in the near future.

3.5.4.1. High Entropy Composites Alloys

Metal matrix composites (MMCs) have widely been studied for many industrial applications due to their high hardness and excellent strength with optimum ductility and toughness [82,133,134]. Several secondary particles as reinforcement, typically ceramics, are incorporated into the metal matrix to enhance the inherent features of the composite structures that can be implemented in various industrial sectors. Considering the attractive properties attained through these composites, HEAs are used as a metal matrix with ceramic reinforcements (i.e., TiC, SiC, WC, Al_2O_3, TiN) developed through different techniques such as induction melting [75,135], plasma cladding [136],

microwave processing [87,88], spark plasma sintering (SPS) [137-139] and additive manufacturing (AM) [140,141]. Thus, a new family of MMCs arose in the field of HEAs known as high entropy composite alloys (HECAs). Together with thermal spraying and cold spraying technologies, HECAs can provide an excellent opportunity to break the bottleneck problems associated with wear and corrosion. One such example is the fatigue fracture (due to cyclic loading of bubble implosions) and plastic deformation failures when exposed to cavitation erosion damage. Therefore, the concurrent high strength and toughness interactions are significant in controlling cavitation damage due to bubble implosions. To the best of the authors' knowledge, only one group investigated the cavitation erosion-corrosion response on AlCoCrFeNi HEAs fabricated through HVOF technique [64]. HEA coatings showed 3.5 times lower cumulative mass loss (CML) than conventional steel (06Cr13Ni5Mo) after 24 hours of testing. The presence of BCC phases in HEA coatings enhance the hardness due to solid solution strengthening that controls damage due to bubble implosions. Lamellar spalling and interlaminar cracks are the dominant damage mechanisms observed after testing. Different HECAs can be designed by tailoring the chemical compositions and with the addition of reinforcement that can be fabricated using deposition techniques depending on the vulnerability of severe degradations.

3.5.5. Perspectives on Other Applications of HEA Coatings

Varying the chemical compositions opens new possibilities for potential benefits of HEAs in their multifunctional roles including catalysis and energy applications. The governing factors, including high configurational entropy and severe lattice distortions, enable HEAs to perform as a catalyst. The most promising attribute for HEAs is the meticulous material selections and their property tuning by varying the chemical compositions in atomic length, which helps to modify the crystal structures to mold them as a feasible catalysis. Employing the established thermal spraying manufacturing routes is considered a top-notch approach to fabricate catalytic HEAs. However, to the best of the author's knowledge, the utilization of HEAs through thermal spraying is still lacking. Being the vast compositional space of HEAs, designing new-generation catalytic HEA coatings would be challenging and require high-throughput screening using computational tools such as machine learning.

Recent studies show the potential features of arc melted HEAs to use in orthopedic implant applications in terms of hip and knee replacements [142-146]. Although the demand for bio implant materials is increasing due to automobile accident rates and sports injuries, premature failure due to localized corrosion in a highly aggressive physiological environment becomes a long-term issue for using traditional materials. The presence of toxic ions is another problem in conventional materials such as stainless steel, which leads to allergic reactions to the human body. The distinguished microstructural features of HEAs, along with anti-wear and anti-corrosion properties, endows the possibility of HEAs to use as a novel type of bioimplant materials [147,148]. Since the field of research is highly unexplored in terms of HEA coatings, the potential benefits of HEAs can provide a helpful hand to develop bioimplant coatings with improved wear and corrosion resistance, excellent strength-weight ratio, and biocompatibility. The perspective for future study associated with thermal spray HEA coatings would invigorate the interests of researchers to focus extensively on the directions of orthopedic implants.

Radiation damage in the nuclear sector is another challenging area of research, where the structural material damages due to the high dose of radiation at high temperatures. The traditional materials for nuclear reactors are unable to overcome high dose neutron irradiations, which eventually results in material embrittlement, hardening, and failure. The salient features of HEAs with topological lattice distortion capability between constituent elements can be able to provide self-healing ability to encounter the high radiation dose. The findings of arc-melted HEAs showed an excellent irradiation response than traditional materials [149,150]. This expands the possibility of such a study in the field of HEA coatings through thermal spray manufacturing routes.

Thermal-sprayed high entropy alloy coating properties can be further enhanced through targeted strategies in order to create next-generation materials with unique properties. One of the main advantages of HEAs is that they provide numerous possibilities in designing alloys including the combinations of transition metals, refractory elements and ceramics. For achieving favorable phase formations and desired mechanical properties such as strength and toughness, selection of plausible alloying elements is paramount. Recently, researchers used the CALPHAD approach for designing numerous high entropy alloys with different variations of alloying

elements and predicted their phase formations, which in turn can identify the strengthening mechanisms of HEAs. For instance, Guo *et al.* [151] used CALPHAD approach coupled with experimentation results to design and develop precipitation strengthened $(FeCoNi)_{95}Al_{2.5}Ti_{5.}$ high entropy alloys. Thermo-Calc software with TTN18 database was used to predict the phase formations of the HEA, as shown in Figure 3.18. Their studies validated that the formation of Ni_3Al based γ' nano precipitates was found for the HEAs using Thermo-Calc software and transmission electron microscopy. Indeed, CALPHAD has been emerged as a profound tool for predicting the phases, microstructure, and materials properties for numerous high entropy alloy systems. CALPHAD in conjunction with machine learning approach is an emerging trend for designing numerous plausible HEA systems that can pave the way for better mechanical properties. Such approach corroborates the research significance in predicting the alloying elements in thermal sprayed HEA coatings. However, the evolution of oxide phases is a common microstructural artefact in thermal sprayed HEA coatings due to their oxygen sensitive elements (typically Al, Cr, Mo, Fe, etc.). Therefore, there is strong need to perform research in predicting the oxide formations using CALPHAD aided approach for high entropy alloys by means of thermal spraying technologies.

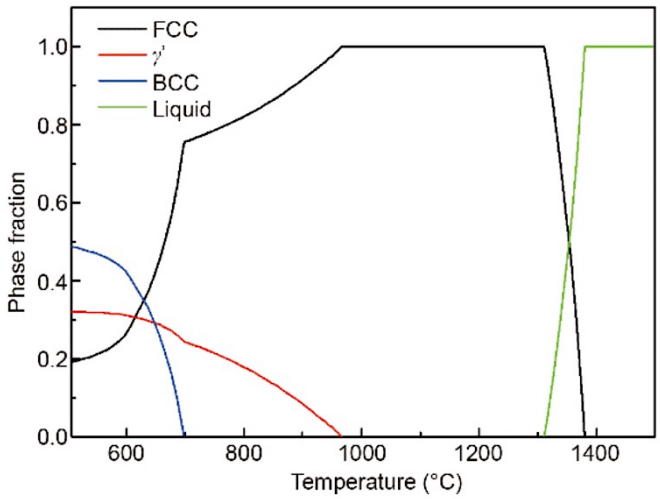

Figure 3.16 Phase diagram of (FeCoNi)92Al2.5Ti5.5 high entropy alloys using Thermo-Calc software (CALPHAD approach) [152].

3.6. Conclusions

High entropy alloys have been shown to have remarkable mechanical properties and considerable potential for future applications. Thermally sprayed high entropy alloys have been advantageous in many ways as compared to traditional alloys or conventional coatings. HEA coatings can be used in many industries due to their excellent wear, friction, corrosion, oxidation behavior and are now replacing some old alloys and techniques eventually. HEA feedstocks can be produced by various methods in which mechanical alloying is a technique followed by researchers in the laboratories. In contrast, gas atomization is the most widely used technique due to the homogeneity of the alloy. Blending is the simplest of all but is not used widely due to the poor composition of the alloy and non-uniform properties. HEAs have been produced as bulk alloys for a long time, but recent advancements of technology have enabled them to be thermally sprayed as a coating over a substrate. Thermal spraying of HEAs is done over a wide range of temperatures depending on the application. High-temperature processes such as APS and HVOF have been shown to develop a harder coating due to oxides and other temperature-induced phases. Cold spray is a low-temperature process that produces a softer coating, and metals with a lower melting point can be sprayed by using this technique easily. However, a study reported that cold sprayed AlCoCrFeNiTi showed higher average hardness than other high-temperature deposition techniques. Cold sprayed HEAs tend to develop a stronger bonding with the substrate due to high velocity impact on to the surface causing mechanical interlocking. Different spraying techniques and process parameters give rise to other mechanical properties and microstructural changes. High-temperature spraying produces higher porosities due to lower particle speeds such as APS. These defects can be treated via post-processing, such as annealing. In addition to that, alloying elements also play an essential role in determining the properties of HEA. HEAs have been showing excellent tribological characteristics from time to time. These coatings offer great potential to be used as wear-resistant coatings. The ability of these coatings to change properties according to the spray parameters make it highly viable to be used for varied applications. Similar layers show different wear and friction behavior when developed via other processes. Coatings produced via high-temperature processes tend to offer higher wear resistance due to oxide formation at elevated temperatures. Softer coatings have lower wear resistance but better friction behavior, possibly due to debris formation. HEA provide

good corrosion resistance due to stable oxides formation. On the contrary, the defects and porosities affect the corrosion behavior negatively. Alongside corrosion, the oxidation resistance of HEAs was also studied to be better than those compared to conventional alloys. Ideally, high-temperature processes should provide a better oxidation resistance due to the formation of an oxide layer protecting the surface. But certain coating develops pores which impact the oxidation resistance negatively. Owing to HEAs outstanding mechanical and tribological properties, a wide range of industries could benefit from these new species of alloys. The aerospace sector will primarily profit from HEAs. They provide the perfect set of characteristics like wear resistance and the ability to withstand erosion at high temperatures beneficial for harsh environments such as gas turbine engines. The lightweight, high strength HEA coatings are the essential factor for many industrial components that can provide energy consumption, better functionality and improved service life. Material degradation can be a harmful cause in the marine sector. HEAs being resistant to corrosion and degradation, can find their space in marine industries. While HEAs have shown promising potential for future applications, environmental awareness is also crucial to study. Production and recycling of HEA coatings should be given importance alongside its industrial benefits. Studies must be performed on how to extract metals elements required for HEA feedstocks and extract those out of wasted HEA feedstocks. The cost-effectiveness of thermal spraying of HEAs is also an important point to be noted.

References:

1. B. Cantor, I. Chang, P. Knight, A. Vincent, Microstructural development in equiatomic multicomponent alloys, Mater. Sci. Eng., A, (2004), 375, p 213-218

2. J.W. Yeh, S.K. Chen, S.J. Lin, J.Y. Gan, T.S. Chin, T.T. Shun, C.H. Tsau, S.Y. Chang, Nanostructured high-entropy alloys with multiple principal elements: novel alloy design concepts and outcomes, Adv. Eng. Mater., (2004), 6(5), p 299-303

3. M.-H. Tsai, J.-W. Yeh, High-entropy alloys: a critical review, Mater. Res. Lett., (2014), 2(3), p 107-123

4. S. Gorsse, J.-P. Couzinié, D.B. Miracle, From high-entropy alloys to complex concentrated alloys, Comptes Rendus Physique, (2018), 19(8), p 721-736

5. D.B. Miracle, Critical Assessment 14: High entropy alloys and their development as structural materials, Mater. Sci. Technol., (2015), 31(10), p 1142-1147

6. B.S. Murty, J.-W. Yeh, S. Ranganathan, High-entropy alloys, Elsevier, New York, 2014, p 388

7. O.N. Senkov, G.B. Wilks, D.B. Miracle, C.P. Chuang, P.K. Liaw, Refractory high-entropy alloys, Intermetallics, (2010), 18(9), p 1758-1765

8. M.C. Gao, J.-W. Yeh, P.K. Liaw, Y. Zhang, High-entropy alloys: fundamentals and applications, 1st ed., Springer, Germany, 2016, p 516

9. D. Tejero-Martin, M.R. Rad, A. McDonald, T. Hussain, Beyond traditional coatings: A review on thermal-sprayed functional and smart coatings, J. Therm. Spray Technol., (2019), 28(4), p 598-644

10. H. Zhang, X. Chen, Y. Gong, Y. Tian, A. McDonald, H. Li, In-situ SEM observations of ultrasonic cavitation erosion behavior of HVOF-sprayed coatings, Ultrason. Sonochem., (2020), 60, p 104760

11. S.A. Galedari, A. Mahdavi, F. Azarmi, Y. Huang, A. McDonald, A comprehensive review of corrosion resistance of thermally-sprayed and thermally-diffused protective coatings on steel structures, J. Therm. Spray Technol., (2019), 28(4), p 645-677

12. A. Meghwal, A. Anupam, B. Murty, C.C. Berndt, R.S. Kottada, A.S.M. Ang, Thermal

spray high-entropy alloy coatings: A review, J. Therm. Spray Technol., (2020), 29, p 857-893

13. J. Li, Y. Huang, X. Meng, Y. Xie, A review on high entropy alloys coatings: fabrication processes and property assessment, Adv. Eng. Mater., (2019), 21(8), p 1900343

14. M. Löbel, T. Lindner, C. Kohrt, T. Lampke, Processing of AlCoCrFeNiTi high entropy alloy by atmospheric plasma spraying, IOP Conference Series: Materials Science and Engineering, March 16-17, 2017 (Germany), IOP Publishing, 2017, p 012015

15. L. Tian, Z. Feng, W. Xiong, Microstructure, microhardness, and wear resistance of AlCoCrFeNiTi/Ni60 coating by plasma spraying, Coatings, (2018), 8(3), p 112

16. A. Anupam, S. Kumar, N.M. Chavan, B.S. Murty, R.S. Kottada, First report on cold sprayed AlCoCrFeNi high-entropy alloy and its isothermal oxidation, J. Mater. Res., (2019), 34(5), p 796-806

17. K.-C. Cheng, J.-H. Chen, S. Stadler, S.-H. Chen, Properties of atomized AlCoCrFeNi high-entropy alloy powders and their phase-adjustable coatings prepared via plasma spray process, Appl. Surf. Sci., (2019), 478, p 478-486

18. S.S. Ghazi, K. Ravi, Phase-evolution in high entropy alloys: Role of synthesis route, Intermetallics, (2016), 73, p 40-42

19. Y.K. Mu, Y.D. Jia, L. Xu, Y.F. Jia, X.H. Tan, J. Yi, G. Wang, P.K. Liaw, Nano oxides reinforced high-entropy alloy coatings synthesized by atmospheric plasma spraying, Mater. Res. Lett., (2019), 7(8), p 312-319

20. L.-H. Tian, W. Xiong, C. Liu, S. Lu, M. Fu, Microstructure and wear behavior of atmospheric plasma-sprayed AlCoCrFeNiTi high-entropy alloy coating, J. Mater. Eng. Perform., (2016), 25(12), p 5513-5521

21. B. Zhu, S. Alavi, C. Cheng, H. Sun, H. Zhao, K.S. Kim, J. Mostaghimi, Y. Zou, Fast and High-Throughput Synthesis of Medium-and High-Entropy Alloys Using Radio Frequency Inductively Coupled Plasma, Adv. Eng. Mater., (2021), 23(3), p 2001116

22. R. Tu, N. Li, Q. Li, S. Zhang, L. Zhang, T. Goto, Microstructure and mechanical properties of B4C–HfB2–SiC ternary eutectic composites prepared by arc melting, J. Eur. Ceram. Soc., (2016), 36(4), p 959-966

23. O. Cedillos-Barraza, D. Manara, K. Boboridis, T. Watkins, S. Grasso, D.D. Jayaseelan, R.J. Konings, M.J. Reece, W.E. Lee, Investigating the highest melting temperature materials: A laser melting study of the TaC-HfC system, Scientific reports, (2016), 6(1), p 1-11

24. A.S.M. Ang, C.C. Berndt, M.L. Sesso, A. Anupam, S. Praveen, R.S. Kottada, B. Murty, Plasma-sprayed high entropy alloys: microstructure and properties of AlCoCrFeNi and MnCoCrFeNi, Metall. Mater. Trans. A, (2015), 46(2), p 791-800

25. J. Davis, Handbook of Thermal Spray Technology, , 1 ed., ASM International, Materials Park, 2004

26. A. Sharma, High Entropy Alloy Coatings and Technology, Coatings, (2021), 11(4), p 372

27. R.W. Smith, R. Knight, Thermal spraying I: Powder consolidation—From coating to forming, JOM, (1995), 47(8), p 32-39

28. P. Bengtsson, T. Johannesson, Characterization of microstructural defects in plasma-sprayed thermal barrier coatings, J. Therm. Spray Technol., (1995), 4(3), p 245-251

29. R. Huang, H. Fukanuma, Study of the influence of particle velocity on adhesive strength of cold spray deposits, J. Therm. Spray Technol., (2012), 21(3-4), p 541-549

30. G. Di Girolamo, M. Alfano, L. Pagnotta, A. Taurino, J. Zekonyte, R. Wood, On the early stage isothermal oxidation of APS CoNiCrAlY coatings, J. Mater. Eng. Perform., (2012), 21(9), p 1989-1997

31. M. Planche, H. Liao, C. Coddet, Oxidation control in atmospheric plasma spraying coating, Surf. Coat. Technol., (2007), 202(1), p 69-76

32. Q. Wei, Z. Yin, H. Li, Oxidation control in plasma spraying NiCrCoAlY coating, Appl. Surf. Sci., (2012), 258(12), p 5094-5099

33. W.-L. Hsu, H. Murakami, J.-W. Yeh, A.-C. Yeh, K. Shimoda, On the study of thermal-sprayed Ni0. 2Co0. 6Fe0. 2CrSi0. 2AlTi0. 2 HEA overlay coating, Surf. Coat. Technol., (2017), 316, p 71-74

34. J. Alcala, F. Gaudette, S. Suresh, S. Sampath, Instrumented spherical micro-indentation of plasma-sprayed coatings, Materials Science and Engineering: A, (2001), 316(1-2), p

1-10

35. R. Neiser, M. Smith, R. Dykhuizen, Oxidation in wire HVOF-sprayed steel, J. Therm. Spray Technol., (1998), 7(4), p 537-545

36. G. Mauer, R. Vaßen, D. Stöver, Plasma and particle temperature measurements in thermal spray: approaches and applications, J. Therm. Spray Technol., (2011), 20(3), p 391-406

37. B. Gludovatz, A. Hohenwarter, D. Catoor, E.H. Chang, E.P. George, R.O. Ritchie, A fracture-resistant high-entropy alloy for cryogenic applications, Science, (2014), 345(6201), p 1153-1158

38. A. Anupam, R.S. Kottada, S. Kashyap, A. Meghwal, B. Murty, C. Berndt, A. Ang, Understanding the microstructural evolution of high entropy alloy coatings manufactured by atmospheric plasma spray processing, Appl. Surf. Sci., (2020), 505, p 144117

39. P. Shi, Y. Yu, N. Xiong, M. Liu, Z. Qiao, G. Yi, Q. Yao, G. Zhao, E. Xie, Q. Wang, Microstructure and tribological behavior of a novel atmospheric plasma sprayed AlCoCrFeNi high entropy alloy matrix self-lubricating composite coatings, Tribology International, (2020), 151, p 106470

40. J. Lehtonen, H. Koivuluoto, Y. Ge, A. Juselius, S.-P. Hannula, Cold gas spraying of a high-entropy CrFeNiMn equiatomic alloy, Coatings, (2020), 10(1), p 53

41. S. Yin, W. Li, B. Song, X. Yan, M. Kuang, Y. Xu, K. Wen, R. Lupoi, Deposition of FeCoNiCrMn high entropy alloy (HEA) coating via cold spraying, Journal of Materials Science & Technology, (2019), 35(6), p 1003-1007

42. S. Matthews, Shrouded plasma spray of Ni–20Cr coatings utilizing internal shroud film cooling, Surf. Coat. Technol., (2014), 249, p 56-74

43. M. Morks, C. Berndt, Corrosion and oxidation properties of NiCr coatings sprayed in presence of gas shroud system, Appl. Surf. Sci., (2010), 256(13), p 4322-4327

44. Z. Salhi, D. Klein, P. Gougeon, C. Coddet, Development of coating by thermal plasma spraying under very low-pressure condition< 1 mbar, Vacuum, (2005), 77(2), p 145-150

45. C. Wang, J. Yu, Y. Zhang, Y. Yu, Phase evolution and solidification cracking sensibility

in laser remelting treatment of the plasma-sprayed CrMnFeCoNi high entropy alloy coating, Materials & Design, (2019), 182, p 108040

46. Y. Xu, W. Li, L. Qu, X. Yang, B. Song, R. Lupoi, S. Yin, Solid-state cold spraying of FeCoCrNiMn high-entropy alloy: an insight into microstructure evolution and oxidation behavior at 700-900° C, Journal of Materials Science & Technology, (2021), 68, p 172-183

47. W.-L. Hsu, Y.-C. Yang, C.-Y. Chen, J.-W. Yeh, Thermal sprayed high-entropy NiCo0. 6Fe0. 2Cr1. 5SiAlTi0. 2 coating with improved mechanical properties and oxidation resistance, Intermetallics, (2017), 89, p 105-110

48. L. Chen, K. Bobzin, Z. Zhou, L. Zhao, M. Oete, T. Königstein, Z. Tan, D. He, Wear behavior of HVOF-sprayed Al0. 6TiCrFeCoNi high entropy alloy coatings at different temperatures, Surf. Coat. Technol., (2019), 358, p 215-222

49. A. Vallimanalan, S.K. Babu, S. Muthukumaran, M. Murali, V. Gaurav, R. Mahendran, Corrosion behaviour of thermally sprayed Mo added AlCoCrNi high entropy alloy coating, Materials Today: Proceedings, (2020), 27, p 2398-2400

50. A. Yurkova, D. Hushchyk, A. Minitsky, Synthesis of High-Entropy AlNiCoFeCrTi Coating by Cold Spraying, Powder Metall. Met. Ceram., (2021), 59(11), p 681-694

51. T. Li, Y. Liu, B. Liu, W. Guo, L. Xu, Microstructure and Wear Behavior of FeCoCrNiMo0.2 High Entropy Coatings Prepared by Air Plasma Spray and the High Velocity Oxy-Fuel Spray Processes, Coatings, (2017), 7(9), p 151

52. P.K. Huang, J.W. Yeh, T.T. Shun, S.K. Chen, Multi-principal-element alloys with improved oxidation and wear resistance for thermal spray coating, Adv. Eng. Mater., (2004), 6(1-2), p 74-78

53. C.-C. Tung, J.-W. Yeh, T.-t. Shun, S.-K. Chen, Y.-S. Huang, H.-C. Chen, On the elemental effect of AlCoCrCuFeNi high-entropy alloy system, Mater. Lett., (2007), 61(1), p 1-5

54. M. Vaidya, G.M. Muralikrishna, B.S. Murty, High-entropy alloys by mechanical alloying: A review, J. Mater. Res., (2019), 34(5), p 664-686

55. T.M. Yue, H. Xie, X. Lin, H. Yang, G. Meng, Microstructure of laser re-melted

AlCoCrCuFeNi high entropy alloy coatings produced by plasma spraying, Entropy, (2013), 15(7), p 2833-2845

56. L. Wang, C. Chen, J. Yeh, S. Ke, The microstructure and strengthening mechanism of thermal spray coating NixCo0. 6Fe0. 2CrySizAlTi0. 2 high-entropy alloys, Mater. Chem. Phys., (2011), 126(3), p 880-885

57. P. Thirathipviwat, S. Sato, G. Song, J. Bednarcik, K. Nielsch, J. Jung, J. Han, A role of atomic size misfit in lattice distortion and solid solution strengthening of TiNbHfTaZr high entropy alloy system, Scripta Mater., (2022), 210, p 114470

58. L. Wang, F. Zhang, S. Yan, G. Yu, J. Chen, J. He, F. Yin, Microstructure evolution and mechanical properties of atmosphere plasma sprayed AlCoCrFeNi high-entropy alloy coatings under post-annealing, J. Alloys Compd., (2021), 872, p 159607

59. Y. Mu, L. Zhang, L. Xu, K. Prashanth, N. Zhang, X. Ma, Y. Jia, Y. Xu, Y. Jia, G. Wang, Frictional wear and corrosion behavior of AlCoCrFeNi high-entropy alloy coatings synthesized by atmospheric plasma spraying, Entropy, (2020), 22(7), p 740

60. L. Tian, M. Fu, W. Xiong, Microstructural Evolution of AlCoCrFeNiSi High-Entropy Alloy Powder during Mechanical Alloying and Its Coating Performance, Materials, (2018), 11(2), p 320

61. R.B. Nair, G. Perumal, A. McDonald, Effect of Microstructure on Wear and Corrosion Performance of Thermally-Sprayed AlCoCrFeMo High Entropy Alloy Coatings, Adv. Eng. Mater., (2022), 2101713, p

62. D.F. Rojas, H. Li, O.K. Orhan, C. Shao, J.D. Hogan, M. Ponga, Mechanical and microstructural properties of a CoCrFe0.75NiMo0.3Nb0.125 high-entropy alloy additively manufactured via cold spray, J. Alloys Compd., (2022), 893, p 162309

63. M. Löbel, T. Lindner, T. Mehner, L.-M. Rymer, T. Lampke, S. Björklund, S. Joshi, Microstructure and Corrosion Properties of AlCoCrFeNi High-Entropy Alloy Coatings Prepared by HVAF and HVOF, Thermal Spray 2021: Proceedings from the International Thermal Spray Conference (ITSC), H.J. O. Ozdemir, F. Toma, Ed., May 24-28, 2021 (Quebec City, Canada), ASM International, pp 416-421

64. Z. Wei, Y. Wu, S. Hong, J. Cheng, L. Qiao, J. Cheng, S. Zhu, Ultrasonic cavitation erosion behaviors of high-velocity oxygen-fuel (HVOF) sprayed AlCoCrFeNi high-

entropy alloy coating in different solutions, Surf. Coat. Technol., (2021), 409, p 126899

65. W.-B. Liao, Z.-X. Wu, W. Lu, M. He, T. Wang, Z. Guo, J. Huang, Microstructures and mechanical properties of CoCrFeNiMn high-entropy alloy coatings by detonation spraying, Intermetallics, (2021), 132, p 107138

66. F. He, Z. Wang, Q. Wu, J. Li, J. Wang, C. Liu, Phase separation of metastable CoCrFeNi high entropy alloy at intermediate temperatures, Scripta Mater., (2017), 126, p 15-19

67. A. Rogachev, S. Vadchenko, N. Kochetov, S. Rouvimov, D.Y. Kovalev, A. Shchukin, D. Moskovskikh, A. Nepapushev, A. Mukasyan, Structure and properties of equiatomic CoCrFeNiMn alloy fabricated by high-energy ball milling and spark plasma sintering, J. Alloys Compd., (2019), 805, p 1237-1245

68. A. Mahdavi, A. Pourasghar, Z. Chen, A. McDonald, Particle–Substrate Transient Thermal Evolution During Cold Spray Deposition Process: A Hybrid Heat Conduction Analysis, J. Therm. Spray Technol., (2020), 29(7), p 1609-1627

69. Y.T.R. Lee, H. Ashrafizadeh, G. Fisher, A. McDonald, Effect of type of reinforcing particles on the deposition efficiency and wear resistance of low-pressure cold sprayed metal matrix composite coatings, Surf. Coat. Technol., (2017), 324, p 190-200

70. A. Meghwal, A. Anupam, V. Luzin, C. Schulz, C. Hall, B.S. Murty, R.S. Kottada, C.C. Berndt, A.S.M. Ang, Multiscale mechanical performance and corrosion behaviour of plasma sprayed AlCoCrFeNi high-entropy alloy coatings, J. Alloys Compd., (2021), 854, p 157140

71. H. Li, J. Li, C. Yan, X. Zhang, D. Xiong, Microstructure and Tribological Properties of Plasma-Sprayed Al 0.2 Co 1.5 CrFeNi 1.5 Ti-Ag Composite Coating from 25 to 750° C, J. Mater. Eng. Perform., (2020), 29(3), p 1640-1649

72. T. Li, Y. Liu, B. Liu, W. Guo, L. Xu, Microstructure and Wear Behavior of FeCoCrNiMo0.2 High Entropy Coatings Prepared by Air Plasma Spray and the High Velocity Oxy-Fuel Spray Processes, Coatings, (2017), 7(9), p

73. T.-T. Shun, L.-Y. Chang, M.-H. Shiu, Microstructure and mechanical properties of multiprincipal component CoCrFeNiMox alloys, Mater. Charact., (2012), 70, p 63-67

74. Z. Wei, Y. Wu, S. Hong, J. Cheng, L. Qiao, J. Cheng, S. Zhu, Effect of WC-10Co on

cavitation erosion behaviors of AlCoCrFeNi coatings prepared by HVOF spraying, Ceram. Int., (2021), 47(11), p 15121-15128

75. H. Wu, S. Huang, H. Zhu, Z. Xie, Strengthening FeCrNiCu high entropy alloys via combining V additions with in-situ TiC particles, Scripta Mater., (2021), 195, p 113724

76. S. Zhu, Z. Zhang, B. Zhang, Y. Yu, Z. Wang, X. Zhang, B. Lu, Microstructure and Properties of Al2O3-13wt.%TiO2-Reinforced CoCrFeMnNi High-Entropy Alloy Composite Coatings Prepared by Plasma Spraying, J. Therm. Spray Technol., (2021), 30(3), p 772-786

77. G.E. Dieter, D.J. Bacon, Mechanical metallurgy, McGraw-hill New York, 1976

78. K.-k. Deng, X.-j. Wang, C.-j. Wang, J.-y. Shi, X.-s. Hu, K. Wu, Effects of bimodal size SiC particles on the microstructure evolution and fracture mechanism of AZ91 matrix at room temperature, Mater. Sci. Eng., A, (2012), 553, p 74-79

79. B. Jin, N. Zhang, S. Guan, Y. Zhang, D. Li, Microstructure and properties of laser re-melting FeCoCrNiAl0.5Six high-entropy alloy coatings, Surf. Coat. Technol., (2018), 349, p 867-873

80. M. Löbel, T. Lindner, T. Mehner, T. Lampke, Microstructure and wear resistance of AlCoCrFeNiTi high-entropy alloy coatings produced by HVOF, Coatings, (2017), 7(9), p 144

81. L. Chen, K. Bobzin, Z. Zhou, L. Zhao, M. Öte, T. Königstein, Z. Tan, D. He, Wear behavior of HVOF-sprayed Al0.6TiCrFeCoNi high entropy alloy coatings at different temperatures, Surf. Coat. Technol., (2019), 358, p 215-222

82. G. Munday, J. Hogan, A. McDonald, On the microstructure-dependency of mechanical properties and failure of low-pressure cold sprayed tungsten carbide-nickel metal matrix composite coatings, Surf. Coat. Technol., (2020), 396, p 125947

83. W.Z. Zhuang, G.R. Halford, Investigation of residual stress relaxation under cyclic load, Int. J. Fatigue, (2001), 23, p 31-37

84. R. McGrann, D. Greving, J. Shadley, E.F. Rybicki, T. Kruecke, B. Bodger, The effect of coating residual stress on the fatigue life of thermal spray-coated steel and aluminum, Surf. Coat. Technol., (1998), 108, p 59-64

85. Y. Oka, H. Ohnogi, T. Hosokawa, M. Matsumura, The impact angle dependence of erosion damage caused by solid particle impact, Wear, (1997), 203, p 573-579

86. Y. Oka, S. Mihara, T. Yoshida, Impact-angle dependence and estimation of erosion damage to ceramic materials caused by solid particle impact, Wear, (2009), 267(1-4), p 129-135

87. H.S. Grewal, R.B. Nair, H.S. Arora, Complex concentrated alloy bimodal composite claddings with enhanced cavitation erosion resistance, Surf. Coat. Technol., (2020), 392, p 125751

88. R.B. Nair, H.S. Arora, H.S. Grewal, Slurry erosion–corrosion of bimodal complex concentrated alloy composite cladding, Adv. Eng. Mater., (2020), 22(12), p 2000626

89. R.B. Nair, H.S. Arora, A.V. Boyana, P. Saiteja, H.S. Grewal, Tribological behavior of microwave synthesized high entropy alloy claddings, Wear, (2019), 436-437, p 203028

90. M. Sexsmith, T. Troczynski, Peel adhesion test for thermal spray coatings, J. Therm. Spray Technol., (1994), 3(4), p 404-411

91. S. Amada, T. Hirose, Influence of grit blasting pre-treatment on the adhesion strength of plasma sprayed coatings: fractal analysis of roughness, Surf. Coat. Technol., (1998), 102(1-2), p 132-137

92. C. Bolis, L. Berthe, M. Boustie, M. Arrigoni, S. Barradas, M. Jeandin, Physical approach to adhesion testing using laser-driven shock waves, J. Phys. D: Appl. Phys., (2007), 40(10), p 3155

93. S. Barradas, R. Molins, M. Jeandin, M. Arrigoni, M. Boustie, C. Bolis, L. Berthe, M. Ducos, Application of laser shock adhesion testing to the study of the interlamellar strength and coating–substrate adhesion in cold sprayed copper coating of aluminum, Surf. Coat. Technol., (2005), 197(1), p 18-27

94. R. Beydon, G. Bernhart, Y. Segui, Measurement of metallic coatings adhesion to fibre reinforced plastic materials, Surf. Coat. Technol., (2000), 126(1), p 39-47

95. M. Löbel, T. Lindner, T. Lampke, High-temperature wear behaviour of AlCoCrFeNiTi0.5 coatings produced by HVOF, Surf. Coat. Technol., (2020), 403, p 126379

96. P. Patel, S.A. Alidokht, N. Sharifi, A. Roy, K. Harrington, P. Stoyanov, R.R. Chromik, C. Moreau, Microstructural and Tribological Behavior of Thermal Spray CrMnFeCoNi High Entropy Alloy Coatings, J. Therm. Spray Technol., (2022), p

97. A. Silvello, P. Cavaliere, S. Yin, R. Lupoi, I. Garcia Cano, S. Dosta, Microstructural, Mechanical and Wear Behavior of HVOF and Cold sprayed High-Entropy Alloys (HEAs) Coatings, J. Therm. Spray Technol., (2022), p

98. R. Nair, H. Arora, S. Mukherjee, S. Singh, H. Singh, H. Grewal, Exceptionally high cavitation erosion and corrosion resistance of a high entropy alloy, Ultrason. Sonochem., (2018), 41, p 252-260

99. Y. Shi, B. Yang, P.K. Liaw, Corrosion-resistant high-entropy alloys: A review, Metals, (2017), 7(2), p 43

100. W. Wang, W. Qi, L. Xie, X. Yang, J. Li, Y. Zhang, Microstructure and corrosion behavior of (CoCrFeNi) 95Nb5 high-entropy alloy coating fabricated by plasma spraying, Materials, (2019), 12(5), p 694

101. A. Vallimanalan, S.P. Kumaresh Babu, S. Muthukumaran, M. Murali, V. Gaurav, R. Mahendran, Corrosion behaviour of thermally sprayed Mo added AlCoCrNi high entropy alloy coating, Materials Today: Proceedings, (2020), 27, p 2398-2400

102. A. Meghwal, A. Anupam, V. Luzin, C. Schulz, C. Hall, B. Murty, R.S. Kottada, C.C. Berndt, A.S.M. Ang, Multiscale mechanical performance and corrosion behaviour of plasma sprayed AlCoCrFeNi high-entropy alloy coatings, J. Alloys Compd., (2021), 854, p 157140

103. Q. Fan, C. Chen, C. Fan, Z. Liu, X. Cai, S. Lin, C. Yang, AlCoCrFeNi high-entropy alloy coatings prepared by gas tungsten arc cladding: Microstructure, mechanical and corrosion properties, Intermetallics, (2021), 138, p 107337

104. A. Aliyu, C. Srivastava, Microstructure-corrosion property correlation in electrodeposited AlCrFeCoNiCu high entropy alloys-graphene oxide composite coatings, Thin Solid Films, (2019), 686, p 137434

105. X.-W. Qiu, C.-G. Liu, Microstructure and properties of Al2CrFeCoCuTiNix high-entropy alloys prepared by laser cladding, J. Alloys Compd., (2013), 553, p 216-220

106. J. Wang, Y. Chen, Y. Zhang, W. Dai, Q. Xu, W. Li, Y. Liu, Corrosion and slurry erosion wear performances of coaxial direct laser deposited CoCrFeNiCu1-xMox high-entropy coatings by modulating the second-phase precipitation, Mater. Des., (2021), 212, p 110277

107. W.-L. Hsu, H. Murakami, H. Araki, M. Watanabe, S. Kuroda, A.-C. Yeh, J.-W. Yeh, A Study of NiCo0.6Fe0.2CrxSiAlTiyHigh-Entropy Alloys for Applications as a High-Temperature Protective Coating and a Bond Coat in Thermal Barrier Coating Systems, J. Electrochem. Soc., (2018), 165(9), p C524-C531

108. W.-L. Hsu, H. Murakami, J.-W. Yeh, A.-C. Yeh, K. Shimoda, On the study of thermal-sprayed Ni0.2Co0.6Fe0.2CrSi0.2AlTi0.2 HEA overlay coating, Surf. Coat. Technol., (2017), 316, p 71-74

109. Y. Xu, W. Li, L. Qu, X. Yang, B. Song, R. Lupoi, S. Yin, Solid-state cold spraying of FeCoCrNiMn high-entropy alloy: an insight into microstructure evolution and oxidation behavior at 700-900 °C, J. Mater. Sci. Technol., (2021), 68, p 172-183

110. O. Senkov, G. Wilks, D. Miracle, C. Chuang, P. Liaw, Refractory high-entropy alloys, Intermetallics, (2010), 18(9), p 1758-1765

111. C. Liu, H. Wang, S. Zhang, H. Tang, A. Zhang, Microstructure and oxidation behavior of new refractory high entropy alloys, J. Alloys Compd., (2014), 583, p 162-169

112. O.N. Senkov, D.B. Miracle, K.J. Chaput, J.-P. Couzinie, Development and exploration of refractory high entropy alloys—A review, J. Mater. Res., (2018), 33(19), p 3092-3128

113. B. Gorr, M. Azim, H.-J. Christ, T. Mueller, D. Schliephake, M. Heilmaier, Phase equilibria, microstructure, and high temperature oxidation resistance of novel refractory high-entropy alloys, J. Alloys Compd., (2015), 624, p 270-278

114. B. Gorr, F. Müller, M. Azim, H.-J. Christ, T. Müller, H. Chen, A. Kauffmann, M. Heilmaier, High-temperature oxidation behavior of refractory high-entropy alloys: effect of alloy composition, Oxid. Met., (2017), 88(3), p 339-349

115. F. Müller, B. Gorr, H.-J. Christ, J. Müller, B. Butz, H. Chen, A. Kauffmann, M. Heilmaier, On the oxidation mechanism of refractory high entropy alloys, Corros. Sci., (2019), 159, p 108161

116. B. Gorr, F. Mueller, H.-J. Christ, T. Mueller, H. Chen, A. Kauffmann, M. Heilmaier, High temperature oxidation behavior of an equimolar refractory metal-based alloy 20Nb20Mo20Cr20Ti20Al with and without Si addition, Journal of Alloys and Compounds, (2016), 688, p 468-477

117. B. Gorr, F. Mueller, H.-J. Christ, H. Chen, A. Kauffmann, R. Schweiger, D.V. Szabó, M. Heilmaier, Development of Oxidation Resistant Refractory High Entropy Alloys for High Temperature Applications: Recent Results and Development Strategy, TMS Annual Meeting & Exhibition, 2018, Springer, pp 647-659

118. B. Gorr, M. Azim, H.-J. Christ, H. Chen, D.V. Szabo, A. Kauffmann, M. Heilmaier, Microstructure evolution in a new refractory high-entropy alloy W-Mo-Cr-Ti-Al, Metallurgical and Materials Transactions A, (2016), 47(2), p 961-970

119. R.E. Chupp, R.C. Hendricks, S.B. Lattime, B.M. Steinetz, Sealing in Turbomachinery, Journal of Propulsion and Power, (2006), 22(2), p 313-349

120. K.R. Lim, K.S. Lee, J.S. Lee, J.Y. Kim, H.J. Chang, Y.S. Na, Dual-phase high-entropy alloys for high-temperature structural applications, J. Alloys Compd., (2017), 728, p 1235-1238

121. H.S. Grewal, R.M. Sanjiv, H.S. Arora, R. Kumar, A. Ayyagari, S. Mukherjee, H. Singh, Activation Energy and High Temperature Oxidation Behavior of Multi-Principal Element Alloy, Adv. Eng. Mater., (2017), 19(11), p 1700182

122. J. Zhou, J. Zhang, F. Zhang, B. Niu, L. Lei, W. Wang, High-entropy carbide: A novel class of multicomponent ceramics, Ceram. Int., (2018), 44(17), p 22014-22018

123. T.J. Harrington, J. Gild, P. Sarker, C. Toher, C.M. Rost, O.F. Dippo, C. McElfresh, K. Kaufmann, E. Marin, L. Borowski, P.E. Hopkins, J. Luo, S. Curtarolo, D.W. Brenner, K.S. Vecchio, Phase stability and mechanical properties of novel high entropy transition metal carbides, Acta Mater., (2019), 166, p 271-280

124. D. Liu, A. Zhang, J. Jia, J. Meng, B. Su, Phase evolution and properties of (VNbTaMoW) C high entropy carbide prepared by reaction synthesis, J. Eur. Ceram. Soc., (2020), 40(8), p 2746-2751

125. Y. Wang, T. Csanádi, H. Zhang, J. Dusza, M.J. Reece, R.Z. Zhang, Enhanced Hardness in High-Entropy Carbides through Atomic Randomness, Advanced Theory and

Simulations, (2020), 3(9), p 2000111

126. B.L. Musicó, D. Gilbert, T.Z. Ward, K. Page, E. George, J. Yan, D. Mandrus, V. Keppens, The emergent field of high entropy oxides: Design, prospects, challenges, and opportunities for tailoring material properties, APL Materials, (2020), 8(4), p 040912

127. R. Witte, A. Sarkar, R. Kruk, B. Eggert, R.A. Brand, H. Wende, H. Hahn, High-entropy oxides: An emerging prospect for magnetic rare-earth transition metal perovskites, Physical Review Materials, (2019), 3(3), p 034406

128. A. Mao, H.-Z. Xiang, Z.-G. Zhang, K. Kuramoto, H. Zhang, Y. Jia, A new class of spinel high-entropy oxides with controllable magnetic properties, J. Magn. Magn. Mater., (2020), 497, p 165884

129. Q. Wang, A. Sarkar, Z. Li, Y. Lu, L. Velasco, S.S. Bhattacharya, T. Brezesinski, H. Hahn, B. Breitung, High entropy oxides as anode material for Li-ion battery applications: A practical approach, Electrochem. Commun., (2019), 100, p 121-125

130. S.H. Albedwawi, A. AlJaberi, G.N. Haidemenopoulos, K. Polychronopoulou, High entropy oxides-exploring a paradigm of promising catalysts: A review, Materials & Design, (2021), p 109534

131. S. Zhou, Y. Pu, Q. Zhang, R. Shi, X. Guo, W. Wang, J. Ji, T. Wei, T. Ouyang, Microstructure and dielectric properties of high entropy Ba (Zr0. 2Ti0. 2Sn0. 2Hf0. 2Me0. 2) O3 perovskite oxides, Ceram. Int., (2020), 46(6), p 7430-7437

132. A. Sarkar, L. Velasco, D. Wang, Q. Wang, G. Talasila, L. de Biasi, C. Kübel, T. Brezesinski, S.S. Bhattacharya, H. Hahn, B. Breitung, High entropy oxides for reversible energy storage, Nat. Commun., (2018), 9(1), p 3400

133. S.T. Dehaghani, A. Dolatabadi, A. McDonald, Thermally sprayed metal matrix composite coatings as heating systems, Appl. Therm. Eng., (2021), 196, p 117321

134. T.W. Clyne, P.J. Withers, An Introduction to Metal Matrix Composites, Cambridge University Press, 1993

135. S. Riva, A. Tudball, S. Mehraban, N.P. Lavery, S.G.R. Brown, K.V. Yusenko, A novel High-Entropy Alloy-based composite material, J. Alloys Compd., (2018), 730, p 544-551

136. S. Zhu, Y. Yu, B. Zhang, Z. Zhang, X. Yan, Z. Wang, Microstructure and wear behaviour of in-situ TiN-Al2O3 reinforced CoCrFeNiMn high-entropy alloys composite coatings fabricated by plasma cladding, Mater. Lett., (2020), 272, p 127870

137. Q.C. Fan, B.S. Li, Y. Zhang, The microstructure and properties of (FeCrNiCo)AlxCuy high-entropy alloys and their TiC-reinforced composites, Materials Science and Engineering: A, (2014), 598, p 244-250

138. E. Colombini, M. Lassinantti Gualtieri, R. Rosa, F. Tarterini, M. Zadra, A. Casagrande, P. Veronesi, SPS-assisted Synthesis of SICp reinforced high entropy alloys: reactivity of SIC and effects of pre-mechanical alloying and post-annealing treatment, Powder Metall., (2018), 61(1), p 64-72

139. Z. Li, X. Liu, K. Guo, H. Wang, B. Cai, F. Chang, C. Hong, P. Dai, Microstructure and properties of Ti(C, N)–TiB2–FeCoCrNiAl high-entropy alloys composite cermets, Materials Science and Engineering: A, (2019), 767, p 138427

140. G.M. Karthik, S. Panikar, G.D.J. Ram, R.S. Kottada, Additive manufacturing of an aluminum matrix composite reinforced with nanocrystalline high-entropy alloy particles, Materials Science and Engineering: A, (2017), 679, p 193-203

141. A. Amar, J. Li, S. Xiang, X. Liu, Y. Zhou, G. Le, X. Wang, F. Qu, S. Ma, W. Dong, Additive manufacturing of high-strength CrMnFeCoNi-based High Entropy Alloys with TiC addition, Intermetallics, (2019), 109, p 162-166

142. M. Todai, T. Nagase, T. Hori, A. Matsugaki, A. Sekita, T. Nakano, Novel TiNbTaZrMo high-entropy alloys for metallic biomaterials, Scripta Mater., (2017), 129, p 65-68

143. T. Hori, T. Nagase, M. Todai, A. Matsugaki, T. Nakano, Development of non-equiatomic Ti-Nb-Ta-Zr-Mo high-entropy alloys for metallic biomaterials, Scripta Mater., (2019), 172, p 83-87

144. T. Nagase, Y. Iijima, A. Matsugaki, K. Ameyama, T. Nakano, Design and fabrication of Ti–Zr-Hf-Cr-Mo and Ti–Zr-Hf-Co-Cr-Mo high-entropy alloys as metallic biomaterials, Materials Science and Engineering: C, (2020), 107, p 110322

145. D. Castro, P. Jaeger, A.C. Baptista, J.P. Oliveira, An overview of high-entropy alloys as biomaterials, Metals, (2021), 11(4), p 648

146. S. Gurel, A. Nazarahari, D. Canadinc, H. Cabuk, B. Bal, Assessment of biocompatibility of novel TiTaHf-based high entropy alloys for utility in orthopedic implants, Mater. Chem. Phys., (2021), 266, p 124573

147. G. Perumal, H.S. Grewal, M. Pole, L.V.K. Reddy, S. Mukherjee, H. Singh, G. Manivasagam, H.S. Arora, Enhanced biocorrosion resistance and cellular response of a dual-phase high entropy alloy through reduced elemental heterogeneity, ACS Applied Bio Materials, (2020), 3(2), p 1233-1244

148. J. Shittu, M. Pole, I. Cockerill, M. Sadeghilaridjani, L.V.K. Reddy, G. Manivasagam, H. Singh, H.S. Grewal, H.S. Arora, S. Mukherjee, Biocompatible High Entropy Alloys with Excellent Degradation Resistance in a Simulated Physiological Environment, ACS Applied Bio Materials, (2020), 3(12), p 8890-8900

149. M. Cusentino, M. Wood, R. Dingreville, Compositional and structural origins of radiation damage mitigation in high-entropy alloys, J. Appl. Phys., (2020), 128(12), p 125904

150. D. Patel, M.D. Richardson, B. Jim, S. Akhmadaliev, R. Goodall, A.S. Gandy, Radiation damage tolerance of a novel metastable refractory high entropy alloy V2. 5Cr1. 2WMoCo0. 04, J. Nucl. Mater., (2020), 531, p 152005

151. L. Guo, J. Gu, X. Gong, S. Ni, M. Song, CALPHAD aided design of high entropy alloy to achieve high strength via precipitate strengthening, Science China Materials, (2020), 63(2), p 288-299

152. J.-K. Xiao, H. Tan, Y.-Q. Wu, J. Chen, C. Zhang, Microstructure and wear behavior of FeCoNiCrMn high entropy alloy coating deposited by plasma spraying, Surf. Coat. Technol., (2020), 385, p 125430

153. L.M. Wang, C.C. Chen, J.W. Yeh, S.T. Ke, The microstructure and strengthening mechanism of thermal spray coating NixCo0.6Fe0.2CrySizAlTi0.2 high-entropy alloys, Mater. Chem. Phys., (2011), 126(3), p 880-885

154. A. Vallimanalan, S.P.K. Babu, S. Muthukumaran, M. Murali, R. Mahendran, V. Gaurav, S. Manivannan, Synthesis, characterisation and erosion behaviour of AlCoCrMoNi high entropy alloy coating, Materials Research Express, (2019), 6(11), p 116543

155. T. Li, Y. Liu, B. Liu, W. Guo, L. Xu, Microstructure and wear behavior of

FeCoCrNiMo0. 2 high entropy coatings prepared by air plasma spray and the high velocity oxy-fuel spray processes, Coatings, (2017), 7(9), p 151

156. Murty BS, Yeh JW, Ranganathan S, Bhattacharjee PP. High-entropy alloys. Elsevier; 2019 Mar 16.

Chapter

4. TRIBOLOGICAL RESPONSE OF AlCoCrFeMo HIGH ENTROPY ALLOY DEPOSITED VIA FLAME SPRAYING AND COLD SPRAYING: A COMPARATIVE EVALUATION

In this chapter…

The tribological studies between the flame sprayed and cold sprayed HEAs have been provided. The testing, characterization and data analysis was performed to understand the friction and wear behavior at varying loads and surface conditions.

4.1. Abstract

High entropy alloys (HEAs) are a promising class of advanced materials composed of multi-component elements that possess outstanding mechanical and corrosion properties, which enable their use in many industrial applications. However, limited studies have focused on the tribological behavior of HEAs fabricated by means of thermal spray technologies. In this study, AlCoCrFeMo equimolar HEAs were fabricated successfully using flame spraying and cold spraying techniques to determine the phase compositions, microstructures, properties, and sliding wear resistance. Scanning electron microscope (SEM), energy dispersive spectroscopy (EDS), X-ray diffraction (XRD), image analysis, and Vickers micro-hardness testing were used to characterize the coatings. The results show the existence of oxides in the flame sprayed HEA coatings due to in-flight oxidation, which led to noticeable increase in the porosity (2.8 ± 1%) compared to the cold sprayed HEA coatings (<1%). Oxide evolutions and body-centered cubic (BCC) phases improve the hardness of flame sprayed HEA coatings compared to that of cold sprayed coatings. The sliding performance was investigated at room temperature by varying the normal loads (i.e., 5N, 10N) with constant sliding speed (i.e., 3.1 cm/s). The cold sprayed coatings showed overall lower coefficient of friction (i.e., ~0.5) with numerous fluctuations compared to the flame sprayed coatings. However, the flame sprayed coatings showed improved wear resistance when compared to HEA deposited by means of cold spray. This correlated well with the observations of ex situ analysis, which showed greater material transfer and increased formation of debris on the cold sprayed coatings compared to the flame sprayed coatings. The results obtained in this study suggest that flame sprayed HEA materials are promising candidates for next-generation tribological interfaces under specific conditions, pointing to new materials designed with improved microstructural features and enhanced mechanical properties.

Keywords: Aerospace Materials, High Entropy Alloys, Interfacial Processes, Tribology, Cold Spray (CS), Flame Spray (FS)

4.2. Introduction

Over the years, the demand for materials that resist damage in extreme environments has been increasing with respect to advancement of aircraft engines and gas turbines. Traditional alloys based on one or two dominating elements have shown limitations in terms of the requirements for the aerospace sectors, in particular due to their limited efficacy to mitigate wear and corrosion challenges. Therefore, it is paramount to develop advanced materials with desirable properties, which enable them to withstand such extreme conditions. With the recent advancements in materials research, a novel class of metallic materials comprised of multiple elements known as "high entropy alloys (HEAs)" was coined in 2004, in the pioneering studies of Yeh *et al.* [1] and Cantor *et al.* [2]. Since the emergence of HEAs, the demand for these alloys has sparked considerable interest in the aerospace community due to their promising microstructural features and remarkable properties, which make them more suitable for extreme environments.

HEAs are alloys that contain five or more principal elements, each of which comprises between 5 at% and 35 at% of the alloy [1]. These alloys possess high configurational entropy exceeding 1.5R, where R is the gas constant ($8.3144\ \mathrm{J\ mol^{-1}K^{-1}}$), which enables the stabilization of face-centered cubic (FCC) or body-centered cubic (BCC) depending upon the explored chemical compositions [3]. For instance, the formation of FCC phase was found in CoCrFeMnNi high entropy alloys, which is one of the most extensively investigated compositions in both bulk materials and coatings [2]. However, the replacement of manganese (Mn) with aluminum (Al) promotes the evolution of BCC structure with high strength [4]. It has been argued that the difference in phase formations was determined by the concurrent interactions between high configurational entropy (ΔS_{conf}) and enthalpy of mixing (ΔH_{mix}) [5]. Nevertheless, distinct features, such as lattice distortion, sluggish diffusion and cocktail effects also benefit HEAs with unique microstructural characteristics and desirable properties [6].

Several recent studies have shown exceptional properties of HEAs as coatings in tribological applications [5-10]. More specifically, HEAs fabricated by means of thermal spray coatings have been explored for their behavior under wear loading. For instance, Tian *et al.* [11] investigated the wear performance at varying temperatures

using Si_3N_4 counterface for atmospheric plasma sprayed (APS) AlCoCrFeNiTi HEA coatings on stainless steel 316L substrates. The authors reported that the reduction in wear rates was achieved for the coatings tested at different temperatures up to 900^0C compared to those of steel substrates. More recently, Liu *et al*. [12] explored the tribological performance of high-velocity air fuel (HVAF) sprayed CoCrFeNiTaAl HEA coatings and compared it to 304 stainless steel substrates at varying temperatures (room temperature to 400^0C). The wear rates for the HEA coatings increased as a function of temperature compared to 304 stainless steels because of the severe oxidative wear mechanism involved at elevated temperature. Another study by Zhou *et al*. [13] investigated sliding wear of $Al_{(1-x)}$ CoCrFeNiTix (x = 0 to 0.25) HEAs developed by high-velocity oxy-fuel (HVOF) techniques against a Si_3N_4 counterface. The authors found that with the increase in titanium (Ti) content, the coatings showed less damage during abrasive wear and consequently improved wear resistance was observed, which was attributed to the hard ordered phases.

While several studies showed improved wear performance of high entropy alloys developed using thermal spraying technologies, the high temperature involved in the process might result in undesirable phase transitions, and oxide contaminations [14]. These phases, contaminants and defects may alter wear mechanisms and consequently impact the wear performance of the HEA coatings. Thus, coating fabrication technologies that operate under low-temperature conditions may be more suitable to overcome some of these challenges. For instance, cold spraying is a solid-state deposition method, where the temperature is maintained far below the melting point of powder materials, and thus eliminates oxide contaminations and phase transformations [15]. As compared to high-temperature deposition technologies, cold spraying is capable of depositing powder particles at high velocities in the range between $300 \text{ and } 1200 \text{ m/s}$, which enable them to produce thick coatings with negligible porosity and oxide inclusions [16]. So far, the exploration of high entropy alloys using cold spraying techniques for wear performance has not been thoroughly investigated. A very recent study by Yin *et al.* [17] explored the wear performance of CoCrFeMnNi HEAs using cold spraying and laser cladding technologies. The authors found that the wear resistance was higher for cold spraying HEA coatings compared to that of the laser-cladded coatings. These studies confirm the potential benefits of thermal spraying HEA coatings in tribological applications. Since solid state thermal

spraying coupled with high entropy alloys is a new research direction in the development of coatings for extreme environments, novel alloy compositions should be explored in order to provide a protection against mechanical damage due to sliding wear.

The main purpose of this study was to fabricate AlCoCrFeMo HEA composition using flame spraying and cold spraying technologies in order to understand how the deposition temperature influences the microstructure, phase formations, and tribological characteristics. The novelty of this study is the comparative evaluation of AlCoCrFeMo high entropy alloys using flame spraying and cold spraying techniques on the tribological behavior, which has not been previously investigated. The wear performance of the cold sprayed and flame sprayed AlCoCrFeMo HEA coatings were examined against alumina counter balls at varying normal loads (i.e., 5 N and 10 N). Ex-situ analysis was performed on the worn surfaces and counterface using scanning electron microscope (SEM) and elemental dispersive spectroscopy (EDS) analysis in order to determine the wear mechanism (tribofilm formations, transfer film formations and wear debris) of the developed coatings.

4.3. Materials and Methods

4.3.1. Preparation of coatings

Mechanically alloyed AlCoCrFeMo high entropy alloy composition was used as a feedstock powder in this study (ABM Nano LLC, Missouri, TX, USA). The nominal composition of AlCoCrFeMo HEA is shown in Table 4.1. Furthermore, the morphology of the HEA powders is shown in Fig. 4.1. It is evident that the powder particles appear irregular in morphologies with particle agglomerations. This can be attributed to the repeated welding and fracturing of powder particles during mechanical alloying. The size distribution of HEA feedstock powders after mechanical alloying was $-30 + 3\,\mu m$ (3 to 30 μm). The chemical composition obtained for the mechanically alloyed HEA powders closely matches the nominal composition, as listed in Table 4.1.

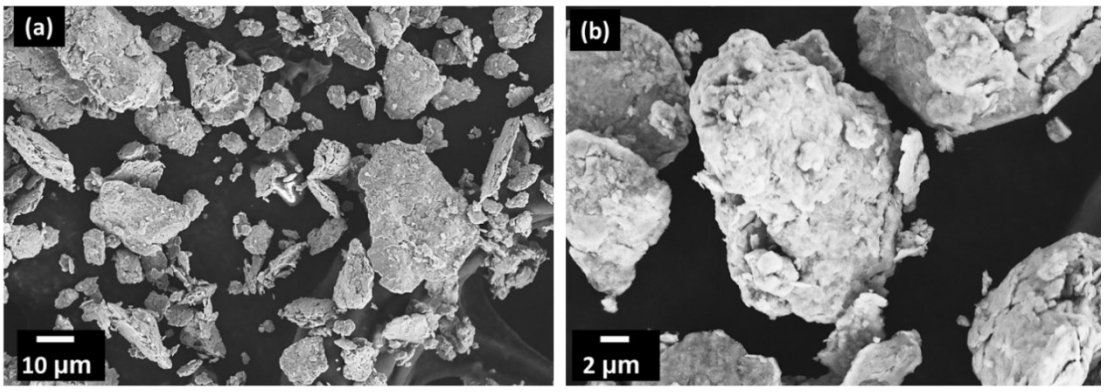

Figure 4.1 Scanning electron microscope of AlCoCrFeMo high entropy alloy feedstock powders.

Table 4.1 Nominal and feedstock composition of AlCoCrFeMo high entropy alloy powder (at%).

Composition	Al	Co	Cr	Fe	Mo
Nominal	20	20	20	20	20
Feedstock	20.5 ± 2.1	19.2 ± 0.9	19.4 ± 0.4	20.4 ± 0.8	20.5 ± 1.1

Commercially available low carbon steel was used as substrates in this study. Prior to deposition of HEA powders, the substrates were roughened using #24-grit alumina (Manus Abrasive Systems Inc., Edmonton, AB, Canada) in order to enhance the surface roughness and to provide better adhesion of coatings with the substrates. The AlCoCrFeMo HEA powders were deposited using portable low-pressure cold spray system (SST series P, CenterLine Ltd., Windsor, ON, Canada). Compressed air was used as a working media for the coating deposition. Depositions were carried out using a constant gas temperature and gas pressure of 450 ^{0}C and 92 psig, respectively. The process parameters are summarized in Table 4.2. For high-temperature deposition, an oxy-acetylene flame spray torch (6PII, Oerlikon Metco, Westbury, NY, USA) equipped with a volumetric powder feeder (5MPE, Oerlikon Metco, Westbury, NY, USA) was utilized for HEA deposition. Argon gas was used as a carrier gas to transfer the HEA powders to spray torch to deposit the coatings. The deposition parameters listed in Table 4.3 were selected based on previous trials performed by the authors of this manuscript and the details can be found elsewhere [20,23]. In both cases, the, coating depositions were manipulated using a programmable robot (HP-20, Motoman,

Yaskawa Electric Corp., Waukegan, IL, USA) to ensure uniform and repeatable deposition of the coatings. At least three samples were fabricated to ensure reproducibility of the deposition process.

Table 4.2 Process parameters for cold sprayed AlCoCrFeMo high entropy alloy coating.

Cold spraying parameters	Values
Accelerating gas (m/s)	Compressed air
Pre-heating temperature (^{0}C)	450
Gas pressure (psig)	92
Transverse speed (mm/s)	5
Stand-off distance (mm)	5
Increment size (µm)	3000

Table 4.3 Process parameters for flame sprayed AlCoCrFeMo high entropy alloy coating.

Flame spray parameters	Values
Acetylene flow (m^3/h)	1.2
Oxygen flow (m^3/h)	1.92
Argon flow (m^3/h)	0.56
Torch velocity (mm/s)	350
Stand-off distance (mm)	177
Particle concentration (ppm)	5000
Increment size (mm)	3
Number of passes	4

4.3.2. Microstructural and mechanical characterization

Microstructural and mechanical characterizations of the HEA coatings were carried out on the cross-sectional samples. The cross-sectional samples were cold mounted using epoxy resin and cured for 24 hours. The samples were polished using 400#, 600#, 800#, 1000#, and 1200# grit silicon carbide papers (LECO, Mississauga, ON, Canada). Final polishing was performed using 3 µm and 1 µm diamond slurry suspensions (LECO, Mississauga, ON, Canada). The samples were cleaned with

alcohol and acetone prior to microstructural investigations. A scanning electron microscope (SEM) (Zeiss Sigma 300 VP-FE, Carl Zeiss Canada Ltd., Toronto, ON, Canada) equipped with energy dispersive spectroscopy (EDS) in backscattered mode, and a working voltage of 15 kV, was used to analyze the microstructure features of the HEA coatings. At least ten micrographs (n =10) were captured in order to determine the average porosity by using image analysis (ImagePro, Media Cybernetics, Bethesda, MD, USA). X-ray diffraction (XRD) (Ultima IV diffractometer Rigaku, Akishima-Shi, TYO, Japan) was conducted at a scanning rate of 2 deg/min with a scan range of 30^0 to 90^0 using Cu-Kα radiation (λ = 1.546 Å) on the coating surfaces. The phase identification was done using the Diffrac.Eva software. Coating's hardness was measured using Vicker hardness tester (VH1102 Vickers hardness tester, Buehler Wilson, Lake Bluff, IL, USA). The indentations were made in accordance with the ASTM Standard E384 [18] with a load of 300 g and a dwell time of 15 s. At least 30 indents (n = 30) were made for all the coatings to obtain the average micro-hardness.

4.3.3. Tribological testing and surface characterization

Tribology tests were performed on a ball-on-flat (reciprocating) configuration using an (Anton Paar TriTec SA, Corcelles, NE, Switzerland) tribometer with parameters established by this research group which were based on the capability of the equipment. The normal loads were varied between 5N and 10N and the total number of cycles was 5000 (i.e., total sliding distance was 100 m). The sliding speed kept constant at 3.1 cm/s (equal to 1 Hz frequency) with a sliding length of 10 mm. The tests were employed at room temperature with humidity maintained between 18% and 22% using desiccants throughout the tests. Alumina (Al_2O_3) ball with a diameter of 6.35 mm was used as the counter face for testing. The sliding wear parameters are shown in Table 4.4.

Table 4.4 Sliding wear test parameters for cold and flame sprayed AlCoCrFeMo high entropy alloy coating.

Sliding wear parameters	Values
Load	5 N and 10 N
Frequency	1 Hz
Amplitude / track length	10 mm
Velocity / sliding speed	3.1 cm/s

Cycles	5000
Sliding distance	100 m
Counter face	Al_2O_3 (alumina ball)
Counter face diameter	6.35 mm
Temperature	25^O C to 28^O C
Relative humidity	18% to 22%

The wear depth measurement was performed on the confocal laser microscope (Olympus LEXT 4000, Houston, USA) along with the optical imaging of the wear tracks and the counter faces. The surface roughness values for the unpolished and polished cold sprayed HEA coatings were around 8.17 ± 0.12 µm and 1.27 ± 0.3 µm, respectively, whereas for the flame sprayed HEA coatings showed approximately 6.81 ± 0.5 µm and 1.67 ± 0.2 µm for unpolished and polished surface coatings. The ex-situ analysis on wear tracks were conducted using field emission scanning electron microscope (OxfordSU3500, Hitachi, Japan) equipped with energy dispersive spectroscopy to determine the involved wear mechanism in both the HEA coatings.

4.4. Results

4.4.1. Microstructure of HEA coatings

Figure 4.2 shows the XRD spectra of HEA coatings and feedstocks. As shown in the figure, the cold sprayed HEA coatings showed formation of BCC phases (i.e., AlCoCrFe-rich BCC1 and CrMo-rich BCC2 phases), where the flame sprayed HEA coatings showed major mixed oxide peaks (Al-rich oxides and spinel-type oxides (AB_2O_4; A = Fe/Mo and B = Al/Cr)) along with the formations of AlCrFe rich BCC1 and Mo-rich BCC2 phases. The weight percentage of spinel oxides were observed to be approximately 25.2 ± 2.5 wt% ($n = 3$), whilst the BCC1 and BCC2 phases weight fractions were observed to be around 46.5 ± 2.2 wt% and 31.5 ± 1.8 wt% . Similar observations with the appearance of spinel oxides were reported for air plasma sprayed AlCoCrFeNi HEA coatings [19]. It is apparent from the XRD profiles that the peaks of feedstock and cold sprayed HEA coatings closely matches, indicating no change in phase transition during cold spraying. Nevertheless, peaks for the flame sprayed HEA coatings showed slight shift to higher angles due to the oxide inclusions.

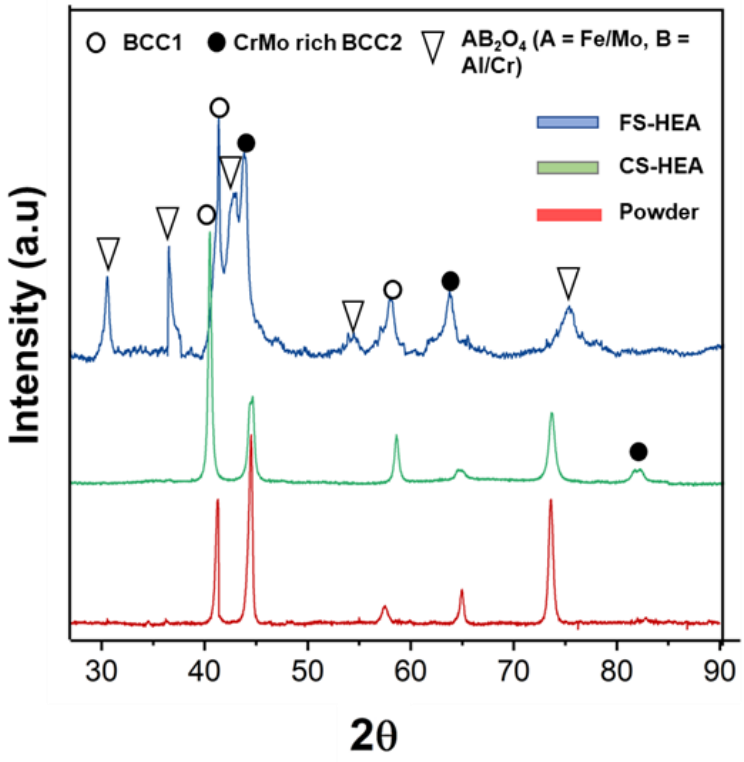

Figure 4.2 X-ray diffraction of feedstock powders, cold sprayed, and flame sprayed AlCoCrFeMo high entropy alloy coatings.

Backscattered cross-sectional SEM images of both the HEA coatings are shown in Fig. 4.3. Overall, the cold sprayed HEA coatings exhibited finer microstructure when compared to the flame sprayed HEA coatings (Fig. 4.3(a)). The average porosity obtained was less than 1%, which was mainly due to the consolidating effect of high-velocity impact of powder particles [16]. However, the different splat morphologies with mixed contrast regions were found for the flame sprayed HEA coatings. The oxide regions were more prominent in all the regions, which is mainly due to the oxidation in-flight during spraying. Different contrast regions that formed on the flame sprayed HEA coatings is likely depends on the process of melting powder particles of different sizes, which has been reported previously by Anupam *et al*. [4] and Nair *et al*. [20]. Numerous inter-lamellar cracks can be seen in the flame sprayed HEA coatings. Furthermore, the apparent porosity was approximately 2.8 ± 1 %, which was 65% higher than that of the cold sprayed HEA coatings.

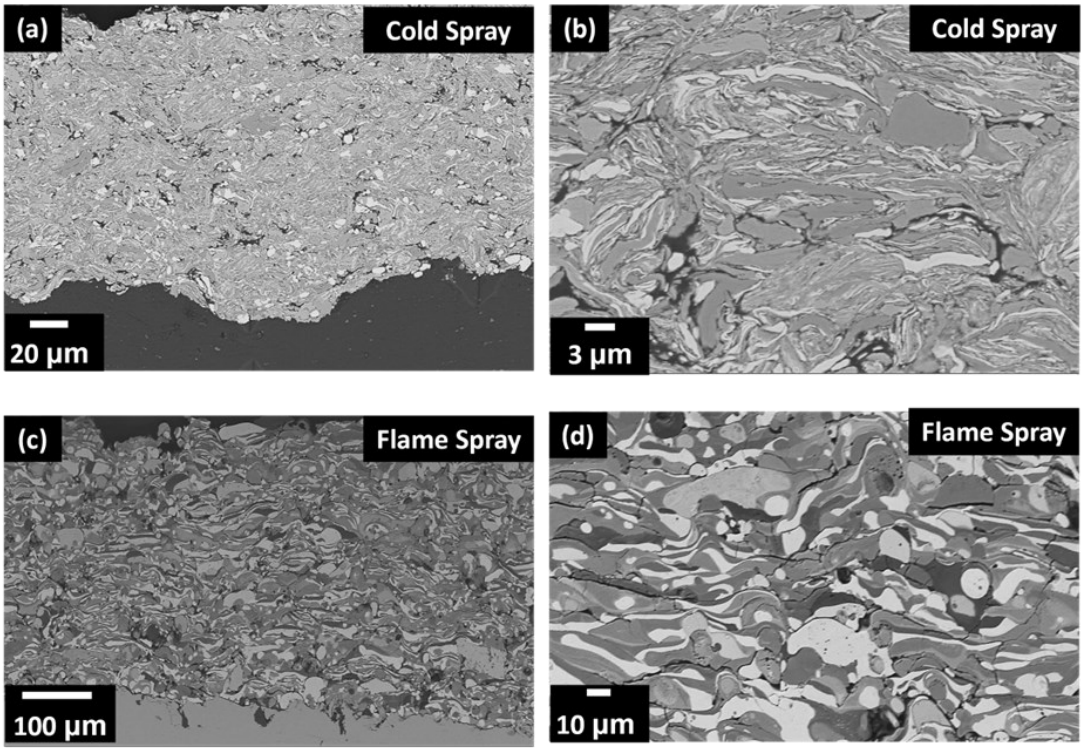

Figure 4.3 Scanning electron microscopy of (a) and (b) Cold sprayed, (c) and (d) Flame sprayed AlCoCrFeMo high entropy alloy coatings.

Figure 4.4 shows the elemental distribution mapping of both the HEA coatings and corresponding atomic percentages obtained for different regions (marked in Fig. 4.4b) of flame sprayed HEA coatings are shown in Fig. 4.5. It is apparent from the elemental mapping that the oxygen concentration in the cold sprayed HEA coatings was negligible, which closely matches the XRD results (Fig. 4.3). Regions corresponding to white and black was mainly comprised of Mo, and Al rich BCC phase regions (see Fig. 4.4). Flame sprayed HEA coatings, on the other hand, showed high concentrations of oxygen in multiple regions (see Fig. 4.4 and Fig. 4.5). The black regions comprised on enriched oxygen concentrations along with Al, Co and Fe, suggesting formation of spinel oxides. White regions showed high concentrations of Mo and Cr coupled with nearly equal concentrations of Al, Co, Fe, and oxygen, indicating the CrMo-rich BCC phases embedded oxides. These results are in line with the XRD results (Fig. 4.2). Gray regions showed Cr enriched oxide regions, indicating the presence of chromium-based oxides and mixed oxide regions.

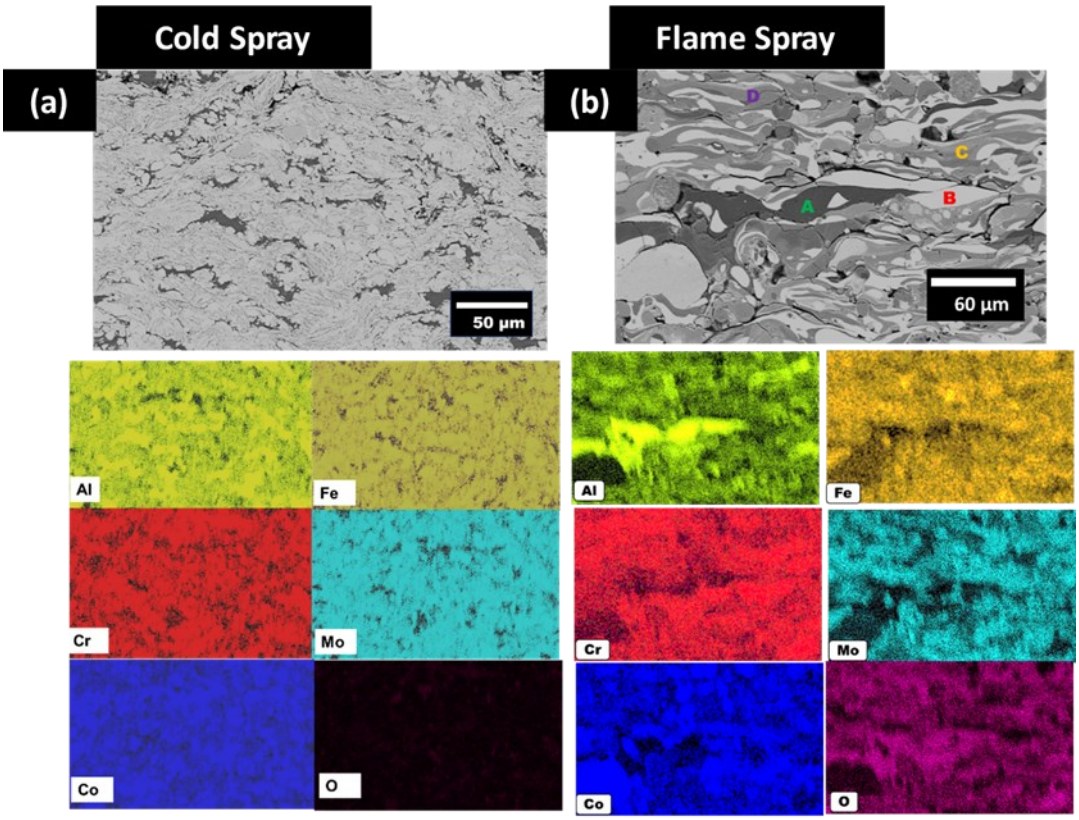

Figure 4.5 Scanning electron microscopy elemental maps of (a) Cold sprayed and (b) Flame sprayed AlCoCrFeMo high entropy alloy coatings.

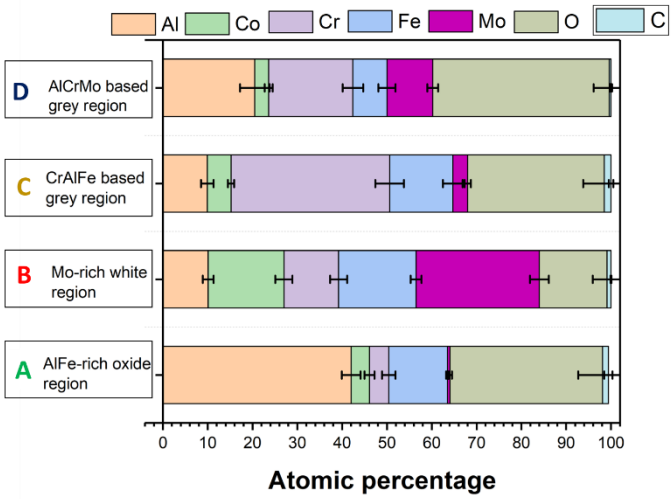

Figure 4.4 Energy dispersive spectroscopy analysis of different regions of the flame-sprayed HEA coatings. The letters (A to D) were the different regions shown in Figure 4.4(b).

4.4.2. Friction coefficient and wear behavior of HEA coatings

The friction coefficients of the cold sprayed and flame sprayed HEA coatings as the function of number of cycles using a 5 N load are shown in Fig. 4.6. Figures 4.6(a) and 4.6(b) depict the unpolished and polished coating surfaces, respectively. As shown in Fig. 4.6, the friction coefficient for the cold sprayed and flame sprayed HEA coatings followed a similar trend for the unpolished and polished surfaces (i.e., $S_a \approx 6.8$ to 8.17 µm for the unpolished surfaces and $S_a \approx 1.2$ to 1.6 µm for the polished surfaces, where S_a denotes surface roughness value). A gradual increase in friction coefficient was observed at the beginning of the test, which is known as the running-in regime (up to approximately 200 cycles) [21]. After the running-in regime, a slight increase in the friction coefficient was found for both the HEA coatings. A steady state was maintained between 200 cycles and 5000 cycles. It is apparent that the friction was slightly reduced for the cold sprayed HEA coatings during steady state compared to that of flame sprayed HEA coatings at both, unpolished and polished surface conditions (see Fig. 4.6). It should be noted that the standard deviations for flame sprayed HEA coatings were higher in case of the unpolished conditions compared to the polished ones. On the other hand, the cold sprayed HEA coatings showed pronounced fluctuations in the friction curves for both surface conditions (i.e., polished and unpolished). Overall, the friction coefficient decreased after polishing for the flame sprayed HEA coatings after testing, whereas the cold sprayed HEA coatings maintained similar value up to 5000 cycles.

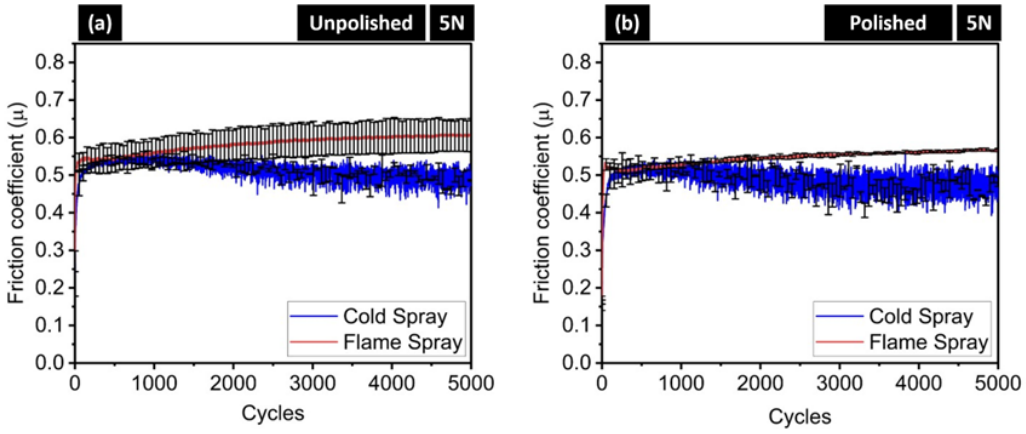

Figure 4.6 Friction behavior of cold sprayed and flame sprayed AlCoCrFeMo high entropy alloy coatings at 5 N normal load for (a) unpolished and (b) polished conditions.

Figures 4.7(a and b) represents the friction coefficient curves of the unpolished and polished HEA coatings performed at 10 N normal load. Similar to the 5N tests, when using a normal load of 10N, the friction coefficient was lower for the cold sprayed coating when compared to the flame sprayed one. With an increase in normal load from 5 N to 10 N, a subtle difference in the average friction coefficient was found for both the HEA coatings. As shown in Fig. 4.7(a and b), the friction behavior for the cold sprayed HEA coatings was consistent for unpolished and polished surface conditions, highlighting the steady state regime throughout the test. Furthermore, similar observations with pronounced fluctuations in the friction coefficient were also found for the cold sprayed HEA coatings tested at 10 N compared to 5 N normal load.

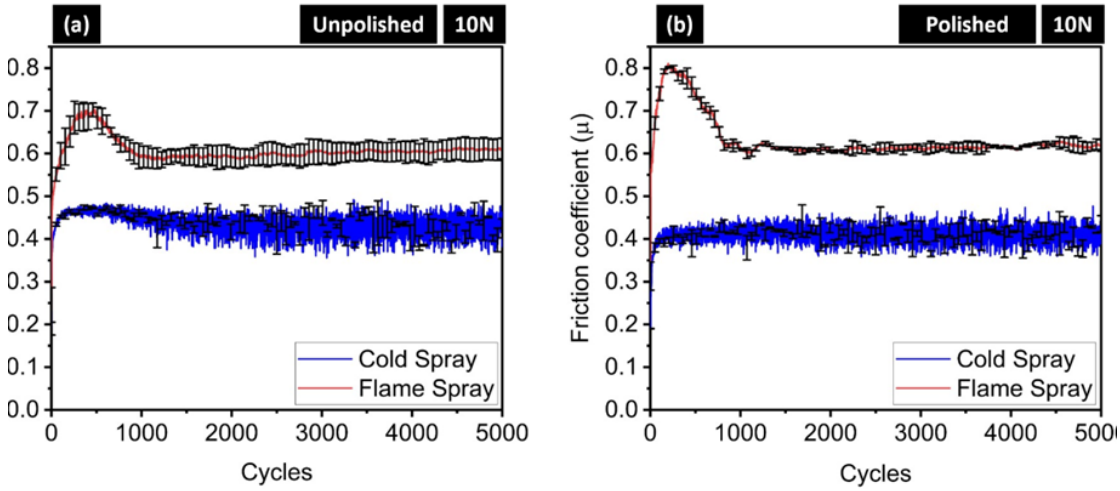

Figure 4.7 Friction behavior of cold sprayed and flame sprayed AlCoCrFeMo high entropy alloy coatings at 10 N normal load for (a) unpolished and (b) polished conditions.

In case of flame sprayed HEA coatings, a steep rise in curves was observed up to approximately 500 cycles, followed by a deceleration (up to 1000 cycles) and steady-state regimes (after 1000 cycles) for both unpolished and polished surface conditions. It should be noted that such a steep rise in curves was not seen for the flame sprayed HEA coatings at 5 N loading. Similar to that observed at 5 N loading conditions, the unpolished surfaces of the flame sprayed HEA coatings showed high standard deviations compared to that of polished surfaces tested at 10 N.

Figure 4.8 shows the average wear depths for both cold sprayed and flame sprayed HEA coatings performed at 5 N load. As shown in Fig. 4.8(a) and 4.8(b), higher

wear depths (~ 60 to 70 µm) were observed for the cold sprayed HEA coatings compared to that of flame sprayed HEA coatings (~ 5 to 10 µm) for both the unpolished and polished surface conditions. The slight variations in the wear depths were found between the unpolished and polished surfaces for both the HEA coatings. However, the average wear depth increased for both the HEA coatings tested at high load, as shown in Fig. 4.9. The wear depth for cold sprayed HEA coatings showed approximately 20 to 30 µm increment for both unpolished and polished surface conditions compared 5 N testing condition. Flame sprayed HEA coatings, on the other hand, exhibited almost similar average wear depths of around 20 µm for unpolished and polished surfaces, respectively, which highlights approximately 10 µm increment at higher loading condition.

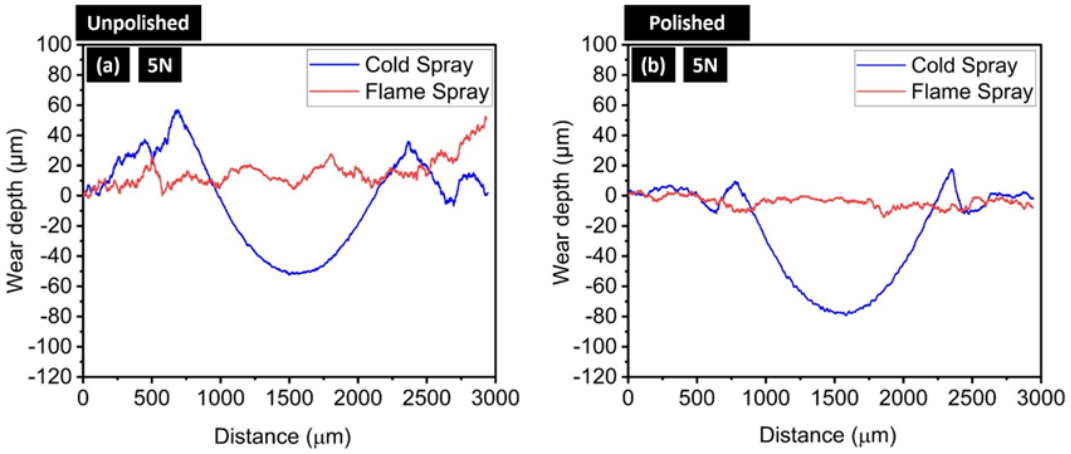

Figure 4.8 Wear profile of cold sprayed and flame sprayed AlCoCrFeMo high entropy alloy coatings at 5 N normal load for (a) unpolished and (b) polished conditions.

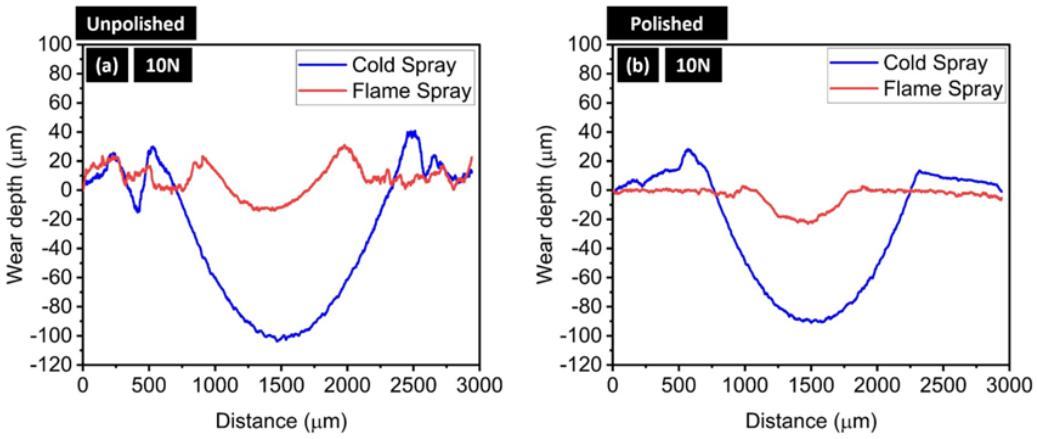

Figure 4.9 Wear profile of cold sprayed and flame sprayed AlCoCrFeMo high entropy alloy coatings at 10 N normal load for (a) unpolished and (b) polished conditions.

The volume wear rates of all the developed HEA coatings at different coating surface conditions with varying loads are shown in Fig. 4.10. It is evident that the flame sprayed HEA coatings showed remarkable wear resistance compared to the cold sprayed HEA coatings in all conditions. The flame sprayed HEA coatings exhibited around 93% lower wear rates compared to that of cold sprayed HEA coatings at both unpolished and polished surface conditions tested at 5 N normal load. However, the wear rates were similar for cold sprayed HEA coatings, approximately $140 \times 10^{-5}\text{mm}^3/\text{Nm}$ at both unpolished and polished surface conditions. With the increase in normal load from 5 N to 10 N, a reduction in wear rates (approximately 35%) was observed for the cold sprayed HEA coatings in polished coating surfaces. The low wear rates achieved for the cold sprayed HEA coatings are in line with friction behavior, which showed lower friction coefficient compared to that of test with a 5 N normal load (see Fig. 4.7(a)). However, the flame sprayed HEA coatings showed higher wear rates under unpolished surfaces conditions, which was approximately 62% compared to that of the 5 N loading condition. No such variations were found in the wear rates for the polished surface conditions when tested at 10 N normal load (see Fig. 4.10).

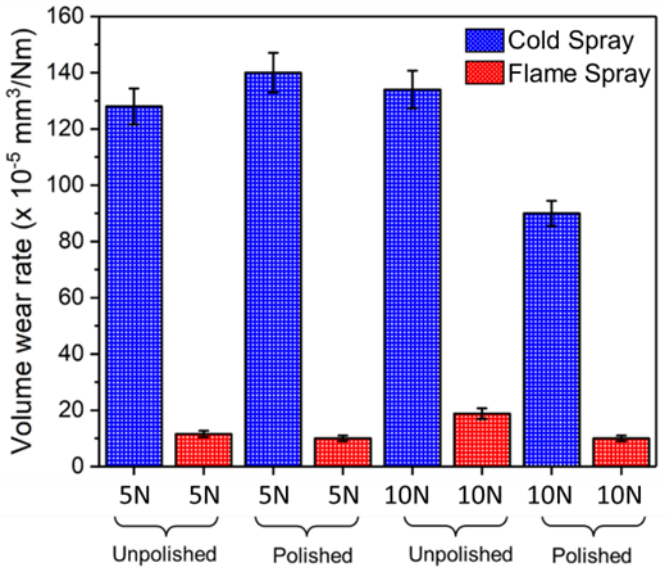

Figure 4.8 Wear rates of cold sprayed and flame sprayed AlCoCrFeMo high entropy alloy coatings at 5 N and 10 N normal load for unpolished and polished conditions.

4.4.3. Ex-situ analysis of wear tracks and counter face

Figure 4.11 shows the worn surface morphologies of unpolished cold sprayed HEA coatings tested at 5 N normal load. As shown in Fig. 4.11(a), it is clearly visible from the wear tracks that the cold sprayed HEA coatings underwent significant damage by means of deep groove scratches parallel to the sliding direction, highlighting abrasive wear mechanism [22]. Numerous loose debris particles were also found on the wear tracks of cold sprayed HEA coatings, indicating the possibility of third-body abrasion. Relatively wider wear track can be seen in the cold sprayed HEA coatings after testing with a wear track dimension of approximately 1.6 mm. Furthermore, the presence of oxide debris was observed in some regions on the wear tracks, as shown in Fig. 4.11(b). In addition, numerous cracks were also found in the regions near the oxide debris, highlighting the brittle nature of oxide layers. The increase oxygen content was further confirmed with the EDS analysis of the wear tracks, as shown in Fig. 4.13, and summarized in Table 4.5. The oxygen concentrations were negligible in case of the unworn cold sprayed HEA coatings (see Fig. 4.3(a)).

The worn surface morphologies of the unpolished flame sprayed HEA coatings are shown in Fig. 4.12 (a & b). When compared to cold sprayed HEA coatings, the damage severity found to be lower in case of flame sprayed HEA coatings. There is no evidence of wide groove scratches and micro-ploughing for the flame sprayed HEA coatings. In contrast, brittle fracture along with numerous cracks and spallation pits were found on the wear tracks of the flame sprayed HEA coatings. The brittle fractures were more evident in the regions mainly comprised of oxide phases.

The oxygen content did not show many variations between the worn and unworn surfaces, (see Fig. 4.13 and Table 4.5). The EDS analysis confirmed that the tribo-layers appear enriched in Cr, Fe, Al and oxygen concentrations with traces of all other elements (see Fig. 4.13 and Table 4.5). When compared to cold sprayed HEA coatings, the width of the wear track dimension was around 0.7 mm, which is approximately 54% lower compared to that of the cold sprayed HEA coatings.

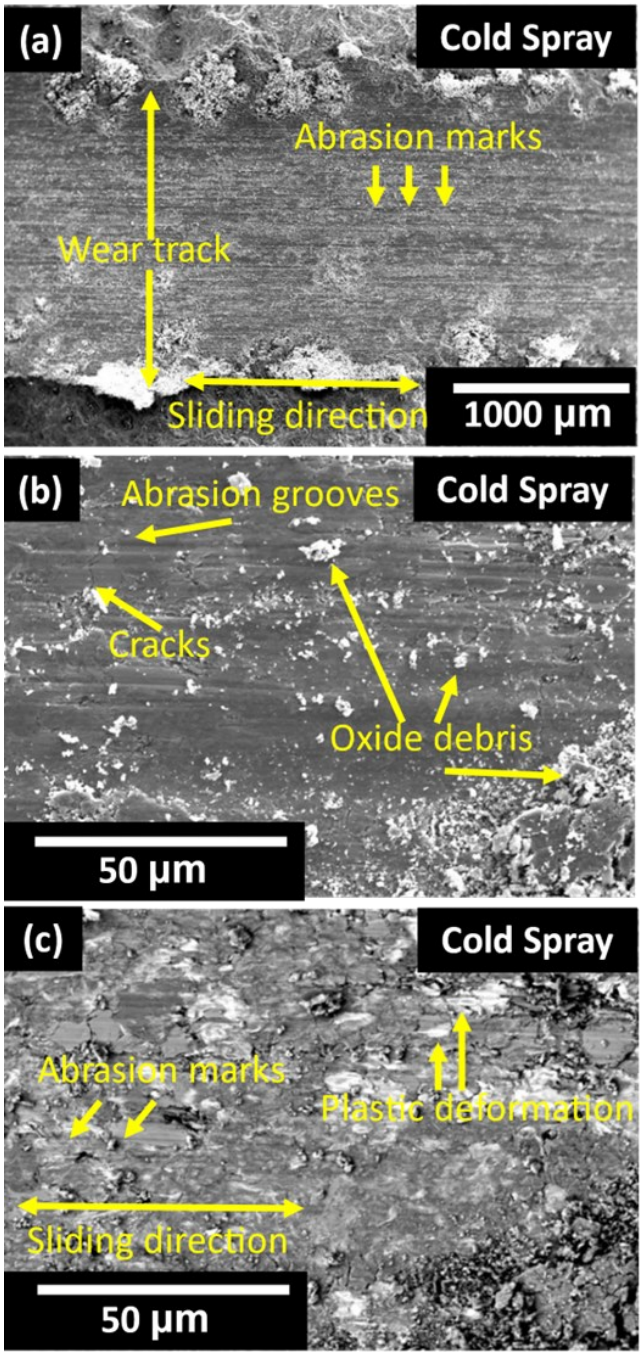

Figure 4.9 Scanning electron microscope shows the (a) low and (b) high magnified images of worn surface morphologies for the cold sprayed HEA.

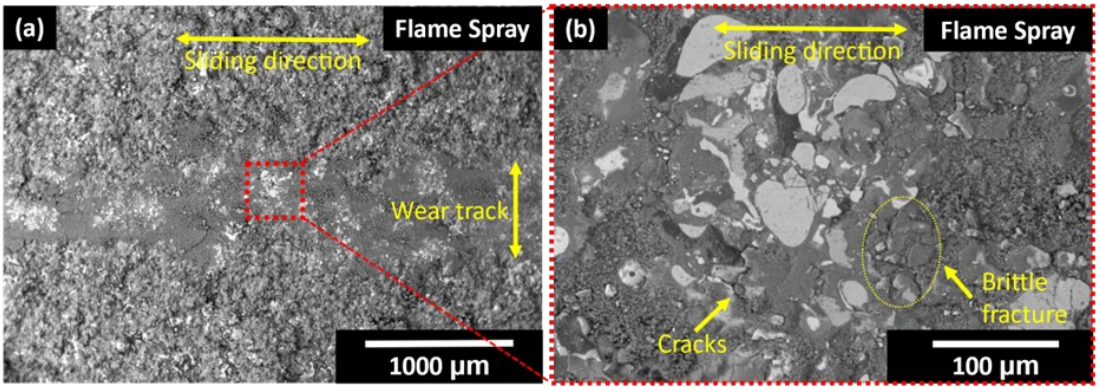

Figure 4.10 Worn surface morphology of (a) low magnification and (b) high magnification of flame sprayed AlCoCrFeMo high entropy alloy coating at 5 N normal load for unpolished condition.

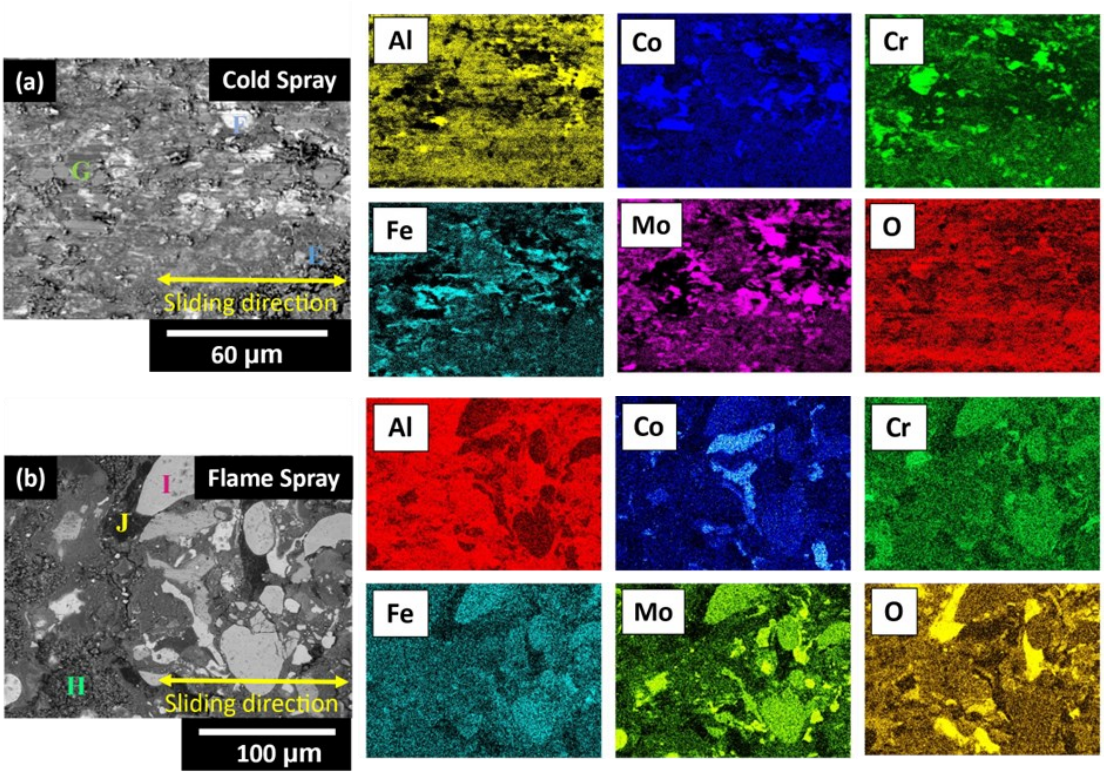

Figure 4.11 Scanning electron microscopy elemental maps of worn surface of (a) Cold sprayed and (b) Flame sprayed AlCoCrFeMo high entropy alloy coatings.

Table 4.5 Elemental distribution on worn surface of cold sprayed and flame sprayed AlCoCrFeMo high entropy alloy coating.

	Elements are in atomic percentage						
Regions	**Al**	**Co**	**Cr**	**Fe**	**Mo**	**O**	**C**
E	13.93	7.94	9.34	11.34	11.68	38.09	7.68
F	0.68	1.81	0.36	1.07	60.19	8.65	27.24
G	6.43	4.30	66.04	1.40	0.48	10.62	10.74
H	7.52	5.78	6.66	6.32	5.85	62.08	5.79
I	7.97	10.78	10.74	10.71	11.76	41.35	6.68
J	26.74	3.10	3.01	2.71	2.51	58.31	3.62

Wear morphologies of alumina counter ball after sliding against HEA coatings are shown in Fig. 4.14. It is apparent from the optical graphs that the amount of transfer film was higher on the counter face after sliding against cold sprayed HEA coatings when compared to the flame sprayed HEA (Fig. 4.14(a and b)). The amount of transfer film formations for the cold sprayed HEA was similar for both unpolished and polished surface conditions. However, the unpolished flame sprayed HEA coatings exhibited higher amount of transfer films when compared to the polished flame sprayed HEA. Furthermore, scratches can be seen on the counter faces, which might have resulted from hard oxide debris particles during sliding. The contact area and wear depth on the counter face was higher when sliding against cold sprayed HEA coatings.

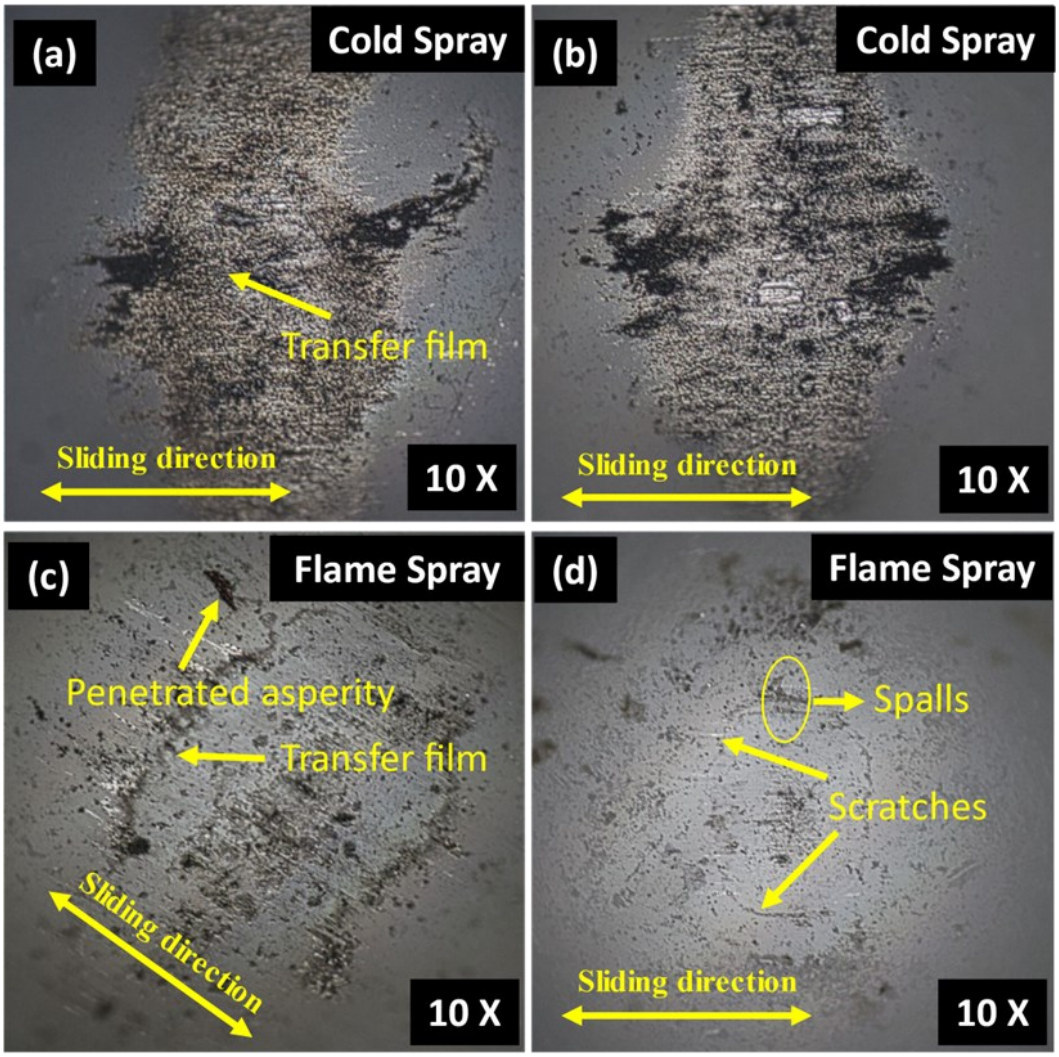

Figure 4.12 Wear morphology of alumina counter ball after sliding at 5 N normal load for (a) unpolished, (b) polished cold sprayed and (c) unpolished, (d) polished flame sprayed AlCoCrFeMo high entropy alloy coatings.

4.5. Discussion

Detailed characterization of the high entropy alloy coatings fabricated by means of cold spraying and flame spraying showed significant differences in the evolved microstructure, phase formations, and wear performance. Among the coatings tested in this study, the polished flame sprayed HEA coatings exhibited the highest wear resistance. The presence of spinel-type oxide contaminations for the flame sprayed HEA coatings due to oxidation in-flight with a phase fraction of 25.2 ± 2 wt% $(n = 3)$ contributed to an increase in hardness when compared to the cold sprayed HEA coating. It is apparent that the evidence of oxide inclusions was negligible in case of cold sprayed HEA coatings. Owing to the high fraction of oxides, a relatively high

hardness value was obtained for the flame sprayed HEA coatings $\left(592 \pm 43\ \text{HV}\ (\text{n} = 30)\right)$, which showed approximately 40% higher than that of cold sprayed HEA coatings $(362 \pm 48\ \text{HV}\ (\text{n} = 30))$. The oxides were predominantly composed of Al-rich and spinel type AB_2O_4 $(\text{A} = \text{Fe/Mo and B} = \text{Al/Cr})$ oxides for the flame sprayed HEA coatings. A recent study by Patel *et al*. [23] reported the average hardness value of 423 HV for high-velocity air-fuel sprayed CoCrFeMnNi HEA coatings, which exhibited mixed oxide phases of Cr_2O_3, and Co_3O_4, respectively. The wear rates for heat treated polished CoCrFeMnNi coatings at similar conditions, however, they were 3.5 times higher compared to flame sprayed HEA coatings. This could possibly be explained by the difference in the formation of oxides and their corresponding phase fractions formed for the flame sprayed HEA coatings. In addition, the existence of solid-solution BCC phases for the AlCoCrFeMo HEA coatings were also a determinative factor for improving the hardness. It has previously been reported that the FCC solid-solution structure favors the low hardness, whereas higher hardness was reported for the BCC structured high entropy alloys [24-26]. Hence, it can be said that the difference in the wear rates for the cold sprayed and flame sprayed HEA coatings was mainly attributed to their difference in microstructure, phase formations and hardness, which is a result from the responses of high-temperature and low-temperature depositions.

The wear track analysis confirmed the existence of severe abrasive wear for the cold sprayed HEA coatings with pronounced plastic deformation (see Fig. 4.11). Indeed, the repetitive fracturing and delamination might have resulted in increase of the wear rates for the cold sprayed HEA coatings tested at both 5 N and 10 N normal loads. A prior study on cold sprayed AlCoCrFeMo HEA coatings showed a lack of cohesive strength between particle-particle interfaces that resulted in high wear rates tested under abrasive loading [20]. Thus, it can be implied that the inferior wear performance for the cold sprayed HEA coatings might be due to the intense delamination, and severe abrasion on the wear tracks compared to that of flame sprayed HEA coatings (see Fig. 4.15). In addition to that, the appearance of debris was also evidently found on wear tracks of the cold sprayed HEA coatings. This debris must have been oxidized due to the frictional heating at the interface performed at open atmospheric conditions during sliding and acted as third-bodies [27]. Previously, Nong *et al.* [28] had reported the formation of oxide layers (also known as glazed layers) in AlCrFeNiTi HEAs, that

protected the surface from delamination. However, they also reported that the continuous delamination and removal of oxide layers from the wear tracks for the $AlCrFeNiTiMn_{0.5}$ alloy increased the wear rates. Hence, it can be inferred that similar mechanism might have occurred in case of the cold sprayed HEA coatings. The formation of oxide debris could be the result of breaking of oxide layers that were formed on the wear tracks during sliding, that might have undergone three-body abrasion, leading to increase in wear rates. Similar observations for high-velocity oxy fuel based CoCrFeMnNi HEA coatings was also reported by Patel *et al.* [23]. Further, it can be seen that the transfer film on the counter face was more prevalent for the cold sprayed HEA coatings than that of flame sprayed HEA coatings (see Fig. 4.14). Alidokht *et al.* [29] reported increase in wear rates for the cold sprayed titanium coatings, which is governed by the monotonous accumulation and annihilation of transfer films on the counter face during sliding. This is consistent with the observations in our study, where a higher amount of transfer was observed on the counter-face against the cold sprayed HEA coatings, which also showed an increase in wear rates when compared to the flame sprayed HEA coating. In addition, for flame sprayed HEA coatings, the evidence of debris was found to be comparatively lower than that of cold sprayed HEA coatings, indicating that the three-body abrasion has not played a role for the flame sprayed HEA coatings. Consequently, a reduction in dimensions (width and depth) of the wear tracks were observed with the flame sprayed HEA (see Fig. 4.12). A study by Wu *et al.* [30] reported occurrence of low wear debris with shallow grooves, which is likely due to high hardness of boronized $Al_{0.1}CoCrFeNi$ high entropy alloys. Similarly, the oxide-rich flame sprayed HEA coating studied here, showed an increase in hardness and consequently, restricted the advancement of abrasive wear, which in turn, resulted in lower wear rates. Similar observations were also reported by Verma *et al.* [31], which suggested that the addition of copper (Cu) in CoCrFeNiCu HEA likely promotes the oxide layer formations during sliding and protected the coating surfaces against wear by preventing a direct contact at the interface. Another study also reported the same observations for the plasma sprayed FeCoNiCrMn high entropy alloys [32].

In terms of the friction behavior, the cold sprayed HEA coatings exhibited lower friction coefficient but greater fluctuations in the curves tested at all conditions (see Fig. 4.6 and 4.7) when compared to the flame sprayed HEAs. The fluctuations could be attributed to the repeated localized fracturing of the coating layers, which may lead to

buildup and loosening of debris on the wear tracks during sliding. Another possible explanation could be that the lower overall friction of the cold sprayed HEA coating is a result of the delamination of the coating layers [33]. In addition, the loose debris particles might have acted as roller bearings and contributed towards the sliding motion thus reducing the overall friction. Similar observations of friction coefficient were also reported previously by Joseph *et al.* [22] and Tüten *et al.* [26]. The friction behavior of the flame sprayed HEA coating was quite intriguing. The steep rise in the friction curves (up to 500 cycles) observed might be due to the removal of contaminant or oxide layer over the surface and thus, exposure of the bare surface which must have given rise to the adhesion and hence, the friction coefficient. Another reason for the rise of friction might be the entrapment of the wear debris between the sliding surfaces, which penetrate both the surfaces and stop the slippage resulting in a rise in friction. The sudden drop (500 to 1000 cycles) in the coefficient of friction may be explained by the gradual removal of asperities from the counter face because wear particles are not able to anchor easily to a polished surface [21]. In addition, for the flame sprayed HEA coating, the compact oxide phases due to oxidation in-flight exhibits strong resilience against deformation and delamination at both unpolished and polished conditions, which could be another possible reason for higher friction coefficients. A similar phenomenon was modelled by Rigney *et al.* [33] which suggested that harder materials exhibit high resistance to deformation which consequently results in high friction coefficient. The presence of scratches and roughened regions over the surface of counterface (see Fig. 4.14) provides more evidence of this phenomenon for the flame sprayed HEA coating.

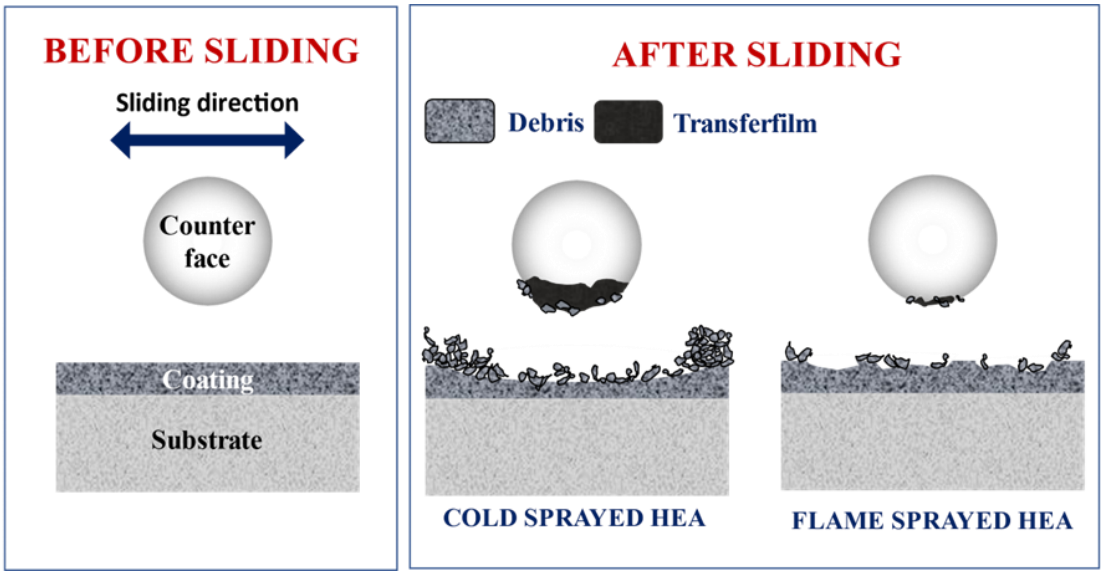

Figure 4.13 Proposed wear mechanism for cold sprayed and flame sprayed AlCoCrFeMo high entropy alloy coatings.

4.6. Conclusion

In this study, AlCoCrFeMo high entropy alloy system developed through flame spraying and cold spraying was evaluated for its tribological behavior at ambient conditions. Flame sprayed AlCoCrFeMo HEA coatings showed higher oxygen concentration compared to the cold sprayed HEA coatings, which resulted in higher hardness and consequently reduced wear rates. In addition, higher number of debris particles were generated throughout the test with the cold sprayed AlCoCrFeMo HEA coatings, which resulted in higher amount of material transfer to the counter face. The wear for the cold sprayed HEA was governed primarily by third-body abrasion and secondarily by delamination, while brittle failure dominated the wear mechanism of flame sprayed HEA coating as evidenced by the ex-situ analysis of the worn surfaces.

The average friction coefficient for cold sprayed AlCoCrFeMo HEA coatings was overall lower compared to that of the flame sprayed HEA coatings. Cold sprayed coating exhibited loose debris acting as roller bearings and offered lesser resistance to deformation as compared to flame sprayed coating, which consequently reduced the friction. Polishing seemed to have a higher effect on friction and wear of flame sprayed AlCoCrFeMo HEA coatings. The results obtained in this study suggest that the flame

sprayed HEA coatings are promising candidates for next-generation tribological interfaces under specific conditions, pointing to new materials designed with improved microstructural features and enhanced mechanical properties.

References:

1. J.W. Yeh, S.K. Chen, S.J. Lin, J.Y. Gan, T.S. Chin, T.T. Shun, C.H. Tsau, S.Y. Chang, Nanostructured high-entropy alloys with multiple principal elements: novel alloy design concepts and outcomes, Adv. Eng. Mater., 6(5), 299-303 (2004)
2. B. Cantor, I. Chang, P. Knight, A. Vincent, Microstructural development in equiatomic multicomponent alloys, Mater. Sci. Eng., A, 375, 213-218 (2004)
3. B.S. Murty, J.-W. Yeh, S. Ranganathan, High-entropy alloys, 1 ed., Elsevier, 2014
4. A. Meghwal, A. Anupam, B.S. Murty, C.C. Berndt, R.S. Kottada, A.S.M. Ang, Thermal Spray High-Entropy Alloy Coatings: A Review, J. Therm. Spray Technol., 29(5), 857-893 (2020)
5. J.M. Torralba, P. Alvaredo, A. García-Junceda, High-entropy alloys fabricated via powder metallurgy. A critical review, Powder Metall., 62(2), 84-114 (2019)
6. D.F. Rojas, H. Li, O.K. Orhan, C. Shao, J.D. Hogan, M. Ponga, Mechanical and microstructural properties of a CoCrFe0.75NiMo0.3Nb0.125 high-entropy alloy additively manufactured via cold spray, J. Alloys Compd., 893, (2022)
7. E. Ma, X. Wu, Tailoring heterogeneities in high-entropy alloys to promote strength–ductility synergy, Nat. Commun., 10(1), (2019)
8. R.B. Nair, H.S. Arora, A. Ayyagari, S. Mukherjee, H.S. Grewal, High Entropy Alloys: Prospective Materials for Tribo-Corrosion Applications, Adv. Eng. Mater., 20(6), (2018)
9. Y. Shi, B. Yang, P. Liaw, K.T.N. Univ. of Tennessee, K.T.N.U.S.A. The University of Tennessee, Corrosion-resistant high-entropy alloys: A review, Metals, 7(2), (2017)
10. M. Vaidya, G.M. Muralikrishna, B.S. Murty, High-entropy alloys by mechanical alloying: A review, J. Mater. Res., 34(5), 664-686 (2019)
11. L.-H. Tian, W. Xiong, C. Liu, S. Lu, M. Fu, Microstructure and wear behavior of atmospheric plasma-sprayed AlCoCrFeNiTi high-entropy alloy coating, J. Mater. Eng. Perform., 25(12), 5513-5521 (2016)
12. S. Liu, Y. Peng, Y. Zhang, Y. Wang, W. Fan, A. Wang, W. Zhang, Y. Tan, Q. Ma, Y.

Lan, Effect of Nanostructure on Wear and Corrosion Behavior of HVAF-Sprayed Eutectic High-Entropy Alloy Coatings, J. Therm. Spray Technol., 1-11 (2022)

13. Y.-k. Zhou, J.-j. Kang, J. Zhang, Z.-q. Fu, L.-n. Zhu, D.-s. She, W. Yue, Microstructure and sliding wear behavior of HVOF sprayed Al (1-x) CoCrFeNiTix high-entropy alloy coatings, Mater. Lett., 131929 (2022)

14. N. Espallargas, Future development of thermal spray coatings: types, designs, manufacture and applications, ed., Woodhead Publishing is an imprint of Elsevier, 2015

15. F. Gärtner, T. Stoltenhoff, T. Schmidt, H. Kreye, The cold spray process and its potential for industrial applications, J. Therm. Spray Technol., 15(2), 223-232 (2006)

16. G. Munday, J. Hogan, A. McDonald, On the microstructure-dependency of mechanical properties and failure of low-pressure cold sprayed tungsten carbide-nickel metal matrix composite coatings, Surf. Coat. Technol., 396, 125947 (2020)

17. S. Yin, W. Li, B. Song, X. Yan, M. Kuang, Y. Xu, K. Wen, R. Lupoi, Deposition of FeCoNiCrMn high entropy alloy (HEA) coating via cold spraying, J. Mater. Sci. Technol., 35(6), 1003-1007 (2019)

18. ASTM E384-17, Standard Test Method for Microindentation Hardness of Materials, ASTM International, West Conshohocken, PA, 2017, www.astm.org, ed.

19. A. Anupam, R.S. Kottada, S. Kashyap, A. Meghwal, B. Murty, C. Berndt, A. Ang, Understanding the microstructural evolution of high entropy alloy coatings manufactured by atmospheric plasma spray processing, Appl. Surf. Sci., 505, 144117 (2020)

20. R.B. Nair, G. Perumal, A. McDonald, Effect of Microstructure on Wear and Corrosion Performance of Thermally Sprayed AlCoCrFeMo High-Entropy Alloy Coatings, Adv. Eng. Mater., 2101713 (2022)

21. K. Holmberg, A. Mathews, Coatings tribology: a concept, critical aspects and future directions, Thin Solid Films, 253(1), 173-178 (1994)

22. J. Joseph, N. Haghdadi, K. Shamlaye, P. Hodgson, M. Barnett, D. Fabijanic, The sliding wear behaviour of CoCrFeMnNi and AlxCoCrFeNi high entropy alloys at elevated temperatures, Wear, 428, 32-44 (2019)

23. P. Patel, S.A. Alidokht, N. Sharifi, A. Roy, K. Harrington, P. Stoyanov, R.R. Chromik, C. Moreau, Microstructural and Tribological Behavior of Thermal Spray CrMnFeCoNi High Entropy Alloy Coatings, J. Therm. Spray Technol., (2022)

24. N. Hua, W. Wang, Q. Wang, Y. Ye, S. Lin, L. Zhang, Q. Guo, J. Brechtl, P.K. Liaw, O.R.T.N. Oak Ridge National Lab, Mechanical, corrosion, and wear properties of biomedical Ti–Zr–Nb–Ta–Mo high entropy alloys, J. Alloys Compd., 861(1), (2021)

25. C. Mathiou, A. Poulia, E. Georgatis, A.E. Karantzalis, Microstructural features and dry - Sliding wear response of MoTaNbZrTi high entropy alloy, Mater. Chem. Phys., 210, 126-135 (2018)

26. N. Tüten, D. Canadinc, A. Motallebzadeh, B. Bal, Microstructure and tribological properties of TiTaHfNbZr high entropy alloy coatings deposited on Ti[sbnd]6Al[sbnd]4V substrates, Intermetallics, 105, 99-106 (2019)

27. K. Razavizadeh, T.S. Eyre, Oxidative wear of aluminium alloys, Wear, 79(3), 325-333 (1982)

28. Z.-S. Nong, Y.-N. Lei, J.-C. Zhu, Wear and oxidation resistances of AlCrFeNiTi-based high entropy alloys, Intermetallics, 101, 144-151 (2018)

29. S.A. Alidokht, V.N.V. Munagala, R.R. Chromik, Role of Third Bodies in Friction and Wear of Cold sprayed Ti and Ti-TiC Composite Coatings, Tribol. Lett., 65(3), 1-15 (2017)

30. Y.H. Wu, H.J. Yang, R.P. Guo, X.J. Wang, X.H. Shi, P.K. Liaw, J.W. Qiao, Tribological behavior of boronized Al0.1CoCrFeNi high-entropy alloys under dry and lubricated conditions, Wear, 460-461, (2020)

31. A. Verma, P. Tarate, A.C. Abhyankar, T. Shanmugasundaram, M.R. Mohape, D.S. Gowtam, V.P. Deshmukh, High temperature wear in CoCrFeNiCux high entropy alloys: The role of Cu, Scr. Mater., 161, 28-31 (2019)

32. J.-K. Xiao, H. Tan, Y.-Q. Wu, J. Chen, C. Zhang, Microstructure and wear behavior of FeCoNiCrMn high entropy alloy coating deposited by plasma spraying, Surf. Coat. Technol., 385, (2020)

33. D.A. Rigney, J.P. Hirth, Plastic deformation and sliding friction of metals, Wear, 53(2),

345-370 (1979)

Chapter

5. INFLUENCE OF TEMPERATURE ON THE TRIBOLOGICAL BEHAVIOR OF AlCoCrFeMo HIGH ENTROPY ALLOY DEPOSITED VIA VARIOUS THERMAL SPRAYING TECHNIQUES

In this chapter…

The response of varying temperatures on friction and wear behavior is presented. Thermal spraying techniques such as cold spray, flame spray and HVOF have been evaluated and compared to identify the most suitable technology for producing wear resistant HEA coatings.

5.1. Abstract

Tribological evaluation of thermally sprayed high entropy alloys have received little attention. High entropy alloys (HEAs) have shown excellent mechanical properties and wear resistance while also retaining their resistance to corrosion damage. In this study, novel AlCoCrFeMo HEA coatings were developed by means of cold spraying, flame spraying and high velocity oxy-fuel (HVOF) technologies. For the first time among the research community, three different thermal spraying techniques were compared for HEAs to determine their tribological behavior, phases, microstructures and mechanical properties. The coatings were characterized by scanning electron microscope (SEM), energy dispersive spectroscopy (EDS), x-ray diffraction (XRD), image analysis, and Vickers micro-hardness testing. The cold sprayed HEA exhibited less porosity (<1 %) while the flame sprayed and HVOF sprayed coating exhibited porosity levels of (2.6 ± 1 %) and (~ 1 %) respectively. This is mainly due to large presence of oxides in the case of flame sprayed and HVOF sprayed HEA coatings. As a result, the flame sprayed and HVOF sprayed coatings exhibited higher hardness values which is also due to the evolution of body centered cubic (BCC) phase structure as opposed to cold sprayed HEA coating.

The dry sliding wear behavior was investigated at two different temperatures (RT and 450^{O}C) at normal load of 5 N and at a constant sliding velocity of 3.14 cm/s for all the samples. The friction coefficient during the first half of the test was highest for the HVOF sprayed HEA followed by flame sprayed HEA and cold sprayed HEA being the least. During the second half of the test, the flame sprayed HEA exhibited higher friction coefficient as compared to HVOF sprayed HEA and cold sprayed HEA which maintained the lowest value for both the temperatures. However, the wear rates of the HVOF sprayed HEA were significantly lower than the others, with the cold sprayed HEA having the most wear among the three for all temperatures. This correlated well with the observations of the ex-situ analysis, which showed greater material transfer and increased formation of debris on the cold sprayed coatings compared to the flame sprayed and HVOF sprayed coatings. In addition, ex-situ analysis suggested the formation of an oxide based tribofilm on the cold sprayed coatings resulting in reduced wear at elevated temperatures. Brittle fracture was still evident with the flame sprayed coating at elevated temperatures which coupled with

increased adhesion, increased the overall wear. These results suggest that HVOF is the most promising thermal spraying technique for AlCoCrFeMo HEA followed by flame spraying for the specific conditions used in this study.

Keywords: Aerospace Materials, High Entropy Alloys, Interfacial Processes, Tribology, Cold Spray, Flame Spray, HVOF

5.2. Introduction

Traditional materials such as Nickel, Cobalt and Titanium are commonly employed in mechanical systems. However, in extreme environmental conditions, these materials fail to operate effectively due to their poor resistance towards temperature and corrosion effects [1,2]. Therefore, there is a strong desire to develop new materials that can operate well in these conditions. The term High Entropy Alloys (HEAs) was coined by Yeh *et al.* [3] in 2004 which was inspired from a prior work of Ranganathan *et al.* [4] that showcased the outstanding properties of multi-metallic cocktail alloys. HEAs not only exhibit excellent tribological behavior but also feature enhanced mechanical properties [5].

HEAs are defined as alloys having five or more principal elements in equimolar proportions. To improve the performance of such HEAs, principal elements are varied in the range on 5% to 35% atomic percentages [3]. HEAs exhibit excellent toughness, hardness and high resistance to wear, corrosion and oxidation damages due to their four core effects namely high entropy effect, lattice distortion effect, sluggish diffusion effect and cocktail effect as discussed by many researchers [2,6-8]. HEAs have high configurational entropy (>1.5R) which helps in stabilizing the atomic structure [9]. Cantor alloy (CoCrFeMnNi), coined by Cantor *et al*. [5] comprises of face centered cubic (FCC) structure which is the most widely studied HEA so far. However, replacing Mn with Al accelerates the formation of body centered cubic structure (BCC) which results in improved strength [6]. HEAs have been repeatedly showing promising results in the form of bulk alloys as well as coatings for tribological applications [10-12].

Joseph *et al.* [12] studied the sliding wear behavior for vacuum arc-melted $Al_{0.3}$CoCrFeNi, $Al_{0.6}$CoCrFeNi and CoCrFeMnNi and compared it with traditionally used Inconel 718 alloy over a wide range of temperatures (25^{O}C to 900^{O}C). The samples were tested against Alumina (Al_2O_3) counter balls, and it was observed that FCC structure of CoCrFeMnNi and $Al_{0.3}$CoCrFeNi resulted in higher wear rates at room temperature due to lower hardness. Whereas $Al_{0.6}$CoCrFeNi, AlCoCrFeNi and Inconel 718 having BCC and/or FCC structure had much more resistance to wear. However, at elevated temperatures, the wear resistance of almost all the HEAs showed higher values as compared to traditionally used Inconel 718. This is mainly due to the presence of oxide based tribo-film over the worn surface which protected the surface underneath as

opposed to traditionally used nickel-based alloy (Inconel 718). As expected, AlCoCrFeNi had a superior performance than any other alloys considered in this study at all temperature ranges due to its pure BCC structure. Similarly, Zhang *et al.* [13] synthesized CoCrFeMnNi and CoCrFeNiV by vacuum hot pressing sintering and tested against Si_3N_4 counter balls at temperatures ranging between 25^OC to 800^OC. The addition of V and removal of Mn from the traditionally studied cantor alloy (CoCrFeMnNi) resulted in precipitation of hard sigma phase that enhanced the hardness (975 ± 11 HV) of the HEA significantly. Evidently, CoCrFeNiV showed improved resistance to wear due to formation of hard V_2O_5 oxide glaze layer as compared to CoCrFeMnNi for all temperature ranges.

Even though bulk HEAs have shown promising results, thermally sprayed HEA coatings are much more effective when it comes to tribological applications. This is due to their flexibility and versatility of operation and ability to be coated over intricate and complex geometries. Properties and tribological performance of HEAs are greatly influenced by the different thermal spraying processes such as HVOF, HVAF, Flame spray and Cold spray due to the variations in particle velocities, operating temperatures and carrier media [14]. Cold spraying being a low temperature process, prevents the formation of oxides and temperature related defects while protecting the surface from oxidative wear [15-17]. However, on the contrary, formation of oxide phases is sometimes beneficial from tribological perspective since the oxides enhance the hardness of the coating and also protect the surface underneath from further wear [6]. Zou *et al*. [18], very recently synthesized a high entropy composite alloy coating (HEC) by reinforcing FeCoNiCrMn with Al_2O_3 particles and cold spraying. The authors observed that the hardness of the HEC with 11 wt% Al_2O_3 was 278.3 ± 13.9 $HV_{0.3}$ and for 20 wt% Al_2O_3 was 302.4 ± 19.9 $HV_{0.3}$ as compared to 258.4 ± 22.6 $HV_{0.3}$ of pure FeCoNiCrMn. This resulted in 50% reduction in wear rates for the reinforced HEC as compared to original HEA which can be attributed to grain size refinement and work hardening effects due to reinforcements. It can be inferred that cold sprayed HEA coatings being softer in nature can be enhanced by implanting ceramic particles within their matrix. However, high temperature deposition processes inherently provide hard coatings due to evolution of oxide phases during spraying which is beneficial for tribological application as compared to cold spray. In addition to that, reinforcements using ceramic particles will improve the resistance against wear damage even further.

For instance, in 2022 Silvello *et al.* [19] compared the wear behavior of FeCoNiCrMn HEA sprayed using HVOF and cold spray at room temperature ($27 \pm 2^{O}C$) against WC-Co counter ball. It was observed that HVOF produced harder coating of 390 ± 10 $Hv_{0.1}$ as compared to cold sprayed coating of 382 ± 6 $Hv_{0.1}$. The hardness of cold sprayed coating was closer to HVOF due to reduced porosity of less than 1% and dense thick coating in case of cold sprayed HEA coating which is comparable to a thin HVOF coating with oxide phases. The HVOF sprayed HEA exhibited lower wear rates as compared to cold sprayed HEA due to their increased hardness and cohesive strength. Also, Löbel *et al.* [20] studied the tribological behavior of HVOF sprayed $AlCoCrFeNiTi_{0.5}$ HEA tested against Al_2O_3 counter ball over a wide range of temperatures ($22^{O}C$ to $900^{O}C$). It was seen that from room temperature to $500^{O}C$, the wear resistance dropped due to thermal softening, but it increased significantly at $900^{O}C$. From temperatures between ambient and $500^{O}C$, the wear was dominated by abrasion as well as third body abrasion of loose debris particles. For temperature ≥ 800 °C, the oxide based tribo-layer significantly increased and covered a larger surface resulting in improved protection. The phases at room temperature were mostly BCC (A2) and BCC (B2) however, at elevated temperatures the inclusions of minor FCC, spinel oxides and tetragonal σ-phase were evident which could be responsible for increased wear resistance. There is no research done on tribological evaluation of flame sprayed HEAs however, some interesting work comparing cold sprayed HEAs with flame sprayed HEAs can be found in the prior studies done by the authors of this current manuscript.

The main purpose of this research is to critically evaluate the effect of temperature ($25^{O}C$ and $450^{O}C$) on the tribological behavior of HEAs developed by three different thermal spraying processes. A novel AlCoCrFeMo HEA coating was developed using cold spraying, flame spraying and HVOF and tested at room temperature as well as $450^{O}C$ against Al_2O_3 counter ball to evaluate its friction and wear performance. The mechanisms were determined by performing detailed ex-situ analysis on the worn surfaces.

5.3. Experimental methods

5.3.1. Thermal spraying of HEA coatings

A novel HEA system was developed and its tribological behavior was studied for extreme environmental applications. AlCoCrFeMo HEA powder developed by ABM Nano LLC, Missouri, TX, USA was used as a feedstock for thermal spraying. Table 5.1 shows the nominal composition of AlCoCrFeMo HEA. Particle agglomerations were observed which can be inferred from their irregular appearance in morphologies. This can be a result of fracturing of powder particles during mechanical mixing, and repeated welding. The powder particles mainly ranged between $-30 + 3$ μm (3 to 30 μm). The mechanically alloyed HEA powder related closely to their nominal compositions. As shown in Table 5.1.

Table 5.1 Nominal and feedstock composition of AlCoCrFeMo high entropy alloy powder.

Composition	Al	Co	Cr	Fe	Mo
Nominal	20	20	20	20	20
Feedstock	20.5 ± 2.1	19.2 ± 0.9	19.4 ± 0.4	20.4 ± 0.8	20.5 ± 1.1

Commercially available low carbon steel was grit blasted using #24-grit alumina (Manus Abrasive Systems Inc., Edmonton, AB, Canada) and used as a substrate. Three different thermal spraying technologies were used to spray the same AlCoCrFeMo HEA and were evaluated for its friction and wear behavior unprecedentedly. A portable low pressure cold spray system (SST series P, CenterLine Ltd., Windsor, ON, Canada) was used to deposit the AlCoCrFeMo HEA coating in which the working fluid for deposition was compressed air. A constant gas temperature of 450^{O}C and a constant gas pressure of 92 psig were maintained throughout the deposition process. Table 5.2 lists the process parameters of this system. Secondly, an oxy-acetylene flame spray torch (6PII, Oerlikon Metco, Westbury, NY, USA) was used for high temperature thermal deposition of the HEA coating which was fitted with a volumetric powder feeder (5MPE, Oerlikon Metco, Westbury, NY, USA). Table 5.3 shows the spraying parameters for flame spray in which it can be seen that the main carrier gas used was Argon. To ensure a homogeneous and reproducible coating, a programmable robot (HP-20, Motoman, Yaskawa Electric Corp., Waukegan, IL, USA) was used for spraying the HEA powders over the substrate which was seen in all three

samples of the HEA coating for each deposition process. The HVOF coating was deposited by using Oerlikon-Metco Diamond Jet^{TM} 2700 Gun. The process parameters shown in table 5.4 for the HVOF coating were derived from previously successful works published by one of the authors of this manuscript [1].

Table 5.2 Process parameters for cold sprayed AlCoCrFeMo high entropy alloy coating.

Cold spraying parameters	Values
Accelerating gas (m/s)	Compressed air
Pre-heating temperature (^{0}C)	450
Gas pressure (psig)	92
Transverse speed (mm/s)	5
Stand-off distance (mm)	5
Increment size (μm)	3000

Table 5.3 Process parameters for flame sprayed AlCoCrFeMo high entropy alloy coating.

Flame spray parameters	Values
Acetylene flow (m^3/h)	1.2
Oxygen flow (m^3/h)	1.92
Argon flow (m^3/h)	0.56
Torch velocity (mm/s)	350
Stand-off distance (mm)	177
Particle concentration (ppm)	5000
Increment size (mm)	3
Number of passes	4

Table 5.4 Process parameters for HVOF sprayed AlCoCrFeMo high entropy alloy coating [1].

HVOF parameters	Values
Feed rate (g/min)	23
Oxygen flow (L/min)	303.5
Propylene flow (L/min)	78.8

Air flow (L/min)	421.8
Transverse speed (m/s)	1
Stand-off distance (mm)	150
Substrate temperature (^{0}C)	350-400
In-flight particle temperature (^{0}C)	2200
Velocity (m/s)	558
Number of passes	30

5.3.2. Coating characterization methods

Cross sections of the coated HEA samples were used for the coating characterization. The cross sectioned samples were cold mounted by utilizing epoxy resin and left to cure for 24 hours. Polishing of the cross sections were done using 400, 600, 800, 1000, and 1200 grit silicon carbide papers (LECO, Mississauga, ON, Canada) and these were cleaned using alcohol and acetone to avoid any contamination. The surface roughness values for the tests done at room temperature were maintained at $S_a \approx 1.2$ to 1.6 μm for all the samples. For high temperature tests, they were maintained between $S_a \approx 6.8$ to 8.17 μm for cold sprayed and flame sprayed samples and $S_a \approx 1.2$ to 1.6 μm for HVOF sprayed samples. Earlier works of the authors have already established that difference in surface roughness values did not have a significant impact on the friction and wear behaviors of cold sprayed and flame sprayed samples for AlCoCrFeMo HEA coatings in this particular range. The microstructural features were observed using an energy disruptive spectroscopy (EDS) (15 kV) in backscatter mode which was fitted to a scanning electron microscope (SEM) (Zeiss Sigma 300 VP-FE, Carl Zeiss Canada Ltd., Toronto, ON, Canada). The average porosity was determined by high quality image analysis (ImagePro, Media Cybernetics, Bethesda, MD, USA) for ten micrographs (n =10). The phases were identified by performing X-ray diffraction (XRD) (Ultima IV diffractometer Rigaku, Akishima-Shi, TYO, Japan) over the coatings withing the scanning range of 30^O to 90^O at 2 deg/min and Cu-Kα radiation (λ = 1.546 Å). Further analysis of phases was performed by Diffrac.Eva software. Vickers hardness tester (VH1102 Vickers hardness tester, Buehler Wilson, Lake Bluff, IL, USA) was used to measure the average micro-hardness of the coatings in accordance with ASTM Standard E384. 30 indents (n = 30) were made at a load of 300 g and for a dwelling time of 15 s. The XRD characterization for HVOF coating

was performed by using a Bruker AXS, Germany, Model: D8 Discover system at k = 1.78 A^O and 2h = 20^O-130^O (Co Kα radiation) with 35 kV power and 45 mA tube current. Cross sectional studies were performed using a SEM (SU3500, Hitachi, Japan) and the elemental maps were obtained using Oxford Aztec X-Max50 SDD energy disruptive spectroscopy (EDS) system.

5.3.3. Dry sliding wear testing

Reciprocating dry sliding wear tests were performed using a ball-on-disc type tribometer (Model: Anton Paar TriTec SA, Switzerland) at 5 N normal load for 5000 cycles and two different temperatures (room temperature & 450^OC). The relative humidity around the sample was maintained by using desiccants between 18% - 20% for all test conditions. The sliding velocity was kept constant at 3.14cm/s (1Hz) with an amplitude of 10 mm. The total sliding distance at this velocity for 5000 cycles was found to be 100 m. Alumina (AL_2O_3) balls with 6.35 mm diameter were used as a counter face for all the tests. The sliding wear parameters were derived from previous studies of the same research group [1,22] for closer comparison and mentioned in Table 5.5.

Table 5.5 Sliding wear test parameters for cold, flame and HVOF sprayed AlCoCrFeMo high entropy alloy coatings.

Sliding wear parameters	Values
Load	5 N / 10 N
Frequency	1 Hz
Amplitude / track length	10 mm
Velocity / sliding speed	3.14 cm/s
Cycles	5000
Sliding distance	100 m
Counter face	Al_2O_3 (alumina ball)
Counter face diameter	6.35 mm
Temperature	25^O C to 28^O C
Relative humidity	18% to 22%

The wear profile characterization and optical imaging of counter faces were performed using a confocal laser microscope (Model: Olympus LEXT 4000). The wear

profiles obtained were used to calculate the wear area at cross-section of the wear track and the material pile-up area was subtracted from it. This wear area was used to calculate the actual wear volume (V mm^3) by multiplying it by the track length (10 mm). The wear rates (W mm^3/Nm) were calculated using these wear volumes (V mm^3) for all the testing conditions by $W = V / L*D$ where, L is the normal load (5 N) and D is the sliding distance of the wear test (100 m).

The worn surface morphology was analyzed using scanning electron microscope (Model: SU3500, Hitachi, Japan) to interpret the wear mechanisms of the three HEA coatings. Elemental mapping and energy disruptive spectroscopy were performed through Oxford Aztec X-Max50 SDD system attached to the SEM.

5.4. Results and discussion

5.4.1. Characterization of HEA coatings

The characterization of cold sprayed and flame sprayed HEA coatings have been discussed in detail in chapter 4, section 4.4.1 of this thesis. Figure 5.1 shows the XRD spectra for HVOF sprayed AlCoCrFeMo HEA coating. As seen from figure 5.1, HVOF coating showed a presence of BCC phases along with mixed complex oxide phases similar to that of flame sprayed HEA coating. However, the coating characterization of HVOF sprayed HEA compared to that of the flame sprayed coating showed slight variations. For instance, flame spraying is a low velocity and high temperature thermal deposition technique which allows more time for the elements to be oxidized in-flight [1,7,37]. Thus, based on the assessment of Ellingham diagram, it can be inferred that Al, Cr, Fe based oxides have a higher tendency of forming in HVOF sprayed HEA coating [38].

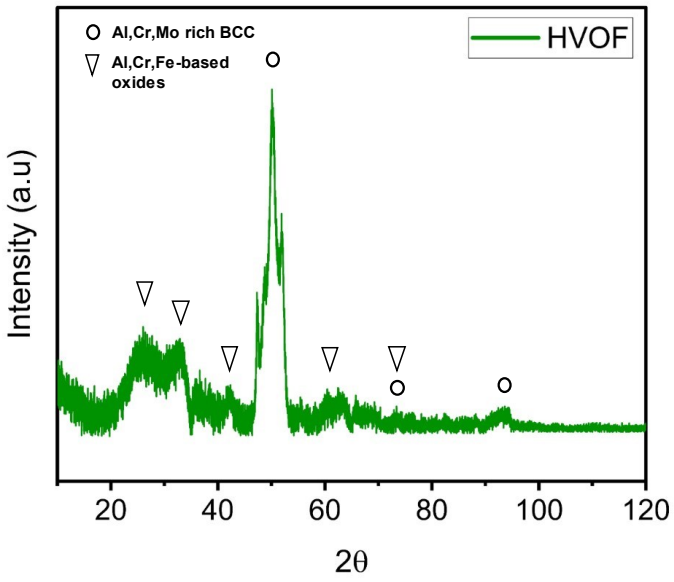

Figure 5.1 X-ray diffraction of HVOF sprayed AlCoCrFeMo high entropy alloy coating.

The backscattered SEM images of HVOF sprayed coating are shown in Figure 5.2. The images suggest that HVOF spraying developed a coating with a finer microstructure, which can possibly be explained by higher particle velocity [23]. The images show a presence of some cracks and faults indicating the brittleness. However, the coating also exhibits plastically deformed splats due to high impact velocities. The microhardness value for cold sprayed HEA was the least ($362 \pm 48\ HV$) among the three followed by flame sprayed HEA ($592 \pm 43\ HV$) and HVOF HEA having the highest hardness ($654 \pm 32\ HV$).

The variations in hardness observed in HVOF sprayed coating as compared to flame sprayed coating can be explained by the differences in their microstructure (see figure 5.2 and figure 4.3). Finer microstructure, deformed phases and lesser porosity in case of HVOF sprayed coating as compared to flame sprayed coating explains the higher hardness values observed in HVOF sprayed HEA coating. Overall, the HVOF sprayed coatings show the characteristics of both flame sprayed as well as cold sprayed HEA coatings.

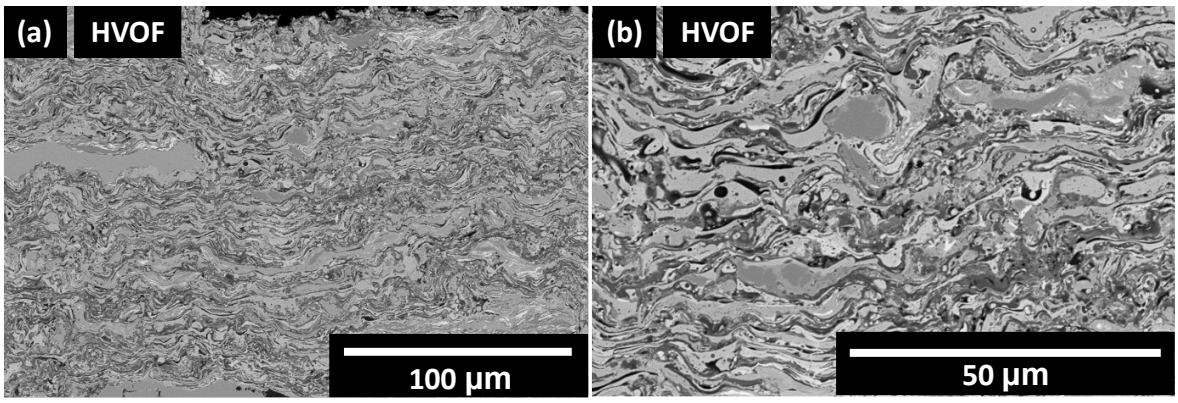

Figure 5.2 Scanning electron microscopy of HVOF sprayed AlCoCrFeMo high entropy alloy coating at (a) low magnification and (b)high magnification.

Figure 5.3 shows the elemental maps of HVOF sprayed HEA coating and table 5.6 summarizes its point analysis data. The results obtained from mapping and analysis align well with the XRD pattern. Figure 5.3 shows a clear presence of oxide concentrations within the coatings. The darker regions of the coating were majorly Al-based and Cr-based oxides whereas the light er regions were rich in Co-based oxides. However, the lighter regions at some locations also exhibited a complex mixture of all the elements along with oxygen suggesting the homogeneity of the coating. Overall, oxides were present throughout the coating along with dominant principal elements in some locations or equally distributed spectra of Al, Co, Cr, Fe, Mo and O which are key for improving the wear behavior of the coating.

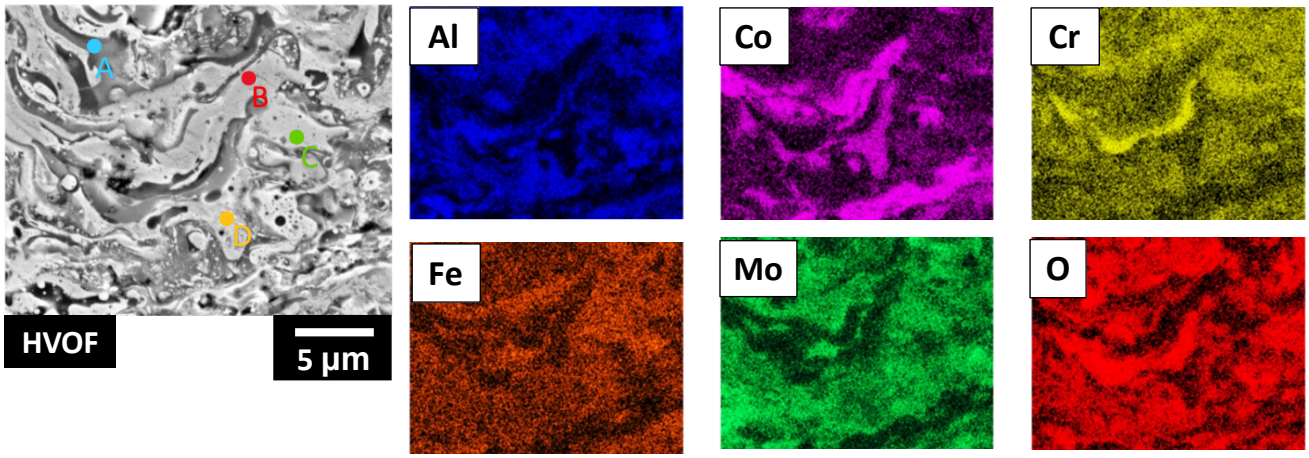

Figure 5.3 Scanning electron microscopy elemental maps of HVOF sprayed AlCoCrFeMo high entropy alloy coating.

Table 5.6 Elemental distribution of HVOF sprayed AlCoCrFeMo high entropy alloy coating.

Regions	Elements are in atomic percentage					
	Al	Co	Cr	Fe	Mo	O
A	9.48	1.86	9.39	5.23	7.44	66.60
B	5.21	68.24	7.21	7.29	8.48	3.57
C	5.80	6.30	26.84	23.92	27.34	9.81
D	1.22	43.39	4.87	15.57	19.82	15.14

5.4.2. Tribological behavior of HEA coatings

The friction coefficient as a function of number of cycles for cold sprayed, flame sprayed and HVOF sprayed AlCoCrFeMo HEA at 5 N normal load is shown in figure 5.4. Figure 5.4(a) shows the friction data for room temperature and figure 5.4(b) for 450^{O}C. At room temperature, a gradual rise in the friction coefficient was observed between 0 to 250 cycles for cold sprayed HEA which is defined as the running-in regime followed by a steady state from 250 to 5000 cycles. The initial rise in the friction is a result of breakage of smooth coating surface and introduction of debris during the first few cycles. Flame sprayed HEA showed a similar running-in and steady state regimes in terms of cycles as compared to cold sprayed HEA. However, for HVOF sprayed HEA, the running-in regime was extended up to approximately 3000 cycles followed by a steady state up to 5000 cycles. The steady state friction values were significantly lower than the running-in regime friction values. This might be due to the delay in formation of smooth tribo-film over the worn surface. The hard oxide phases proved to be resistant against sliding for the initial 3000 cycles until the surface was broken down and transformed into a smooth groove. The initial breakage of oxide-based phases was uneven and created a hinderance in sliding motion which also explains the large fluctuation in friction values during the first 3000 cycles. In comparison, the cold sprayed HEA showed the least friction coefficients for the steady state as compared to flame sprayed and HVOF sprayed HEAs. At steady state, the HVOF still performed much better than the flame sprayed HEA. Large number of debris particles were observed in the case of cold sprayed HEA as compared to the other two. This explains the fluctuations observed throughout the 5000 cycles of cold sprayed HEA. The higher hardness values coupled with strain hardening during sliding of

HVOF sprayed and flame sprayed HEAs resulted in increased shear forces required to break-off the asperities and resisted the sliding motion [24]. The softer nature of the cold sprayed HEA delaminated easily and as a result showed the least value for friction coefficient. Similar theory was proposed by Reid *et al* [25]. in 1987 for Cu-Sn and Cu-Al alloys.

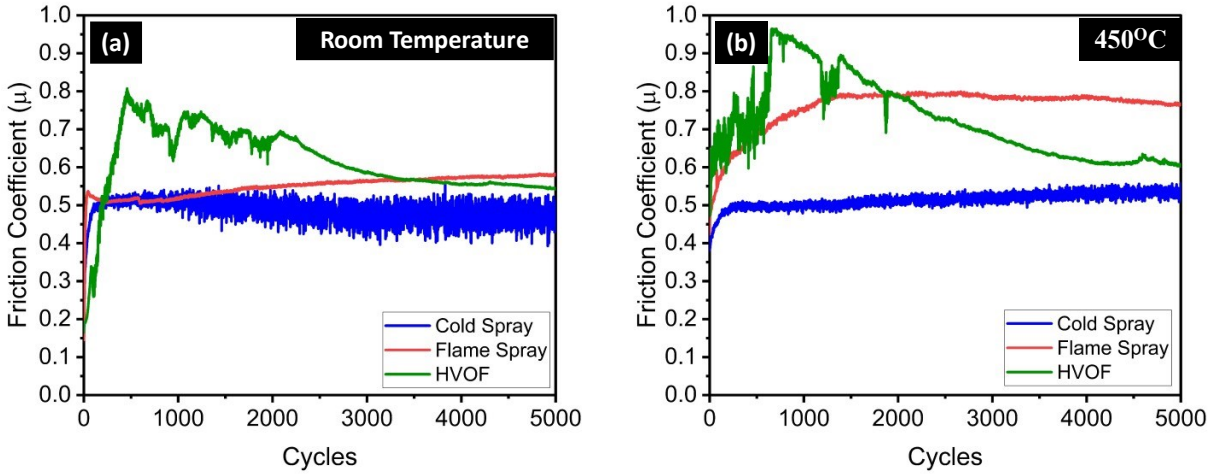

Figure 5.4 Friction coefficient vs. cycles at 5 N load for (a) Room temperature and (b) 450^{O}C.

At 450^{O}C, the friction behavior followed a very similar trend that was observed at room temperature as it is evident from figure 5.4(b). cold sprayed HEA performed better than other two in terms of friction followed by HVOF and lastly flame sprayed HEA. The friction coefficient values and operating regimes remained similar for cold sprayed HEA for both the test temperatures. This might be since the easy delaminating nature of the coating overcame the adhesion caused at elevated temperatures. Flame sprayed HEA showed a delay in steady state at 1500 cycles as compared to 250 cycles at room temperature. This delay in converging to a steady state might be due to initial softening of the HEA with no significant transfer. Increased adhesion of the debris particles to the counter ball must have formed a transfer film after 1500 cycles which resulted in rise in friction coefficient. A steady state was maintained after 1500 cycles until 5000 cycles. Overall friction coefficient of the flame sprayed HEA was observed to be higher at elevated temperatures as compared to the room temperature due to increased adhesion and formation of larger number of debris particles comparatively. The HVOF sprayed HEA showed a slight increase in the friction coefficient at running-in (0 to 2500 cycles) as well as steady-state (2500 to 5000 cycles) regimes also due to the increase in adhesive component introduced by the rise in temperature. At both

temperatures, HVOF sprayed HEA showed friction coefficient values closer to cold sprayed HEA during steady state.

Figure 5.5 shows the wear depth profiles of cold sprayed, flame sprayed and HVOF sprayed HEAs at 5 N normal loads at both testing temperatures. Figure 5.5(a) shows the wear depth profiles at room temperature. It can be clearly seen that higher wear depth of about ~ 70 to 80 µm was observed for cold sprayed HEA but the depths for flame sprayed and HVOF sprayed HEAs were almost negligible for these test conditions. However, the flame sprayed HEA revealed a more uneven wear profile with non-uniform patches of wear throughout the wear track. HVOF HEA even though having negligible wear depth, still showed a distinct groove. The wear depth profiles show that cold sprayed HEA had a significantly wider groove followed by the flame sprayed HEA and lastly the HVOF sprayed HEA. Figure 5.5(b) shows the wear profiles for 450^{O}C. It can be observed that cold sprayed HEA and HVOF sprayed HEA showed a reduction in wear depth at elevated temperatures by almost ~30 µm and ~5 µm respectively. However, the flame sprayed HEA surprisingly showed a significant increase in the wear depth which also follows its rising trend of friction coefficient at elevated temperature.

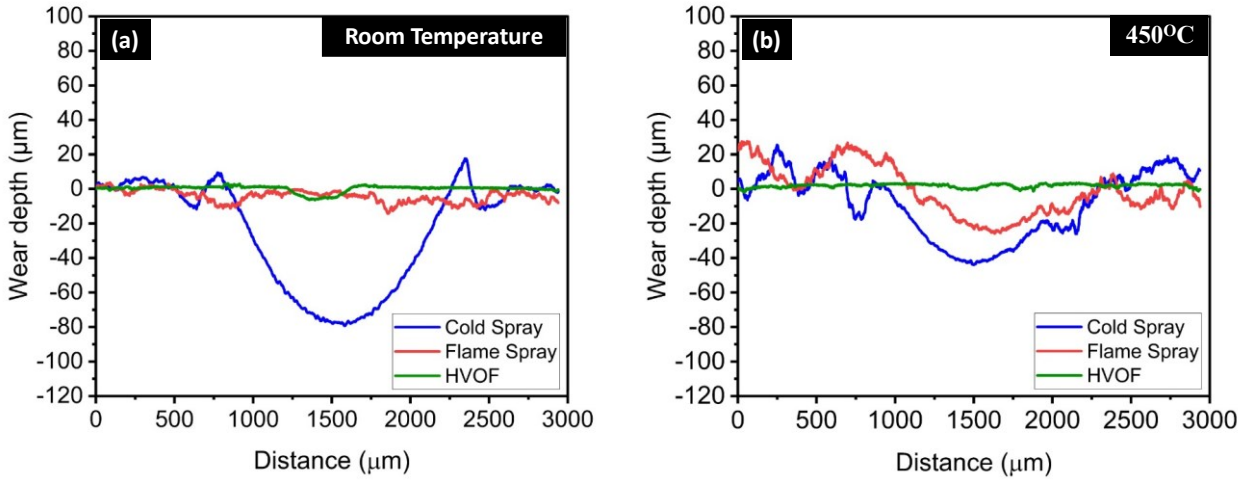

Figure 5.5 Wear depth profile of cold sprayed, flame sprayed and HVOF sprayed samples at 5 N load for (a) Room temperature and (b) 450^{O}C.

The wear rates for all the HEAs at all test temperatures have been depicted in figure 5.6. Similar to the wear depth profiles, it is evident that cold sprayed HEA showed the highest wear rates at room temperature (140 x 10^{-5} mm^3 Nm^{-1}) as well as 450^{O}C (71.8 x 10^{-5} mm^3 Nm^{-1}) compared to the other two with a reduction of almost 50% at elevated temperature. The wear rates of the HVOF sprayed HEA reduced from 3.96 x 10^{-5} mm^3 Nm^{-1} at room temperature to 0.7 x 10^{-5} mm^3 Nm^{-1} at 450^{O}C. Whereas, that of flame sprayed HEA increased from 10 x 10^{-5} mm^3 Nm^{-1} at room temperature to 21.68 x 10^{-5} mm^3 Nm^{-1} at 450^{O}C. More discussion on wear behavior at elevated temperatures has been provided in the next section (section 5.4.3).

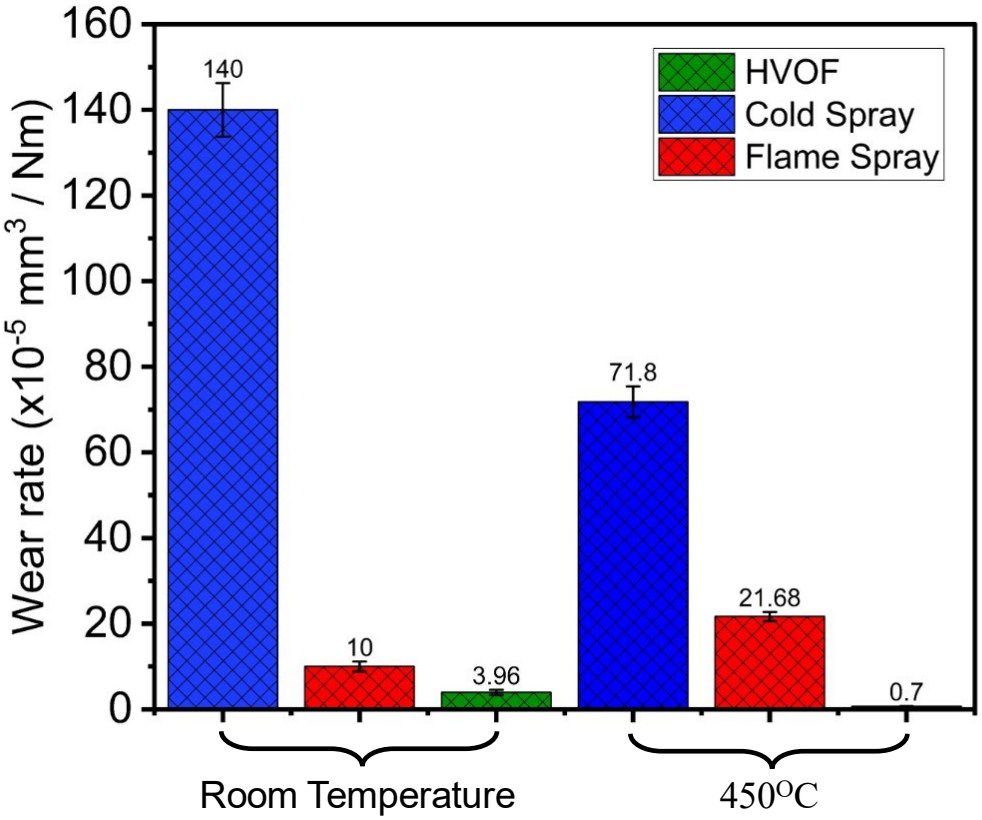

Figure 5.6 Wear rates of cold sprayed, flame sprayed and HVOF AlCoCrFeMo high entropy alloy coatings at 5 N normal load for room temperature and 450^{O}C.

The evolution of microstructure was evidently different in cold sprayed HEAs as compared to flame sprayed and HVOF sprayed HEAs as discussed in detail in the previous sections (section 4.4.1 and section 5.4.1) of this thesis. Large presence of oxides due to in-flight oxidation was observed in the case of flame sprayed and HVOF sprayed HEAs due to the difference in the deposition temperatures. These oxide phases

coupled with the microstructure formed, contributed towards the hardness of the coatings (see previous section). The cold sprayed HEA had almost negligible oxide inclusions and hence exhibited lower hardness values. The differences in the wear rates between the different coatings correlates well with the differences in their hardness values. Further investigation on wear behavior has been carried out on worn surfaces and the discussion has been provided in the following section (section 5.4.3).

5.4.3. Ex-situ analysis of worn surfaces and counter ball after sliding tests

To understand the variations and the mechanisms of the wear behavior of the HEA coatings, the worn surfaces were further characterized using scanning electron microscopy (SEM), electron disruptive spectroscopy (EDS) analysis and elemental mapping. The elemental maps for the cold sprayed and flame sprayed HEAs (figure 4.13) along with the EDS analysis table (table 4.5) at room temperature has been presented in the previous chapter (chapter 4) of this thesis. Table 5.7 summarizes the EDS analysis data for HVOF sprayed HEA for room temperature and Figure 5.7 shows the elemental maps for HVOF sprayed HEA at room temperature. Figure 5.8 shows the worn surface morphologies of HEA coatings at room temperature tests. Figure 5.8(a, b) shows the worn surfaces of cold sprayed HEA at room temperature. It was observed that the worn surface was covered by wear scars parallel to the sliding direction throughout the wear track. This signifies that the wear was dominated by abrasive mechanism [12]. The wear track also showcased delamination and plastically deformed phases with a very minute presence of cracks which indicates that the resistance to wear was very low. The worn surface as showcased in figure 4.11 (b), also had a presence of oxide debris particles which must have acted as third bodies and accelerated the wear. These oxide debris particles must have resulted from frictional heating at the interface of the counter ball and surface of the coating which also explains the fluctuation observed in the friction graph of the HEA. It can be inferred that the wear mechanism for this system was mostly ploughing/abrasion along with third body abrasion.

Figure 5.8(c, d) shows the worn surfaces of the flame sprayed HEAs that showcase the brittle nature of the coating. The observed wear was non uniform and abrupt throughout the wear track with almost negligible presence of abrasion marks. The higher hardness of the coating contributed towards increased wear resistance as

compared to cold sprayed HEA coating. Unlike the worn surface of the cold sprayed HEA, the worn surface of the flame sprayed HEA exhibited numerous cracks with clear evidence of brittle fracture. Fragmented debris was observed with no evidence of plastic deformation which is an indicator of higher hardness. The absence of abrasive wear scars and the distinct phases with large number of cracks indicate that the wear was dominated mostly through brittle failure mechanisms. Oxide debris particles were found adhered to the surface of the wear track which indicates that an oxide based tribo-film was formed which protected the surface underneath from further wear. Elemental maps shown in figure 4.13 (b) and EDS analysis (table 4.5) proves that there was no significant change in the oxide contents after the sliding wear as compared to unworn surface and the oxide inclusions mainly originated from the high temperature deposition process.

The worn surface of the HVOF sprayed HEA at room temperature is shown in figure 5.8(e, f). HVOF sprayed HEA possessed the highest hardness as compared to other which played a key role in improving the wear resistance. Similar to flame sprayed HEA, it also showed numerous cracks and evidence of brittle failure. However, abrasive wear scars and plastically deformed asperities were also observed along with homogenized phases which explains the smooth uniform wear groove. Evidence of large oxide-based debris layer was found adhered to the surface which protected the surface and resisted the wear similar to flame sprayed HEA. The elemental analysis suggested that oxide percentage over the surface did not change significantly after sliding. Large patches of oxide debris were found with presence of all principal elements in a uniform fashion.

Table 5.7 Elemental distribution on worn surface of HVOF sprayed AlCoCrFeMo high entropy alloy coating at room temperature.

Regions	Elements are in atomic percentage					
	Al	Co	Cr	Fe	Mo	O
A	7.74	6.67	7.07	7.63	8.66	62.23
B	19.94	11.81	13.39	17.99	23.13	13.74
C	4.68	53.82	3.01	3.39	3.51	31.59

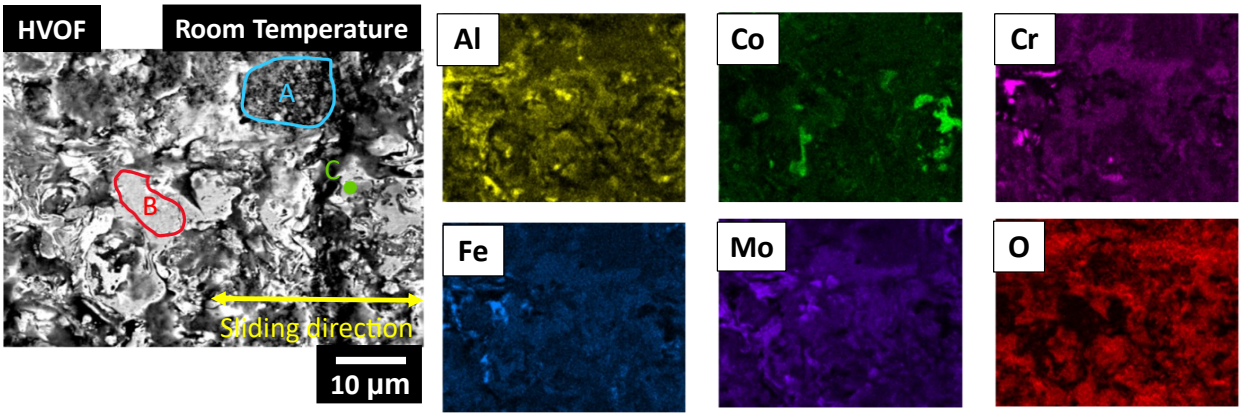

Figure 5.7 Scanning electron microscopy elemental maps of worn surface of HVOF sprayed AlCoCrFeMo high entropy alloy coating at room temperature.

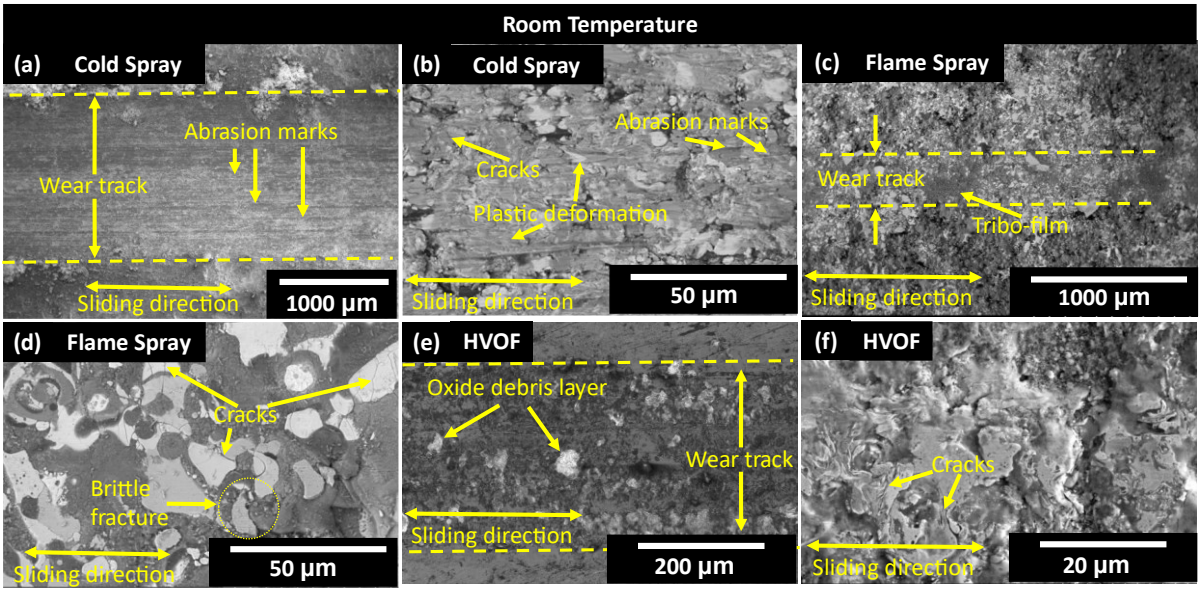

Figure 5.8 Worn surface morphology of (a, b) Cold sprayed, (c, d) Flame sprayed and (e, f) HVOF sprayed AlCoCrFeMo high entropy alloy coatings at 5 N normal load for room temperature.

Figure 5.9 shows the worn morphologies of the alumina counter balls for all testing conditions. As seen from figure 5.9(a), the counter face of the cold sprayed HEA showed significantly larger transfer of frictionally heated debris particles as compared to the other two. The transfer film suggests that large amount of delamination occurred in cold sprayed coating and increased the wear rates as a result. The flame sprayed HEA counter ball (figure 5.9(b)) showed less transfer at room temperature with visible scratches and cracks at the area of contact which implies that the hard coating resisted the sliding motion leading to increased friction and reduced wear. On the contrary, the

HVOF sprayed HEA counter ball at room temperature as observed in figure 5.9(c), showed less transfer compared to the cold sprayed and flame sprayed coatings. The area of contact appears to be the lowest among the three with harsh wear damage on the alumina ball due to hardness of coating. These findings align well with the low wear rates of this coating. Presence of wear scars and lack of cracks also confirms that abrasion played a part in wearing out the coating however, the hardness and oxide layer prevented the wear rates from inflating as inferred from the wear track analysis.

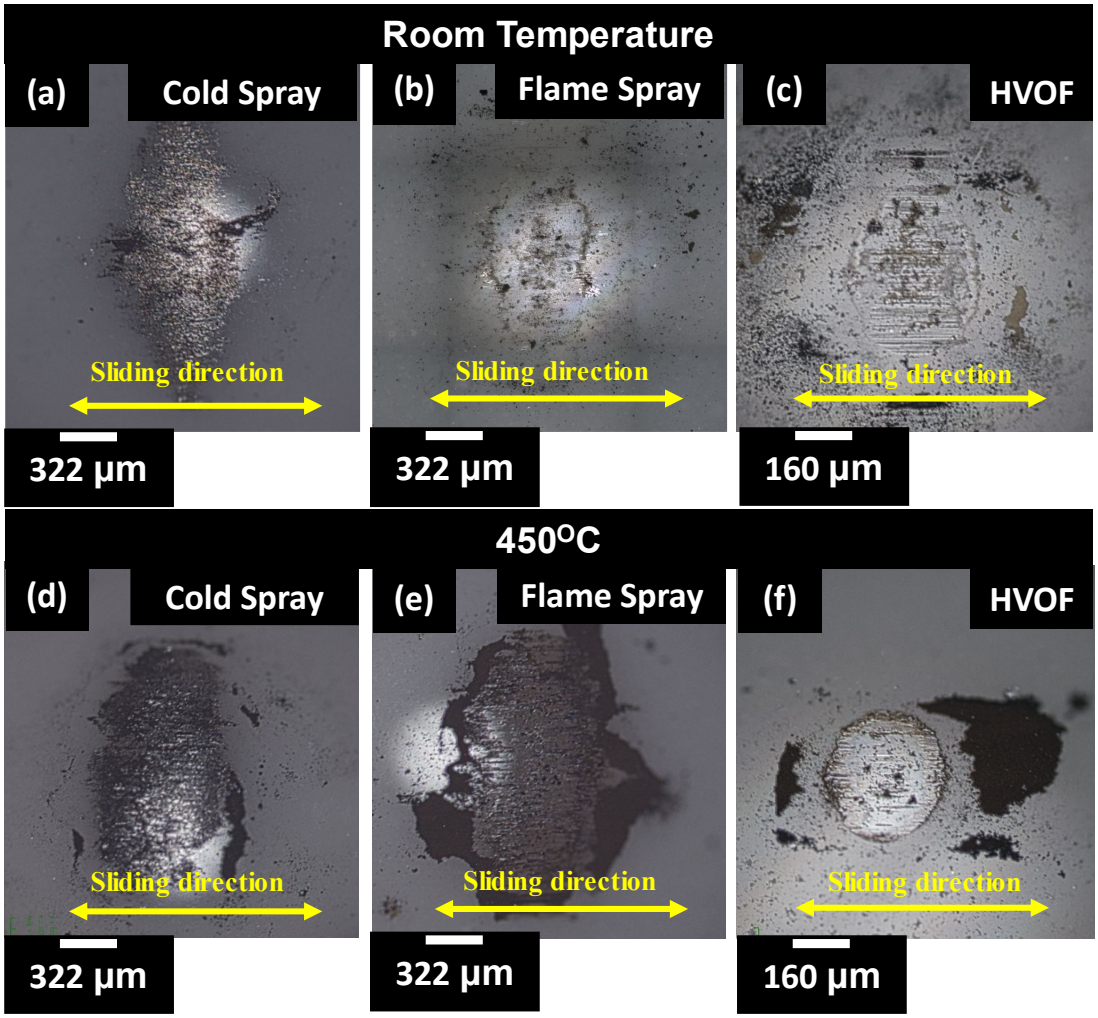

Figure 5.9 Wear morphology of alumina counter ball after sliding at 5 N normal load for (a) Cold sprayed HEA, (b) Flame sprayed HEA, (c) HVOF sprayed HEA at room temperature and (d) Cold sprayed HEA, (e) Flame sprayed HEA, (f) HVOF sprayed HEA at 450^{O}C.

Overall, the oxide inclusion and atomic phase structure played an integral part in determining the wear rates of the HEA coatings. As discussed earlier, aluminum supported the formation of BCC phase structure in addition to the oxides formed due to high temperature deposition processes in case of flame sprayed and HVOF sprayed

HEA coatings which increased the hardness of the coating significantly as discussed by many researchers [26-28]. The increased hardness proved to be vital in increasing the wear resistance of flame sprayed and HVOF sprayed HEA. Severe wear occurred in cold sprayed HEA due to continuous delamination of surface due to weak cohesive strength, large number of debris particles resulting in three body abrasion, large amount of transfer on the counter ball resulting in harsh ploughing damage and lack of oxide based tribo-film to protect the surface underneath [7]. Poza et al [29] have suggested that Al-based coatings tend to show plastic deformation leading to delamination. It was also noticed that the wear mechanism was mostly adhesive type during initial sliding however during latter cycles, the creation of hard oxidized debris acted as third bodies and caused massive abrasive wear which matched perfectly with the observations made in this current study. In case of flame sprayed HEA coating, the oxide phases protected the surface from severe delamination and abrasive wear [30,31]. However, the brittle failure of coating led to uneven wear leading to severely worn patches at some locations. The oxidized loose debris was hard enough to initiate cracks on the worn surface and cause wear, but contrastingly adhered debris formed a tribo-film over the wear track protecting further wear. The evidence of loose debris observed was significantly low owing to the hardness which resulted in shallower groove due to lack of enough ploughing [32]. The wear mechanism appears to be dominated by brittle failure coupled with some amount of adhesion. Interestingly, HVOF sprayed HEA coating exhibited characteristics which were a combination of the other two HEA coatings. Similar to flame sprayed HEA, the worn surface analysis provided evidence of brittle failure with minor cracks indicating high hardness. The hardness of the coating being highest among comparison group, showed the least wear rate. Howsoever, the worn surfaces also exhibited abrasion marks and plastic deformation which resulted in smooth groove avoiding non uniform patches of wear. The counter ball surface showed no significant transfer which proved that the adhesive component of wear was not exaggerating. The wear occurred due to mild abrasion causing deformation of asperities and brittle failure to some extent. The hard oxide phases, oxide-based tribofilm and plastically deformed asperities improved the wear resistance of the coating. The non-uniform wear of flame sprayed HEA and uniform wear of cold sprayed and HVOF sprayed HEA could be a characteristic of the size of phases observed in figure 5.8. The variations in size of phases were introduced due to variations in splats morphology as

a result of high particle velocities in case of cold sprayed and HVOF sprayed coating as opposed to flame sprayed coating [33,34].

Figure 5.10 shows the worn morphologies of all the coating systems at 450^{O}C. As observed from figure 5.10(a, b), the cold sprayed HEA coating exhibited a very similar mechanisms for wear and the wear track width reduced to ~1.4mm from 1.6mm as temperature increased. Abrasion marks are clearly visible similar to the tests at room temperature with presence of minor cracks. However, a smoother tribofilm was visible at elevated temperatures. Figure 5.11(a) show the elemental maps of cold sprayed HEA from which it can be inferred that the smooth tribofilm showed a large presence of oxide content which was also confirmed from table 5.8 showing the EDS analysis. Visible pits over worn surface signifies the brittle nature, a characteristic of harder surface, of the coating which arises from fracturing of oxide-based tribo-layer. The worn surface morphologies of the counter ball at 450^{O}C shown in figure 5.9(d) suggests that the transfer of material was almost similar to that observed at room temperature with a slight increase in heated debris particles. The frictionally heated debris was mostly found adhered to the wear track or the counter-ball at 450^{O}C as opposed to the loose particles observed at room temperature.

Wear track morphology of flame sprayed HEA at 450^{O}C can be found in figure 5.10(c, d). Surprisingly, the track width increased to ~1.1mm at 450^{O}C from 0.7mm at room temperature. It was observed that the wear groove was much more uniform as compared to that at room temperature which signifies wear by ploughing through asperities. On a closer analysis it was observed that the brittle failure and cracks were still evident at 450^{O}C. The elemental analysis confirmed that no significant difference in oxide concentrations was seen between these operating temperature ranges. Significantly large amounts of debris particles were observed at elevated temperatures which signifies that the asperities were easily broken off at higher temperatures. The worn surface of the counter ball shown in figure 5.9(e) shows significantly larger amount of transfer made up of frictionally heated debris particles. This is a sign of increased adhesion leading to adhesive type of wear and ploughing through the coating. The area of contact was clearly large at 450^{O}C due to deeper penetration of counter ball in the coating. All the evidence suggests that the hardness of the coating might have been decreased at 450^{O}C which explains the increased wear rates.

The HVOF sprayed HEA at 450^{O}C as observed in figure 5.10(e, f), shows a reduction in track width from ~0.3mm at room temperature to ~0.2mm at 450^{O}C. Magnified images show that the wear track was covered with a large oxide based tribo-film which protected the surface from wear. The elemental maps suggest that this oxide was majorly Co-based. Similar to that at room temperature, the surface showed minor abrasion marks with a small amount of plastically deformed phases. The worn surface had no visible cracks or loose debris particles. The counter ball shown in figure 5.9(f) presents a clear reduction in area of contact and much cleaner surface with the exception of transfer-film which suggests that the surface might be harder at 450^{O}C as compared to room temperature.

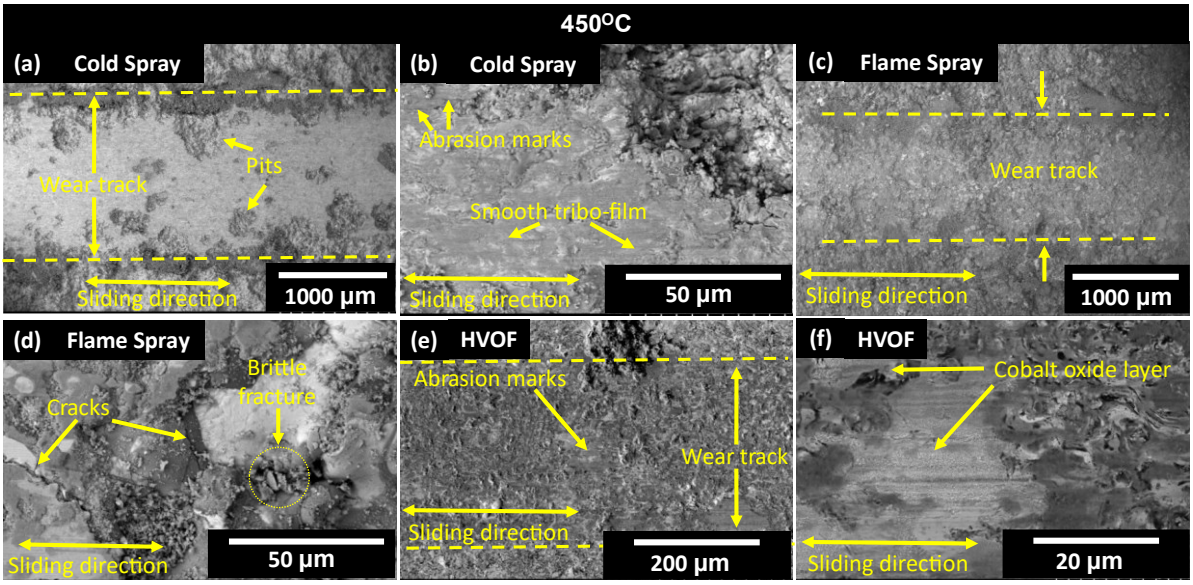

Figure 5.10 Worn surface morphology of (a, b) Cold sprayed, (c, d) Flame sprayed and (e, f) HVOF sprayed AlCoCrFeMo high entropy alloy coatings at 5 N normal load for 450^{O}C.

Table 5.8 Elemental distribution on worn surface of cold sprayed, flame sprayed and HVOF sprayed AlCoCrFeMo high entropy alloy coating at 450^{O}C.

Regions	Elements are in atomic percentage					
	Al	Co	Cr	Fe	Mo	O
A	0.18	32.4	0.55	0.44	8.11	58.32
B	40.03	2.03	0.49	12.83	3.87	40.75
C	8.64	4.73	18.52	5.90	6.98	55.23

D	0.0	16.16	2.88	15.32	30.70	34.94
E	1.39	8.28	22.25	12.40	16.19	39.47
F	28.04	1.91	30.09	12.91	1.23	25.82
G	8.29	8.47	6.85	7.33	9.12	59.94
H	0.15	58.23	0.57	0.33	0.12	40.59
I	5.21	38.68	11.04	13.67	16.75	14.66

In comparison among the deposition processes, the wear behavior of cold sprayed, flame sprayed and HVOF sprayed HEAs showed similar results. At elevated temperatures, the wear rates of the cold sprayed HEAs reduced significantly due to the

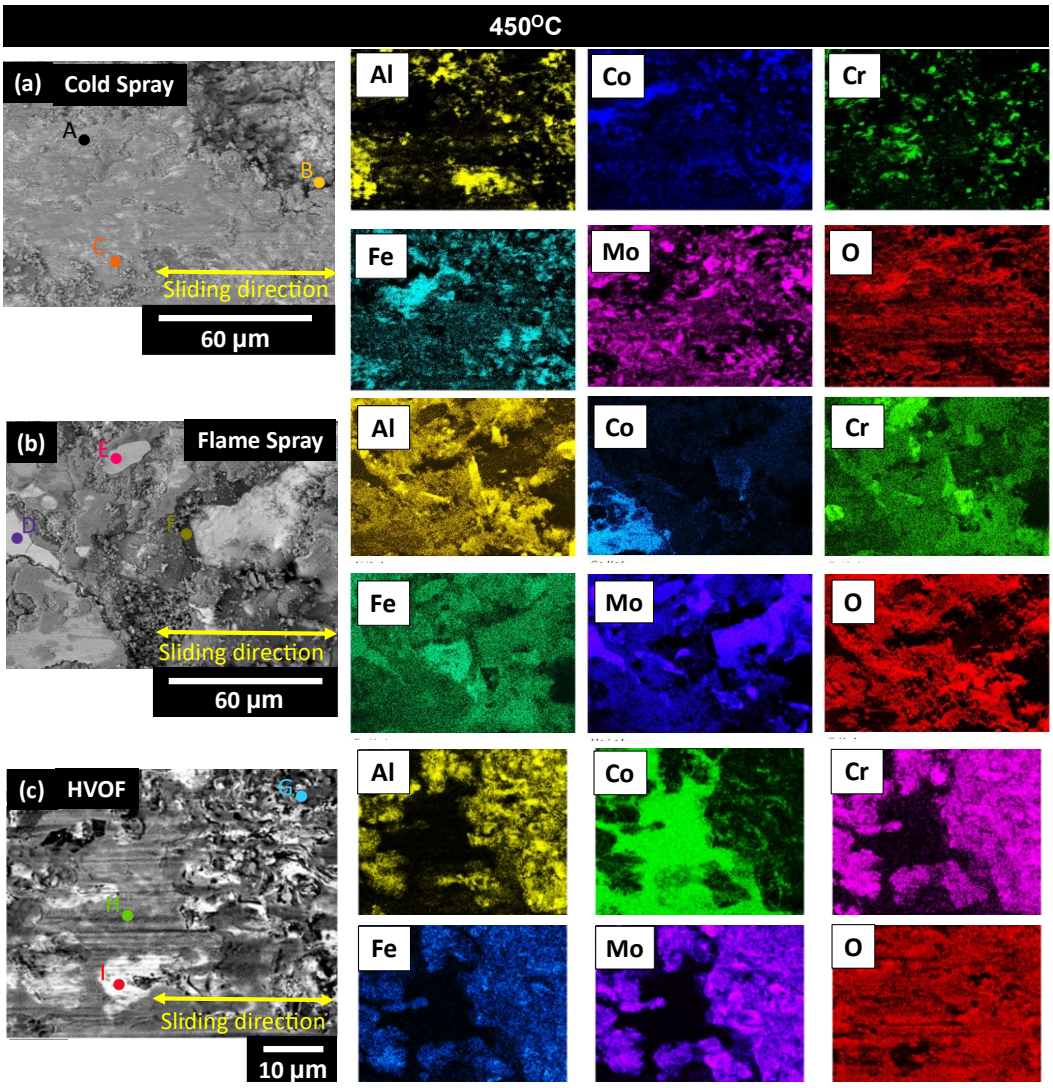

Figure 5.11 Scanning electron microscopy elemental maps of worn surface of (a) Cold sprayed, (b) Flame sprayed and (c) HVOF sprayed AlCoCrFeMo high entropy alloy coating at 450°C.

increase in oxide based tribo-films formed over the surfaces and possible increase in

hardness. The reduction of loose debris mitigated the three-body abrasion and the oxide based tribofilm protected the surface from further wear. At both the temperatures, the cold sprayed HEA showed similar mechanisms of delamination and abrasive type of wear However, for the flame sprayed HEA, the increase in adhesion component and debris formation leading to abrasive wear at 450^{O}C with probable decrease in hardness, increased the wear rates significantly. The flame sprayed HEA still exhibited large amount of brittle fracture and cracks and the wear mechanism was dominated by adhesion and mild abrasion for high temperature tests. The HVOF sprayed HEA showed a large increase in Co-based oxide layer over the surface which must have been hindered in formation of Al-based or Cr-based oxides, which are mostly abrasives, in larger quantities. Ceramic layers usually protect the surface from wear however, they are brittle and fail due to mechanical loading and eventually end up increasing the wear [35]. Interesting work done by Viat *et al*. [36] suggests that Co-based oxides, on the other hand, exhibit ductility as opposed to brittleness at elevated temperatures and reduces wear. This phenomenon might have plastically deformed the phases instead of fracturing them and prevented the coating from severe third body abrasive wear due to broken ceramic debris particles. This explains the reduced wear rates of HVOF sprayed HEA at high temperatures.

5.4.4. Proposed mechanisms

The proposed mechanism for the cold sprayed and flame sprayed HEA has been discussed in detail in the previous chapter of this thesis (chapter 4). The proposed mechanism has been derived through rigorous analysis of the friction, wear behavior and ex-situ analysis of the worn surfaces. At room temperature, the HVOF sprayed HEA showed the least wear rates as a characteristic of its highest hardness in comparison. The higher hardness could have potentially contributed to a decrease in the amount of abrasion. In addition, a smooth oxide based tribo-film was formed over the surface which helped decrease the overall wear. With progression of sliding, the surface of the coating succumbed to fatigue stresses leading to brittle failure giving rise to some loose debris particles. These debris particles caused minor abrasion which was evident from the wear scars observed in some regions of the wear track.

At 450^{O}C, the cold sprayed HEA showed an increased amount oxide content over the worn surface indicating a presence of a more uniform tribo-film as compared

to that at room temperature. In addition, the wear track was observed to be smooth with negligible presence of cracks or brittle failure. Reduction in the fluctuations observed on the friction graph indicates that lesser number of loose debris particles were formed hence mitigating the three-body abrasive wear. The wear rates at elevated temperatures were reduced due to possible increase in the hardness and formation of hard oxide phases over the worn surface indicated by pits observed on the wear track due to brittleness of the coating.

The flame sprayed HEA coating at 450^{O}C, showed increased wear rates due to significant increase in the adhesive component and possibility of reduced hardness. The surface of the coating was subjected to adhesive type of wear which is evident from the area of contact of counter-ball and friction graphs during the initial sliding. Large amounts of cracks and loose debris was observed over the worn surface at elevated temperatures which suggests that the brittle fatigue failure also increased due to softening of asperities. Overall, the wear mechanism at high temperatures can be said to be dominated by breakage of asperities and formation of loose debris particles which accumulated on the counter ball forming transfer-film that penetrated the coating deeper than the coating at room temperature and accelerated the wear.

The HVOF sprayed HEA coating at 450^{O}C, showed significant reduction in wear rates which can be attributed to a smooth and uniform oxide-based tribo-film (i.e., Co-rich). The wear of the coating showed similar mechanisms compared to the room temperature wear. The wear track of the coating exhibited a slight increase in adhesion during the initial sliding cycles which can be inferred from friction graph and blackened transfer observed over counter ball. The worn surface of the coating showed a reduction in brittle failure and evidence of plastic deformation with some amount of abrasion. Figure 5.12 illustrates a schematic representation of the proposed wear mechanisms in

worn state of cold sprayed, flame sprayed and HVOF sprayed AlCoCrFeMo HEA coatings at room temperature as well as 450^{O}C.

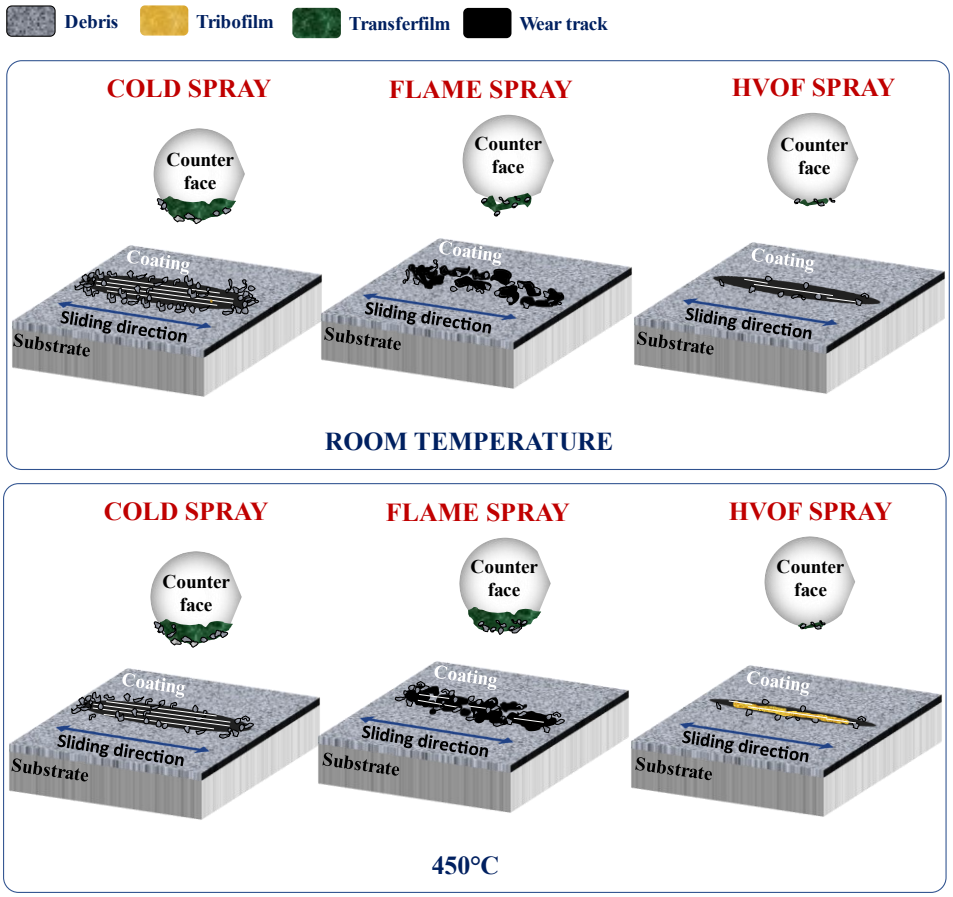

Figure 5.12 Proposed wear mechanism for cold sprayed, flame sprayed and HVOF sprayed AlCoCrFeMo high entropy alloy coatings at room temperature and 450^{O}C.

5.5. Conclusions

In this study, AlCoCrFeMo high entropy alloy coatings were developed using cold spray, flame spray and HVOF. These coatings were tested to evaluate their friction and wear behavior at room temperature as well as 450^{O}C. A comparative evaluation of the coatings was drawn, and the following conclusions were deduced:

- HVOF sprayed and flame sprayed HEA coatings exhibited large concentrations of oxide inclusions compared to cold sprayed HEA coating at both operating temperatures leading to increased hardness values.

- At room temperature, the cold sprayed HEA (0.49) had the least steady state friction coefficient followed by HVOF sprayed HEA (0.56) and flame sprayed HEA (0.55). The wear was dominated by abrasive mechanisms due to large number of debris formation for cold sprayed HEA, brittle failure with minor adhesion for flame sprayed HEA and minor abrasion coupled with brittle failure due to the hard nature of the coatings. The HVOF sprayed HEA performed better than the rest with minimal wear rates followed by flame sprayed HEA and cold sprayed HEA being the worst. The high wear rates for cold sprayed HEA are a direct result of low hardness values as compared to other two.
- At $450^{O}C$, the friction coefficients of all the systems increased as a result of rise in adhesive component. The steady state friction coefficient of the flame sprayed HEA (0.78) was the highest followed by HVOF (0.64) and cold sprayed HEA (0.52) coating. The wear for the cold sprayed HEA was still dominated by ploughing/abrasion and delamination however, the wear rates reduced at elevated temperatures due to formation of oxide-based tribo-film giving rise to small degree of brittle failure characterized by pits over the wear track. The wear rates for the flame sprayed HEAs reduced because of significant increase in adhesive component followed by deeper penetration of counter ball and possible decrease in the hardness. The wear mechanisms at elevated temperature showed evidence of increased abrasion with significant increase in debris formation due to brittle failure. HVOF sprayed HEA coating showed a rise in Co-based tribo-film formation over the worn surface which prevented wear. As a result, the wear rates at $450^{O}C$ for HVOF sprayed coating were the least among all the other tested systems. The wear occurred due plastic deformation of asperities followed by minor abrasion and adhesion.
- HVOF spraying seems to be the most suitable thermal deposition technique for producing wear resistant AlCoCrFeMo high entropy alloy coating followed by flame spraying. Cold spraying, even though having performed better in friction as compared to other two, shows significantly large wear rates.

References:

1. P. Patel, S.A. Alidokht, N. Sharifi, A. Roy, K. Harrington, P. Stoyanov, R.R. Chromik, C. Moreau, Microstructural and Tribological Behavior of Thermal Spray CrMnFeCoNi High Entropy Alloy Coatings, Journal of Thermal Spray Technology, (2022)
2. R.B. Nair, H.S. Arora, A. Ayyagari, S. Mukherjee, H.S. Grewal, High Entropy Alloys: Prospective Materials for Tribo-Corrosion Applications, Advanced Engineering Materials, 20(6), (2018)
3. J.W. Yeh, S.K. Chen, S.J. Lin, J.Y. Gan, T.S. Chin, T.T. Shun, C.H. Tsau, S.Y. Chang, Nanostructured High-Entropy Alloys with Multiple Principal Elements: Novel Alloy Design Concepts and Outcomes, Advanced Engineering Materials, 6(5), 299-303 (2004)
4. S. Ranganathan, Alloyed pleasures: Multimetallic cocktails, Current science, 85(10), 1404-1406 (2003)
5. B. Cantor, I.T.H. Chang, P. Knight, A.J.B. Vincent, Microstructural development in equiatomic multicomponent alloys, Materials science & engineering. A. Structural materials : properties, microstructure and processing., 375(1), 213 (2004)
6. A. Meghwal, A. Anupam, B.S. Murty, C.C. Berndt, R.S. Kottada, A.S.M. Ang, Thermal Spray High-Entropy Alloy Coatings: A Review, Journal of Thermal Spray Technology, 29(5), 857-893 (2020)
7. R.B. Nair, G. Perumal, A. McDonald, Effect of Microstructure on Wear and Corrosion Performance of Thermally Sprayed AlCoCrFeMo High-Entropy Alloy Coatings, Advanced Engineering Materials, 2101713 (2022)
8. M. Vaidya, G.M. Muralikrishna, B.S. Murty, High-entropy alloys by mechanical alloying: A review, Journal of Materials Research, 34(5), 664-686 (2019)
9. B.S. Murty, J.-W. Yeh, S. Ranganathan, High-entropy alloys, 1 ed., Elsevier, 2014
10. B. Jin, N. Zhang, H. Yu, D. Hao, Y. Ma, AlxCoCrFeNiSi high entropy alloy coatings with high microhardness and improved wear resistance, Surface & Coatings Technology, 402, (2020)
11. A. Erdogan, K.M. Doleker, Comparative study on dry sliding wear and oxidation performance of HVOF and laser re-melted Al0.2CrFeNi(Co,Cu) alloys, Transactions of

Nonferrous Metals Society of China, 31(8), 2428-2441 (2021)

12. J. Joseph, N. Haghdadi, K. Shamlaye, P. Hodgson, M. Barnett, D. Fabijanic, The sliding wear behaviour of CoCrFeMnNi and AlxCoCrFeNi high entropy alloys at elevated temperatures, Wear =, 428, 32-44 (2019)

13. M. Zhang, X. Zhang, M. Niu, Z. Jiang, H. Chen, Y. Sun, High-temperature tribological behavior of CoCrFeNiV high-entropy alloys: A parallel comparison with CoCrFeNiMn high-entropy alloys, Tribology International, 174, 107736 (2022)

14. P. Patel, A. Roy, N. Sharifi, P. Stoyanov, R.R. Chromik, C. Moreau, Tribological Performance of High-Entropy Coatings (HECs): A Review, Materials (Basel, Switzerland), 15(10), (2022)

15. C. Chen, Y. Xie, L. Liu, R. Zhao, X. Jin, S. Li, R. Huang, J. Wang, H. Liao, Z. Ren, Cold spray additive manufacturing of Invar 36 alloy: microstructure, thermal expansion and mechanical properties, Journal of Materials Science & Technology, 72, 39-51 (2021)

16. N. Fan, J. Cizek, C. Huang, X. Xie, Z. Chlup, R. Jenkins, R. Lupoi, S. Yin, A new strategy for strengthening additively manufactured cold spray deposits through in-process densification, Additive Manufacturing, 36, 101626 (2020)

17. S. Yin, M. Hassani, Q. Xie, R. Lupoi, Unravelling the deposition mechanism of brittle particles in metal matrix composites fabricated via cold spray additive manufacturing, Scripta Materialia, 194, 113614 (2021)

18. Y. Zou, Z. Qiu, C. Huang, D. Zeng, R. Lupoi, N. Zhang, S. Yin, Microstructure and tribological properties of Al2O3 reinforced FeCoNiCrMn high entropy alloy composite coatings by cold spray, Surface & Coatings Technology, 434, (2022)

19. A. Silvello, P. Cavaliere, S. Yin, R. Lupoi, I. Garcia Cano, S. Dosta, Microstructural, Mechanical and Wear Behavior of HVOF and Cold sprayed High-Entropy Alloys (HEAs) Coatings, Journal of Thermal Spray Technology, (2022)

20. M. Lobel, T. Lindner, T. Lampke, High-temperature wear behaviour of AlCoCrFeNiTi_{0.5} coatings produced by HVOF, Surface and Coatings Technology, 403, (2020)

21. H. Wu, S. Zhang, Z. Wang, C. Zhang, H. Chen, J. Chen, New studies on wear and corrosion behavior of laser cladding FeNiCoCrMox high entropy alloy coating: The role of Mo, International Journal of Refractory Metals and Hard Materials, 102, 105721 (2022)

22. P. Tonge, A. Roy, P. Patel, C.J. Beall, P. Stoyanov, Tribological Evaluation of Lead-Free MoS2-Based Solid Film Lubricants as Environmentally Friendly Replacements for Aerospace Applications, Lubricants, 10(1), 7 (2022)

23. G. Munday, J. Hogan, A. McDonald, On the microstructure-dependency of mechanical properties and failure of low-pressure cold sprayed tungsten carbide-nickel metal matrix composite coatings, Surf. Coat. Technol., 396, 125947 (2020)

24. D.A. Rigney, J.P. Hirth, Plastic deformation and sliding friction of metals, Wear, 53(2), 345-370 (1979)

25. J.V. Reid, J.A. Schey, The effect of surface hardness on friction, Wear, 118(1), 113-125 (1987)

26. N. Hua, W. Wang, Q. Wang, Y. Ye, S. Lin, L. Zhang, Q. Guo, J. Brechtl, P.K. Liaw, O.R.T.N. Oak Ridge National Lab, Mechanical, corrosion, and wear properties of biomedical Ti–Zr–Nb–Ta–Mo high entropy alloys, Journal of Alloys and Compounds, 861(1), (2021)

27. C. Mathiou, A. Poulia, E. Georgatis, A.E. Karantzalis, Microstructural features and dry - Sliding wear response of MoTaNbZrTi high entropy alloy, Materials Chemistry and Physics, 210, 126-135 (2018)

28. N. Tüten, D. Canadinc, A. Motallebzadeh, B. Bal, Microstructure and tribological properties of TiTaHfNbZr high entropy alloy coatings deposited on Ti[sbnd]6Al[sbnd]4V substrates, Intermetallics, 105, 99-106 (2019)

29. P. Poza, M.Á. Garrido-Maneiro, Cold sprayed coatings: Microstructure, mechanical properties, and wear behaviour, Progress in Materials Science, 123, (2022)

30. J.-K. Xiao, H. Tan, Y.-Q. Wu, J. Chen, C. Zhang, Microstructure and wear behavior of FeCoNiCrMn high entropy alloy coating deposited by plasma spraying, Surface & Coatings Technology, 385, (2020)

31. A. Verma, P. Tarate, A.C. Abhyankar, T. Shanmugasundaram, M.R. Mohape, D.S. Gowtam, V.P. Deshmukh, High temperature wear in CoCrFeNiCu_x high entropy alloys: The role of Cu, Scripta Materialia, 161, 28-31 (2019)

32. Y.H. Wu, H.J. Yang, R.P. Guo, X.J. Wang, X.H. Shi, P.K. Liaw, J.W. Qiao, Tribological behavior of boronized Al0.1CoCrFeNi high-entropy alloys under dry and lubricated conditions, Wear, 460-461, (2020)

33. S. Chandra, P. Fauchais, Formation of Solid Splats During Thermal Spray Deposition, Journal of Thermal Spray Technology, 18(2), 148-180 (2009)

34. R.C. Dykhuizen, Review of impact and solidification of molten thermal spray droplets, Journal of Thermal Spray Technology, 3(4), 351-361 (1994)

35. S. Nsoesie, R. Liu, K. Jiang, M. Liang, High-temperature hardness and wear resistance of Cobalt-based Tribaloy alloys, Inter. J. Mater. Mech. Eng, 2, 48-56 (2013)

36. A. Viat, G. Guillonneau, S. Fouvry, G. Kermouche, S. Sao Joao, J. Wehrs, J. Michler, J.-F.o. Henne, Brittle to ductile transition of tribomaterial in relation to wear response at high temperatures, Wear, 392-393, 60-68 (2017)

37. Nelson, G.M., Nychka, J.A. and McDonald, A.G., 2011. Flame spray deposition of titanium alloy-bioactive glass composite coatings. Journal of Thermal Spray Technology, 20(6), pp.1339-1351 (2011)

38. Hasegawa, Masakatsu. "Ellingham diagram." Treatise on Process Metallurgy. Elsevier, pp. 507-516 (2014)

Chapter

6. CONCLUSIONS AND FUTURE WORK

In this chapter…

The overall conclusions of the thesis have been summarized and proposed future work has been presented.

6.1. Conclusions

HEAs have been widely studied since 2004 in their bulk form however, thermally sprayed HEAs have only been investigated since recent years. This thesis explores the available literature on thermally sprayed HEAs and provides a critical comparative evaluation of their tribological performance through the manuscripts. The conclusions for the individual manuscripts have been discussed in detail within their respective chapters. The overall conclusions of the thesis have been summarized in this chapter:

1. Thermally sprayed HEAs show a great potential for wear resistant coatings due to their excellent tribological properties. HEAs can be synthesized by variety of methods such as mechanical alloying, gas atomizing, blending and arc-melting which lead to different mechanical properties. The properties and performance of the coating is largely affected by the deposition technique. For instance, high temperature deposition such as HVOF and flame spray tends to produce hard oxidized coatings having high porosities whereas a low temperature deposition method such as cold spray produces a soft coating with lesser porosity. The versatility of thermal spraying techniques makes it feasible to produce coatings of desired properties depending on the particular application.
2. A novel AlCoCrFeMo HEA coating was developed using cold spray, flame spray and HVOF and their tribological performance was evaluated at varied conditions. Flame sprayed and HVOF sprayed HEA coatings exhibited higher hardness due to formation of oxide phases and showed lesser wear rates as compared to cold sprayed HEA coatings. Polishing had a higher effect on the friction and wear of flame sprayed HEA coating.
3. At room temperature, cold sprayed HEAs had higher fluctuation in friction coefficients due to large number of loose debris particles but showed the least value among the comparison group due to its soft nature. Flame sprayed and HVOF sprayed coatings exhibited higher friction due to the increased hardness and resistance to break asperities with HVOF performing better in the latter part of the tests. The cold sprayed HEA showed the highest wear rates followed by flame sprayed HEA and finally HVOF sprayed HEA having the least. The varying wear rates are a direct result of the hardness of coating.

4. At 450^{O}C, the friction coefficients increased due to enhanced adhesion. Flame prayed HEA showed highest friction followed by HVOF sprayed and cold sprayed HEA respectively. The wear rates for the cold sprayed and HVOF sprayed HEAs reduced drastically due to formation of hard oxide phases over the worn surface. However, the wear rates for flame sprayed HEA coating reduced as a result of increased adhesive and abrasive type of wear and possible softening of the coating at elevated temperatures. Overall, HVOF sprayed HEA coating showed the highest wear resistance at elevated temperatures among all the other tested systems and cold sprayed HEA showed the least wear resistance with flame sprayed HEA being in the middle.
5. Cold spraying seems to be a better performer in terms of friction, but its severe wear rates deem it incapable for tribological applications. HVOF was found to be the most suitable thermal spray deposition technique for producing AlCoCrFeMo HEA coating with excellent tribological behavior.

6.2. Future Work

1. Higher temperature tribological evaluation should be performed (i.e., up to 1000^{O}C) on these coating systems in order to closely mimic applications in hot sections of gas turbine engines.
2. Other thermal spraying techniques having much higher deposition efficiencies, such as High Velocity Air Fuel (HVAF) should be explored for developing AlCoCrFeMo HEA wear resistant coatings in order to improve efficiency and reduce the costs.
3. The principal elements of the HEA should be modified to achieve enhanced performance. Refractory metals such as tungsten (W) and vanadium (V) can be imparted to the existing composition for raising its high temperature performance. For instance, AlCoCrFeMoW and AlCoCrFeMoV can be deposited with HVOF, since it was found to be the most effective technique, and its tribological behavior can be investigated in-depth.
4. Advanced tribological evaluation should be performed on these HEAs using component-based rigs in order to fully capture their abilities under application-relevant conditions. This will help mature coating to a higher TRL.